University of Massachusetts Medical School
eScholarship@UMMS

GSBS Dissertations and Theses | Graduate School of Biomedical Sciences

2014-10-29

Role of Mycobacterium Tuberculosis-Induced Necrotic Cell Death of Macrophages in the Pathogenesis of Pulmonary Tuberculosis: A Dissertation

Teresa S. Repasy
University of Massachusetts Medical School

Let us know how access to this document benefits you.
Follow this and additional works at: https://escholarship.umassmed.edu/gsbs_diss

 Part of the Bacteriology Commons, Immunopathology Commons, Respiratory Tract Diseases Commons, and the Virology Commons

Repository Citation
Repasy TS. (2014). Role of Mycobacterium Tuberculosis-Induced Necrotic Cell Death of Macrophages in the Pathogenesis of Pulmonary Tuberculosis: A Dissertation. GSBS Dissertations and Theses. https://doi.org/10.13028/M28K5C. Retrieved from https://escholarship.umassmed.edu/gsbs_diss/747

This material is brought to you by eScholarship@UMMS. It has been accepted for inclusion in GSBS Dissertations and Theses by an authorized administrator of eScholarship@UMMS. For more information, please contact Lisa.Palmer@umassmed.edu.

ROLE OF *MYCOBACTERIUM TUBERCULOSIS*-INDUCED NECROTIC CELL DEATH OF MACROPHAGES IN THE PATHOGENESIS OF PULMONARY TUBERCULOSIS

A Dissertation Presented

By

TERESA S. REPASY

Submitted to the Faculty of the
University of Massachusetts Graduate School of Biomedical Sciences, Worcester
in partial fulfillment of the requirements for the degree of

DOCTOR OF PHILOSOPHY

October 29, 2014

Interdisciplinary Graduate Program

ROLE OF *MYCOBACTERIUM TUBERCULOSIS*-INDUCED NECROTIC CELL DEATH OF MACROPHAGES IN THE PATHOGENESIS OF PULMONARY TUBERCULOSIS

A Dissertation Presented
By

TERESA S. REPASY

The signatures of the Dissertation Defense Committee signify completion and approval as to style and content of the Dissertation

_____
Hardy Kornfeld, M.D., Thesis Advisor

_____
Samuel Behar, M.D., Ph.D., Member of Committee

_____
Jon Goguen, Ph.D., Member of Committee

_____
Mary Munson, Ph.D., Member of Committee

_____
Natkunam Ketheesan, M.D., Ph.D., Member of Committee

The signature of the Chair of the Committee signifies that the written dissertation meets the requirements of the Dissertation Committee

_____
Christopher Sassetti, Ph.D., Chair of Committee

The signature of the Dean of the Graduate School of Biomedical Sciences signifies that the student has met all graduation requirements of the school

_____
Anthony Carruthers, Ph.D.,
Dean of the Graduate School of Biomedical Sciences

Interdisciplinary Graduate Program
October 29, 2014

Acknowledgements

Firstly, I would like to thank my mentor, Dr. Hardy Kornfeld, for allowing me to join his lab and participate in his research efforts. He provided an enriching environment where I could grow at my own pace as a scientist. He granted me independence yet has always been there to provide support, guidance and advice. He has been exceptionally caring and understanding about me and I am grateful to have been his student.

I would like to thank my thesis and dissertation examination committee members, Dr. Mary Munson, Dr. Francis Chan, Dr. Jon Goguen, Dr. Sam Behar and Dr. Natkunam Ketheesan for taking time from their busy schedules to show interest in my studies and provide me with their guidance and support. I would like to extend my deepest appreciation to my committee chair, Dr. Chris Sassetti. Chris has been an outstanding chair and an awesome advisor who has definitely gone far above and beyond his duties. He has opened his lab me and offered his resources and has always made me feel so welcomed.

I would also like to thank the Kornfeld lab members, past and present, for all their support in my studies. Dr. Nuria Martinez and Kim West have been so generous with their time and assisted me with my experiments. I would like to especially acknowledge Dr. Jinhee Lee. I am immensely thankful to him for all that he has taught me and for always taking the time to answer my questions and providing me with guidance throughout the years. I am exceptionally lucky to have someone as honest, inspiring and giving like him as a lab member.

I wish to thank the Sassetti lab members, past and present, who have kindly provided me with their advice, training and time. They have always made the time for me whenever I needed their help. Special thanks to Xavier Meniche, Christina Baer and of course, "Sundaram" Kadamba Papavinasasundaram for all your help.

I want to thank my family for their support and love. I am especially thankful to my ever-caring mother, Jung-Ja Yang, and cheerleading sister, Angie Pledger, for being so patient and understanding, year after year.

Lastly, I am most grateful to my wonderful husband, Michael. Without his emotional support, practical and wise advice and endless love, I would not have been able to come this far. He has been my biggest cheerleader and a constant source of encouragement. He has always tried to keep me grounded, especially throughout my academic career, and kept me focused on the goal at hand. He has endured and sacrificed, more than anyone will know, and continues to kindly indulge me. Thank you for everything.

Teresa S. Repasy
October 2014

Abstract

Mycobacterium tuberculosis, the causative agent of tuberculosis, can manipulate host cell death pathways as virulent strains inhibit apoptosis to protect its replication niche and induce necrosis as a mechanism of escape. *In vitro* studies revealed that similar to lytic viruses, *M. tuberculosis* has the ability to induce cytolysis in macrophages when it reaches an intracellular burden of ~25 bacilli. Base on this finding, we proposed the burst size hypothesis that states when *M. tuberculosis* invades a macrophage at a low multiplicity of infection it replicates to a burst size triggering necrosis to escape the cell and infect naïve nearby phagocytes, propagating the spread of infection. The first part of this study investigated if the *in vitro* observations of *M. tuberculosis* cytolysis were relevant to cell death of infected phagocytes during pulmonary tuberculosis *in vivo*. Mice infected with a low dose of *M. tuberculosis* revealed during TB disease, the major host cell shifted from one type of phagocyte to another. Enumeration of intracellular bacilli from infected lung cells revealed the predictions of the hypothesis were confirmed by the distribution of bacillary loads across the population of infected phagocytes. Heavily burdened cells appeared nonviable sharing distinctive features similar to infected macrophages from *in vitro* studies. Collectively, the data indicates that *M. tuberculosis* triggers necrosis in mononuclear cells when its number reaches the threshold burst size.

The previous study showed during the period of logarithmic bacterial expansion, neutrophils were the primary host cell for *M. tuberculosis* coinciding with the timeframe of the highest rate of burst size necrosis. The second part of this study examined this link

by infecting mice with one of four different *M. tuberculosis* strains ranging in virulence. Mice infected with the most virulent strain had the highest bacterial burden and elicited the greatest number of infected neutrophils with the most extensive lung inflammation and greater accounts of cell death. Treating these mice with a bacteriostatic agent decreased the bacterial load and infected neutrophils in a dose-dependent manner indicating necrosis induced by virulent *M. tuberculosis* recruited neutrophils to the lungs. Infected neutrophils can serve as a biomarker in tuberculosis as evidenced by poorly controlled infection and increased severity of lung immune pathology.

Table of Contents

List of Tables

List of Figures

List of Abbreviations

AFB	acid-fast bacilli
AFB^+	*M. tuberculosis* infected
Atg	autophagy-related
AM	alveolar macrophage
ATPase	adenosine triphosphatase
BAL	bronchoalveolar lavage
BCG	*Mycobacterium bovis* bacille Calmette-Guérin
BMDM	bone marrow derived macrophages
CFU	colony forming units
COX2	cyclooxygenase 2
CR	complement receptor
CTL	cytotoxic T lymphocyte
CXCL1	C-X-C motif ligand 1
CXCL2	C-X-C motif ligand 2
DAMP	damage-associated molecular pattern molecule
DAPI	4',6-diamidino-2-phenylindole
DC	dendritic cell
DMEM	Dulbecco's modified Eagle medium
EEA1	early endosomal autoantigen-1
Eis	enhanced intracellular survival
EM	electron microscopy
EMB	ethambutol
ESAT-6	early antigenic target-6
FasL	Fas ligand
GKO	interferon-γ knockout mice
H&E	hematoxylin and eosin
HMGB1	high mobility group box 1
IFN-γ	interferon-gamma
IL	interleukin
IRG	immunity-related guanosine triphosphatase
iNOS	inducible nitric oxide synthase
KC	keratinocyte chemoattractant
LC3	light chain 3
LMP	lysosomal membrane permeabilization
LTBI	latent tuberculosis infection
LXA_4	lipoxin A_4

ManLAM	mannosylated lipoarabinomannan
mDC	myeloid dendritic cell
MIP-2	macrophage inflammatory protein 2
MOI	multiplicity of infection
MOMP	mitochondrial outer membrane permeability
MP	mononuclear phagocyte
MPO	myeloperoxidase
MPT	mitochondrial permeability transition
Mtb	*Mycobacterium tuberculosis*
NADPH	nicotinamide adenine dinucleotide phosphate
Ndk	nucleoside diphosphate kinase
NET	neutrophil extracellular trap
NF-κB	nuclear factor-κB
NOD	nucleotide-binding oligomerization domain
PAMP	pathogen-associated molecular pattern
PCD-1	programmed cell death-1
PDIM	phthiocerol dimycocerosate
PGE_2	prostaglandin E_2
p.i.	post infection
PPD	purified protein derivatives
PRR	pattern recognition receptor
PS	phosphatidyl serine
RD	region of difference
REML	restricted maximum likelihood
RIP	receptor-interacting protein kinase
RM	recruited monocyte/macrophage
RNI	reactive nitrogen intermediates
ROS	reactive oxygen species
STPK	serine/threonine protein kinase
TB	tuberculosis
TNF-α	tumor necrosis factor-α
TLR	Toll-like receptor
TUNEL	terminal deoxynucleotidyl transferase dUTP nick end labeling
U/SA	uncertainty and sensitivity analysis
WT	wild type

CHAPTER I: Introduction

1.1 The Life Cycle of *Mycobacterium tuberculosis*

Tuberculosis (TB) is an infectious disease primarily caused by the intracellular bacterium *Mycobacterium tuberculosis* (*Mtb*). The pathogen spreads from one host to another when it becomes aerosolized in particles called droplet nuclei from the cough of a person with active pulmonary TB. The inhalation of infectious droplets by an uninfected person initiates the dissemination of the bacilli. As the droplet nuclei make their way into the alveoli of the lungs, they are encountered by resident alveolar macrophages. Engulfment of the pathogen incites an inflammatory response from the infected macrophage releasing proinflammatory signals, cytokines and chemokines, to recruit neighboring phagocytic cells (neutrophils, monocytes, dendritic cells (DCs) and alveolar macrophages) to the site of infection. As *Mtb* hijacks the macrophage for its residence for replication, the incoming naïve phagocytic cells eventually become the new host cells for the expanding mycobacteria population (1). The newly recruited cells will also serve as the foundation for the formation of the granuloma (2). For the next three weeks *Mtb* will replicate logarithmically, unabated, as it deploys its evasion strategies to counter the host's response to the invading pathogen.

The tuberculous granuloma is a definitive pathological hallmark feature of TB. The formation of the granuloma usually starts as an accumulation of various phagocytes such as macrophages, monocytes, dendritic cells and neutrophils surrounding infected macrophages (3). The macrophages in this aggregate differentiate into foamy

macrophages laden with lipid droplets, epithelioid macrophages and multinucleated giant cells (2, 4). With the onset of adaptive immunity, lymphocytes are also recruited to the granuloma. By this point, tissue architecture has dramatically changed and the granuloma resembles a more organized and structured cellular composition. The center is enriched with macrophages and it is encased by a shell of collagen and other extracellular matrix material forming the fibrous outer layer while lymphocytes (mostly $CD4^+$ T cells, some $CD8^+$ T cells and B cells (5)) encircle the periphery of the granulomatous lesion (2, 6). The arrival of lymphocytes to the granuloma is an indicator that the host adaptive immune system has commenced. Each granuloma, within the same host, exhibits individual stages of development indicating the impact of localized environment over its current state (2). The onset of adaptive immunity restricts mycobacterial replication, halting the logarithmic expansion of the bacilli. While there are numerous mediators of host immunity that combat the pathogen, the major factors that are critical in immunity against *Mtb* are $CD4^+$ T cells and the cytokines, TNF-α, IFN-γ and IL-12 (5).

Although the host immune response is quite effective against *Mtb*, for most infected individuals complete eradication of the pathogen is not likely (7). However, even if many humans still harbor the bacilli, the pathogen is successfully contained as infected individuals are asymptomatic and do not produce infectious droplets. This marks the stage of latent TB infection (LTBI). Most people that are initially infected with *Mtb* reach the state of LTBI and remain in this condition lifelong. Approximately 5-10% of infected individuals will progress to develop active TB disease. Triggers that suppress the immune system significantly increase the chance of getting active disease. Some of those risk

factors include HIV infection, TNF-neutralizing therapy for rheumatoid arthritis or Colitis and diabetes (8). As disease progresses, the structure and composition of the granuloma changes as well. A caseous center starts to develop, most likely due to the increase in the number of foamy macrophages (4). The necrotic center eventually liquefies and cavitates causing the once contained bacilli to be released into the airway (4). This triggers the host to cough, releasing infectious droplet nuclei into the environment thus completing the life cycle of *Mtb*.

1.2 Experimental Tuberculosis

TB is primarily a human disease but it is worth noting that without the use of animal models, the discoveries that have been made towards better understanding the disease simply would not exist. The use of nonhuman primates, rabbits, guinea pigs, mice and even zebrafish have all offered tremendously valuable insight into *Mtb* infection and the disease. To dissect the host response to *Mtb*, it is necessary to analyze the progression of disease *in vivo*. The mouse model has been invaluable in this role as their utilization has provided us with critical knowledge such as the importance of interferon-γ (IFN-γ), tumor necrosis factor-α (TNF-α), interleukin-12 (IL-12) and $CD4^+$ T cells in controlling *Mtb* infection ─ findings all confirmed in human disease studies (5). The TB mouse model has served as a powerful tool in understanding many aspects of TB, from *Mtb* virulence to the host immune response and the mechanisms of innate and adaptive immunity against *Mtb*. However, it is important to note that there are differences in the host-pathogen interactions amongst the host species. For example, the standard wild type (WT) mice, C57BL/6 or BALB/c, when infected with *Mtb* present a very different

pathology than TB disease in humans. Mice granulomas are poorly structured and are not hypoxic, necrotic nor fibrotic; the bacterial burden are relatively high and remain at a steady level as disease progresses; and for mice, *Mtb* infection is lethal (8). Additionally, mice infected with *Mtb* do not present latency of infection to active disease, as seen in humans (8). Due to these and other differences, new findings from mouse TB may only be inferred to be actually occurring in humans until they are validated in human TB. Other animal models may be preferential in studying certain aspects of the disease, such as latent infection or efficacy of new drugs and vaccines, because they reflect more accurately human disease. Nonetheless, the value of the mouse model and its expansive contribution to our current knowledge cannot be overlooked. There is still a lot we don't know about TB and with the wide availability of targeted mutant strains and the abundance of analytical reagents available, the mouse, as a host species, has not exhausted its usefulness in our goal to gain a better understanding of *Mtb*-host interaction.

1.3 Immunity against *M. tuberculosis*

1.3.1 Innate Immunity

Macrophages, one of the major host cells for *Mtb*, are equipped with numerous receptors to bind and phagocytose the bacilli. Complement receptor 3 (CR3) has been shown to be a major macrophage receptor, but macrophages can bind to *Mtb* via other surface receptors: CR1, CR4, mannose receptors, CD14, scavenger receptors, Fcγ receptors and receptors of surfactant protein A Sp-A (9). Pattern recognition receptors

(PRRs) also recognize *Mtb* through specific types of molecules expressed on the pathogen called pathogen-associated molecular patterns (PAMPs). The interaction between PAMPs and PRRs initiates the innate immune response which leads to the production of cytokines and elicits the adaptive immune response (10). One of the most important types of receptors involved in immunity against *Mtb* is Toll-like receptors (TLRs). To date, three TLRs have been identified that recognize mycobacteria. TLR2 is the most dynamic in recognizing *Mtb*. It can distinguish various mycobacterial lipoproteins as well as cell wall components such as mannosylated lipoarabinomannan (ManLAM) and phosphatidylinositol dimannoside. TLR9 detects mycobacterial DNA while TLR4 has been shown to be activated by the bacilli's heat shock protein 60/65 (10). The interaction between *Mtb* and TLRs initiates a signaling cascade through a common TLR adaptor protein, MyD88. The recruitment of other proteins eventually leads to the activation of transcription factor nuclear factor-κB (NF-κB) which translocates to the nucleus. This results in the production of effector molecules for innate host defense, primarily proinflammatory cytokines TNF-α, IL-1, IL-6, IL-8 and IL-12, chemokines and nitric oxide. In addition, co-stimulatory molecules that leads to Th1 adaptive immune response (10, 11). The proinflammatory cytokines along with mycobacterial antigens prime T cells. Thus, TLRs bridge the innate and adaptive immune responses to *Mtb*.

Studies that looked into the *in vivo* significance of TLR-mediated signaling in defense against *Mtb* examined mice lacking TLRs or MyD88. Mice lacking single TLR or double or triple knockouts yielded varying results in terms of immune response and the outcome of the disease (12). However, mice lacking MyD88 were extremely susceptible to *Mtb*

infection, succumbing quickly to death with significantly increased bacterial loads, extensive lung damage and decreased expressions of IL-12, TNF-α, IFN-γ, and nitric oxide synthase 2 (13, 14). Similar results were found with IL-1R$^{-/-}$ mice supporting the concept that the importance of TLR signaling in MyD88-dependent innate response to *Mtb* was the IL-1 signaling which is downstream of MyD88 (13).

A key finding in studying TLRs in the context of *Mtb* infection was the discovery of IFN-γ independent antimycobacterial pathway in human macrophages. Vitamin D deficiency has been identified as a risk factor for TB and the Vitamin D3 pathway has been shown to control bacterial replication in human macrophages. Liu et al. revealed that through TLR2 activation, macrophages increased their expression of Vitamin D receptor and upregulated Vitamin-D-1-hydroxylase genes which led to the production of cathelicidin, an antimicrobial peptide (15). This study also demonstrated that a correlation between TB susceptibility and cathelicidin, where African Americans who were more vulnerable to infection and disease had defective induction of cathelicidin mRNA. Cathelicidin has also been recognized to induce autophagy in THP-1 cells and human primary monocytes (16).

Nucleotide-binding oligomerization domain (NOD) proteins are intracellular PRRs that recognize PAMPs. Interaction of NOD2 with mycolyl-arabinogalactan peptidoglycan, a major component of mycobacterial cell wall, was shown to initiate the production of proinflammatory cytokines and nitric oxide (17). NOD2-deficient mice showed similar phenotype to WT mice when challenged with *Mtb* with comparable bacterial burden and pathology. However, Divangahi et al. (18) revealed the importance

of NOD2 in both innate and adaptive immune response to *Mtb* as NOD2-deficient mice infected with *Mycobacterium bovis* bacille Calmette-Guérin (BCG) had reduced type 1 cytokines with less $CD8^+$ and $CD4^+$ T cells along with reduced Ag-specific T cell responses. Long term *in vivo* experiment demonstrated that NOD2-deficient mice infected with *Mtb* had greater bacterial burden at 6 months p.i. than WT mice and had shorter survival times.

Other immune cells from the innate host response are DCs, neutrophils, γδ T cells, NK cells and NKT cells. The importance of DCs during *Mtb* infection is clear ─ they are the primary antigen presenting cells and their role directly links innate immunity to adaptive immunity. The role of the remaining innate immune cells during *Mtb* infection has yet to be defined clearly, especially in humans. γδ T cells have been shown to secrete IFN-γ and TNF-α after activation in addition to IL-17 in response to IL-23 secretion from DCs, demonstrating a protective role against infection. *Mtb*-infected mice that are deficient in γδ T cells have been shown to have varying results depending on the route of infection and dose (19). NK cells can be another source of IFN-γ and when activated, lyse infected macrophages in a TLR-dependent manner. NKT cells are T cells with NK markers that can recognize *Mtb* cell wall lipids as antigens. They also have the ability to secrete IFN-γ as well as IL-4 and IL-10. A subset of NKT cells, invariant NKT cells has been shown to directly restrict mycobacterial replication and reduce bacterial lung burden in *Mtb*-infected mice (20). A recent finding from TB patients showed increased NKT cells expressing programmed cell death-1 (PCD-1), a negative regulator of T cells, from patients with higher sputum bacillary load. PCD-1 correlated with higher apoptotic cell

death of IFN-γ producing NKT cells while permitting NKT cells that produced IL-4 to live, skewing the T cell response towards Th2, thus favoring the pathogen (21).

Neutrophils are recruited into the lungs in the early stage of *Mtb* infection. They are the primary cells that harbored *Mtb* in patients with active pulmonary TB (22) however, their role in TB disease is contradictory. Many studies showed neutrophils to play a negative role in TB pathogenesis while others have revealed host defense. Even their ability to kill *Mtb* is controversial. It is common to observe accumulation of neutrophils at active sites of disease and the disease severity seems to be associated with the amount of localized neutrophil influx (23). Nandi and Behar (24) showed that when neutrophils were depleted in IFN-γR$^{-/-}$ mice this proved to be protective for the host, although there was no decrease in bacterial burden, there was an increase in the survival time. Neutrophils were associated with lung inflammation and contributed to the decline of disease outcome. This study also showed that IFN-γ reduced neutrophil viability and it directly prevented neutrophil recruitment in the lungs (24). A different study showed mice depleted of neutrophils prior to *Mtb* challenge had increased bacterial burden demonstrating their protective role in early defense against the pathogen (23). Neutrophils have been shown to facilitate in the induction of adaptive immunity by functioning with DCs. Mice infected with a proapoptotic *Mtb* mutant lacking nuoG, showed quicker DC acquisition of mycobacterial antigens and faster migration to lymph nodes resulting in faster priming of T cells (25). In a different study, depletion of neutrophils was shown to decrease trafficking of DCs to the lymph nodes resulting in the delay and activation of naïve T cells. Additionally, *Mtb*-infected neutrophils engulfed by

DCs promoted better migration to lymph nodes than DCs that directly phagocytosed *Mtb* demonstrating that neutrophils contributed to the initiation of adaptive immunity (25). However, there is growing amount of evidence that neutrophils are associated with TB pathology and disease severity. Their protective role during infection may be limited to early stage of infection and the robustness of their response to the pathogen may lead to detrimental outcome.

Cell death is also an innate host defense mechanism against *Mtb*. *Mtb*-infected macrophages undergo apoptosis as a means to control infection and reduce bacterial viability. This subject is discussed in detailed in Section 1.6.

1.3.2 Adaptive Immunity

In almost all cases, the innate immune response is inadequate at controlling mycobacterial infection. Immunity against *Mtb* is dependent on the adaptive immune response requiring the activation of antigen specific $CD4^+$ T cells. The appreciation for the essential role of $CD4^+$ T cells against *Mtb* in humans is underscored in HIV infected individuals. The depletion of T cells in this group of immunocompromised individuals renders them extremely susceptible to mycobacterial infection (26). Mice lacking $CD4^+$ T cells are unable to control bacterial growth and quickly succumb to death (26). Naïve T cells are activated by the presentation of antigens by DCs infected with *Mtb* that migrate to the draining lymph node. Once activated, $CD4^+$ T cells traffic to the sites of infection where they activate macrophages by releasing IFN-γ and other cytokines. Specifically, immunity against *Mtb* is predominantly a Th1-mediated response driven by IFN-γ as mice that are unable to produce this cytokine or lack its receptors fail to inhibit bacterial

growth and the infection quickly becomes lethal (27). IL-12, which is released by macrophages and DCs, is essential in its contribution to the differentiation of naïve T cells into Th1 cells. *Mtb*-infected mice incapable of producing IL-12 cannot defend against the pathogen (28). Additionally, for humans that have mutations in the genes for IFN-γ receptor, IL12p40 subunit or IL-12 receptor β1 chain, TB is a severe systemic disease (29).

The arrival of $CD4^+$ T cells to the site of infection marks the event when logarithmic bacterial expansion is inhibited as the antimicrobial mechanisms of macrophages are activated. The production of nitric oxide by inducible nitric oxide synthase (iNOS) and the production of reactive oxygen by nicotinamide adenine dinucleotide phosphate (NADPH) are the two primary defenses against the pathogen. The importance of reactive nitrogen intermediates (RNI) against the pathogen is demonstrated by the highly susceptible phenotype of NOS2 deficient mice challenged with *Mtb* (30). IFN-γ is absolutely necessary to fully activate macrophages to produce iNOS. Mice that are unable to produce reactive oxygen species (ROS) are only slightly susceptible to *Mtb* or equivalent in susceptibility to WT mice, demonstrating the importance of nitric oxide over reactive oxygen in killing mycobacteria (26).

The relative contribution of $CD8^+$ T is still unclear and perhaps more likely to be significant in humans than in mice. $CD8^+$ T cell have the potential to activate macrophages through cytokine production and kill infected cells through cytotoxic mechanisms, but these observations have only been made from *in vitro* studies, thus their relevance in TB disease is unclear (31). A study with nonhuman primates revealed that

$CD8^+$ T cells contributed to protecting the host against TB in vaccinated rhesus macaques. Depletion of $CD8^+$ T cells resulted in significantly reduced protection of BCG vaccine-induced immunity against *Mtb* and depletion of $CD8^+$ T cells from previously cured rhesus macaques with antibiotic therapy reduced anti-*Mtb* immunity upon re-infection (32). B cells have also been studied in BCG-vaccinated animals. A study demonstrated that B cells regulate neutrophils via IL-17 during both *Mtb* infection and BCG immunization and that efficacious protection with BCG vaccination required B cells. B cell deficient mice showed increased inflammation and neutrophil infiltration in the lungs of infected mice and vaccinated mice showed reduced Th1 response (33). Another study showed that mice with defective B cells that were incapable of secreting immunoglobulin were more susceptible to TB than WT mice or mice completely depleted of B cells (34).

1.3.3 M. tuberculosis-*Induced Cytokines*

Recognition of mycobacterial components by mononuclear phagocytes (MPs), composed of mostly macrophages and dendritic cells (and later monocytes), triggers an inflammatory response that activates them and initiates the production and secretion of cytokines. This propagates further cytokine production and initiation of the adaptive immune response. There are numerous cytokines, proinflammatory and anti-inflammatory, secreted during *Mtb* infection that shapes the outcome of infection. Although the proinflammatory response is to protect the host, excessive amount of proinflammatory cytokines can lead to tissue damage, whereas an overpowering anti-inflammatory response can favor the pathogen. A fine balance must be maintained in

order to provide continued protection against the pathogen. The following is a table of only the major cytokines involved during *Mtb* infection.

Cytokine	Main Producer	Effect
TNF-α	Activated MPs, Th1 cells	Key cytokine in host defense, induces production of cytokines & chemokines, granuloma formation & maintenance
IFN-γ	Th1 cells, $CD8^+$ T cells, MPs, γδ T cells, NKT cells, NK cells	Key cytokine in host defense, promotes antigen presentation, activates macrophages, recruits CD4+ T cells
IL-12	Activated MPs	With IL-18 induces differentiation of T cells into Th1 cells that produce IFN-γ, DC maturation & migration to lymph nodes
IL-18	Activated MPs	With IL-12 induces production of IFN-γ and other cytokines, chemokines and transcription factors
IL-1β	Activated MPs, Th1 cells	Independent of TNF-α/IFN-γ/iNOS/IL-12 protection of host, triggers PGE_2 synthesis & negatively regulates type I IFNs
IL-6	Activated MPs	Varying effects dependent on bacterial burden and stage of infection, shown to inhibit production of TNF-α and IL-1β in *M. avium* infection model
IL-23	Activated MPs	In concert with IL-12 promotes activation of CD4+ T cells
IL-8 (aka CXCL8)	Activated MPs	Chemokine that recruits neutrophils and T cells to site of infection
IL-4	Th2 cells	Suppresses IFN-γ production in macrophages, with IL-13 downregulates TLR2 & TNF-α
IL-10	Activated MPs, T cells	Downregulates IL-12 and TNF-α and blocks phagosome maturation in macrophages, inhibits antigen presentation in MPs, reduces IFN-γ and inhibits T cell responses, blocks trafficking of DC to lymph node and Th1 cells to lungs
TGF-β	Activated MPs, T cells	Inhibits ROS and RNI in macrophages, suppresses proliferation of T cells
Type I IFNs	Activated macrophages, virus-infected epithelial cells & plasmacytoid DCs	Inhibits macrophage functions, suppresses IL-1, IL-12 and TNF-α, induces IL-10, blocks macrophage activation by Th1 cells

Table 1.1. Major cytokines during *Mtb* infection (5, 10, 35, 36).

1.3.4 Autophagy

Autophagy is a form of cellular house cleaning where unwanted cytoplasmic components of the cell are degraded. Intracellular stress such as starvation or infection can trigger autophagy which is regulated by autophagy-related (Atg) proteins. The process is initiated by sequestering the targeted cellular component and forming a double membrane around the target known as an autophagosome. During the maturation process, the autophagosome fuses with the lysosome degrading the internal contents via the caustic lysosomal hydrolases (37). Autophagy directly kills mycobacteria and plays a key role in both innate and adaptive immunity against *Mtb*. There are several factors that modulate autophagy in context of mycobacterial infection, cytokines like IFN-γ and TNF-α, certain drugs, vitamin D and signals downstream of TLR ligation. Other functions of autophagy in regards to *Mtb* infection are suppressing proinflammatory cytokines, such as IL-1β and IL-18, and antigen presentation (38).

Although *Mtb* has evolved to evade host immune responses, such as blocking the phagosome maturation process and inhibiting its fusion with the lysosome, the cell counters this evasion with autophagy which delivers the pathogen directly to the lysosome. Therefore, autophagy reduces mycobacterial viability. Guiterrez et al. (39) showed that when autophagy was induced in BCG-infected macrophages, the mycobacterial phagosome became acidified and possessed markers of matured phagosome with co-localization of late endosome and lysosomal markers such as cathepsin D, LAMP-1 and vacuolar H^+-ATPase. These phagosomes also displayed markers for autophagy, light chain 3 (LC3). This study also revealed that autophagy

could be induced with IFN-γ and virulent H37Rv was susceptible to killing by autophagy (39). In both mice and humans, immunity-related guanosine triphosphatases (IRGs) were shown to induce autophagy (40). In mice, IFN-γ induced autophagy required Irgm1, although this was not the case for human Irgm1 ortholog, IRGM. Nonetheless, in U937 human macrophage cells, inducing autophagy reduced mycobacterial viability (40). Another study showed that when TLR2 was stimulated by mycobacterial lipoprotein LpqH, autophagy was induced via vitamin D receptor signaling in human primary monocytes (41). Others TLRs, including TLR4, also induced autophagy in murine macrophages recruiting the adaptor protein MyD88 or Trif which interacted with Beclin 1, a key factor in autophagosome formation (42). Watson et al. (43) showed that within 4 hours p.i., approximately 30% of intracellular *Mtb* colocalized with LC3 in infected BMDM and autophagy was ESX-1 dependent. Autophagy was induced by cytosolic sensing of *Mtb* DNA and targeted mycobacteria were associated with host ubiquitin. *In vivo* results revealed the importance of autophagy to host defense. *Atg5*$^{-}$ mice were highly susceptible to *Mtb* infection surviving only about four weeks with excessive pulmonary damage, 1000-fold increase in lung bacillary burden and significant increase in proinflammatory cytokines TNF-α, IL-1α, IL-1β and IL-6 without any changes in IFN-γ when compared to *Atg5*$^{+}$ mice (43). IL-4 and IL-13, two Th2 cytokines, inhibit autophagy in both murine and human monocytes and macrophages. IL-4 and IL-13 also prevented autophagy-dependent killing of intracellular *Mtb* as well as phagosome maturation (44). The importance of autophagy was revealed when Kumar and colleagues (45) performed a genome-wide analysis to screen for host factors that regulated *Mtb* in

THP-1 cells infected with virulent *Mtb* and found that autophagy was a major pathway in controlling infection.

As a successful pathogen, *Mtb* has developed strategies to resist autophagy. Virulent H37Rv and attenuated strains, H37Ra and BCG, were used to infect human primary DCs. Only H37Rv was able to impede autophagy by preventing the autophagosome-lysosome fusion. Complementation strains that restored ESX-1/ESAT-6 to the attenuated strains reinstated autophagy inhibition (46). The *Mtb* protein, enhanced intracellular survival (Eis), was also shown to inhibit autophagy (47). This protein promotes the intracellular survival of *Mycobacterium smegmatis,* a nonpathogenic bacterium. When BMDM were infected with the *eis* deletion mutant, it resulted in an upregulation of proinflammatory cytokines, TNF-α and IL-6, and ROS generation along with an increase in autophagic vacuoles and autophagosomes suggesting that Eis modulates autophagy in the host. Mice infected with *eis* deletion mutant mirrored the results from the *in vitro* experiment (47). Furthermore, the mycobacterial cell wall component ManLAM, a key virulence factor of *Mtb*, was shown to not only contribute in blocking phagosomal maturation, but also prevented accumulation of autophagosomes in murine macrophages (48). In a proteomics approach, purified ManLAM coated latex beads were fed to macrophages and the phagosomal membrane proteins were quantified. Compared to *M. smegmatis* LAM or *E. coli* LPS, there was 30% less LC3 in ManLAM containing phagosomes indicating that virulent *Mtb* inhibits autophagy (48).

1.4 Immune Evasion of *M. tuberculosis*

The success of *Mtb* as a pathogen is due to its ability to evade the host immune response. The bacilli have acquired numerous methods to manipulate the host cell from both the innate and adaptive responses to the pathogen. One evasion strategy of *Mtb* is the ability to manipulate the phagosome. For most microbes that enter the airspace their encounter with the macrophage means their inevitable demise due to its potent antimicrobial mechanisms. Upon phagocytosis of the pathogen, it is encased in a phagosome, a membrane bound vesicle headed towards destruction by way of fusing with the lysosome. Through the maturation process, the phagosome becomes acidified enabling the optimal condition for the destructive enzymes of the lysosome to function properly and ultimately to destroy the internalized invader (49). For *Mtb*, however, the scenario is quite different. *Mtb* does not just survive within the hostile confines of the phagosome but alters it and preserves an environment capable of bacterial replication. Upon engulfing the bacilli, the phagosome maturation process is halted resembling an early endosome. The phagosomal membrane is associated with Rab5 but not Rab7 which suppresses the recruitment of early endosomal autoantigen-1 (EEA1) (50). This protein is required for fusing the phagosome to the lysosome enabling the proper delivery of lysosomal hydrolases. A mycobacterial component of the cell wall, ManLAM, has been identified with interfering with the phagosomal maturation process and preventing the fusion of the two organelles by blocking vesicular trafficking between the phagosome and trans-Golgi network and thus preventing the necessary molecules for the phagosome to mature (50, 51). *Mtb* protein kinase G has also been implicated to disrupt the transfer

of the *Mtb*-residing phagosome to the lysosome (52). *Mtb* arrests the acidification of the vacuole by preventing the acquisition of vesicular proton-adenosine triphosphatases (ATPases) resulting in approximately 6.4 pH (53, 54). At this pH level, most lysosomal hydrolases are inert, limiting their enzymatic capacity to destroy. *Mtb* also prevents the phagosome from recruiting iNOS, the machinery necessary to generate nitric oxide that kills *Mtb* (55).

Activation of macrophages by IFN-γ, TNF-α and IL-1β overrides the mycobacterial hold on the arresting phagosome and iNOS is activated. The generation of RNI is toxic causing damage to mycobacterial DNA, proteins and lipids (31). While bacterial replication is controlled, *Mtb* is not eliminated due to its countermeasures for RNI toxicity. The bacterial genome contains several mycobacterial genes that encode for proteins to handle nitrosative stress. AhpC, Lpd, SucB and AhpD work together to form an antioxidant complex (56). The *msrA* gene encodes for a reductase that also catalyzes the oxidizing agent (57). And *nox1* and *noxR3* have been implicated in protection against nitrosative and oxidative stress (58, 59). *Mtb* also encodes for superoxide dismutase proteins (Sod) and catalase (KatG) to protect against ROS (60, 61).

Another immune evading strategy of *Mtb* is in the interference of antigen presentation. Several studies have shown that MHC class II expression on *Mtb*-infected macrophages was reduced thus diminishing the ability for $CD4^+$ T cells to recognize them. The reduced expression was attributed to defective transportation and processing of MHC class II molecules in the endosomal pathway (62) or downregulation of the class II transactivator, a protein that controls the expression of MHC class II genes (63). Another

study found that *Mtb* decreased the level of MHC-II mRNAs (64). A follow-up study revealed that a 19 kDa lipoprotein of *Mtb* inhibited MHC class II processing and presentation along with blocking the effects of IFN-γ induced upregulation of the molecule in a TLR2-dependent manner (65). Additionally, when *Mtb*-residing phagosomes were isolated from IFN-γ activated macrophages, there was a reduction in MHC class II antigen processing from phagosomes with live bacteria versus those with heat-killed bacteria (66).

The pathogen's ability to manipulate the fate of the host cell indicates the importance of cell death in its strategy to survive. Many studies have demonstrated that the cellular fate of the infected macrophage is dependent on whether the mycobacterial strain is virulent or attenuated. *Mtb* has developed strategies to alter the host cell death pathway to inhibit apoptosis and induce necrosis. The subject of *Mtb* and host cell death is featured in Section 1.6.

1.5 Review of Cell Death

Cell death in the context of an infection is the host response to eradicate infected cells harboring the invading pathogen. However, both viral and bacterial pathogens have evolved to counter this measure by manipulating the host cell death pathway to evade eradication and promote survival. Infected cells engage in one of these principal forms of programmed cell death: apoptosis, necrosis, and pyroptosis. Each mode of cell death differs in morphology and the mechanism in which the cell determines its demise. This is a brief overview of the major modes of cell death involved in microbial infections.

1.5.1 Apoptosis

Apoptotic cell death usually protects the host from invading pathogens. There are three major pathways for apoptosis to occur: extrinsic, intrinsic and granzyme B. The key components involved in these pathways are initiator and effector caspases (cysteine-dependent proteases). Initiator caspases begin the apoptotic cell death process by activating the downstream effector caspases by cleaving them into their active form. Effector caspases cause the cellular changes that promote the death of the cell, the execution phase.

The extrinsic apoptotic pathway is triggered by death receptors, members of the TNF receptor superfamily with a cytoplasmic death domain that is crucial for signaling. The two well characterized receptors, TNFR1 and Fas, upon binding to their respective cognate ligand, TNF-α and Fas ligand (FasL), oligomerize and initiate a cascade of signaling events through the death domain. The binding of FasL to Fas recruits the adaptor protein FADD via its death domain, whereas the TNF-α/TNFR1 pathway binds the adaptor protein TRADD with the recruitment of FADD. The association of FADD with procaspase-8 initiates the formation of a death-inducing signaling complex which causes the self cleavage of procaspase-8 into its activated form (67). Caspase-8 goes on to activate downstream effector caspases (caspases-3, -6, -7) to promote the execution phase of apoptosis (68).

Intrinsic apoptosis is initiated when the cell is under some form of intracellular stress such as ultraviolet irradiation, DNA damage, lack of nutrients or oxidative stress. Any one of these stressors can damage the outer membrane of the mitochondria. If

mitochondrial outer membrane permeability (MOMP) develops, cytochrome c, which resides in the intermembrane space, is released into the cytosol. Once in the cytosol, cytochrome c associates with an adaptor protein, apoptosis protease activating factor-1, causing it to oligomerize. This initiates the formation of a massive protein complex called the apoptosome which recruits and activates caspase-9, an initiator caspase (69). The activation of caspase-9 causes the downstream effector caspases to be cleaved and activated, inducing apoptosis. The triggering of the intrinsic pathway is hinged on the release of cytochrome c which is regulated by the interaction of proteins in the Bcl-2 family. The Bcl-2 family of proteins is generally categorized into two groups: those that promote apoptosis and those that inhibit it (70). Pro-apoptotic proteins such as Bax and Bak can directly bind to the outer membrane of the mitochondria, forming pores to release cytochrome c. Anti-apoptotic proteins like Bcl-2, Bcl-X_L, Bcl-w and Mcl-1 promote cell survival. Bid is another pro-apoptotic Bcl-2 family member that coordinates with Bax and Bak to promote the release of cytochrome c (71). Bid is activated when it is cleaved which can be performed by number of proteases including caspase-8 and -9, allowing cross-talk between intrinsic and extrinsic pathways of apoptosis.

The third pathway for apoptosis involves cytotoxic T lymphocytes (CTLs) and NK cells. Apoptosis is induced by the release of perforin, a transmembrane pore-forming molecule, by CTLs or NK cells that creates pores on the targeted cell's surface. Following pore formation, cytoplasmic granules are released including serine protease granzyme B. Once inside the target cell, granzyme B can cleave procaspase-10 or procaspase-8 to

activate the mitochondrial pathway or directly cleave procaspase-3 to induce the execution phase (67, 68).

In the presence of an infection, apoptosis is designed to silently kill the pathogen without sounding the alarm of an inflammatory response. The morphological features of apoptosis include shrinking of the cell, condensation of the nucleus, DNA fragmentation and blebbing of the cell membrane resulting in the formation of apoptotic vesicles (72). These membrane-bound vesicles encase the cytoplasmic content of the cell, including the phagosomal residing pathogen, and are engulfed by neighboring phagocytes through the process of efferocytosis (73). Once phagocytosed, the efferocytic phagosome or efferosome, fuse with the lysosome allowing for the degradation of the apoptotic body including the pathogen (73, 74).

1.5.2 Necrosis

Necrotic cell death is strikingly different from apoptotic cell death as many of the morphological features are opposite to that of apoptosis. Cells dying of necrosis undergo swelling of organelles and the rupturing of the plasma membrane which releases cytoplasmic content into the extracellular space (72). This cellular event is pro-inflammatory as necrotic debris, such as damage-associated molecular pattern molecules (DAMPs), triggers inflammation and causes tissue damage. Unlike apoptosis with a well defined signaling pathway, necrotic cell death is caspase independent and can be triggered by a variety of stimuli leading to different signaling pathways to initiate necrosis. Cells that undergo necrosis commonly present some of these cellular events: mitochondrial membrane injury, production of ROS, ATP depletion, disruption of Ca^{2+}

homeostasis, activation of calpains and cathepsins and lysosomal membrane permeabilization (LMP) and the loss of plasma membrane integrity (75, 76).

There are several types of regulated necrosis that have been observed in infected cells. Necroptosis is probably the most mechanistically understood of the necrotic cell death pathways. This form of cell death is dependent on the receptor-interacting protein kinase 1 (RIP1) and RIP3 and can be induced by several factors such as death ligands, TLR ligands or microbial infections (72). In the TNF signaling pathway, upon inhibition of caspase-8, a complex called a necrosome which includes RIP1, RIP3, caspase-8 and FADD is assembled resulting in LMP, ROS production and the activation of calpains and calcium-dependent cysteine proteases (72, 76). Another form of regulated necrosis is ROS induced NETosis and ETosis. First observed from dying infected neutrophils, this novel mode of cell death induces the release of neutrophil extracellular traps (NETs). A combination of chromatin, histones, neutrophil elastase and other antimicrobial molecules trap and kill invading pathogens (77). Other immune cells such as mast cells, eosinophils, and macrophages have been observed to undergo this form of cell death as well. Depending on the conditions in which NETS are released they can suppress inflammation or enhance it (77).

1.5.3 Pyroptosis

Having features of apoptosis and necrosis, pyroptosis was first observed from macrophages infected with *Shigella flexneri* (72). Pyroptosis is inherently dependent on the activation of caspase-1 which is activated by a large protein complex in the cytosol known as the inflammasome. There are four types of inflammasomes and the particular

inflammasome that is assembled is based on the type of microbial or viral detection from the cytosol by NOD-like receptors. Once activated, caspase-1 processes proIL-1β and proIL-18, two proinflammatory cytokines, as well as the induction of pyroptosis. In certain bacterial infections, caspase-11 (also known as caspase-4) has been implicated as a requirement for caspase-1 activation (78). This mode of cell death is proinflammatory. During pyroptosis, the formation of pores in the plasma membrane causes the cell to swell leading to osmotic lysis and eventually the release of cellular contents into the extracellular space. This event is very similar to necrosis, however, in pyroptosis, apoptotic features of nuclear condensation and DNA fragmentation are also present (72). Pyronecrosis, another proinflammatory cell death, is similar to pyroptosis and is mediated by inflammasomes without the dependence on caspase-1 or caspase-11 (76).

1.6 *M. tuberculosis*-Induced Cell Death

Cell death of the host is an intimate part of the mycobacterial life cycle. To initiate infection, *Mtb* must be able to alter the intracellular environment conducive for replication. This requires the pathogen to evade host defenses and keep the cell viable long enough until its utility has been expended. For *Mtb* to complete its life cycle, infection must be first established in the lungs of one host in order to transmit to another host. Since this is carried out via infectious droplet nuclei, *Mtb* must shift from an intracellular to an extracellular environment. This transition requires the pathogen to exit the host cell. To evade host defenses and exit the cell, *Mtb* must have the capacity to modulate the cell death pathways of the host.

1.6.1 Mycobacterial Genes and Host Cell Death

The discovery of mycobacterial genes that are directly involved in host cell death pathways suggests the importance of the fate of infected cells to the pathogenesis of *Mtb*. The mycobacterial gene, *nuoG*, encodes a subunit of type I NADH dehydrogenase complex that upon its deletion, the mutant *Mtb* strain is proapoptotic. THP-1 cells and BMDM challenged with *nuoG* deletion mutant showed increased levels of apoptosis over WT *Mtb*. Mice infected with the *nuoG* deletion mutant showed benefits to the host as they survived much longer, had reduced bacterial lung burden and presented with decreased lung damage compared to WT *Mtb* (79). In a gain-of-function experiment, when *nuoG* was expressed in nonpathogenic strain of mycobacteria, *Mycobacterium kansasii*, and used to infect immunodeficient SCID mice, the mutant strain exhibited increased virulence by shortening host survival time in concert with increased lung pathology (79). Another study showed that primary murine and human alveolar macrophages infected with the *nuoG* deletion mutant had an increase in ROS level in the phagosome and an increase in TNF-α secretion over WT *Mtb*. This revealed that virulent *Mtb* neutralizes ROS in the phagosome in order to inhibit TNF-α mediated apoptosis in a *nuoG*-dependent manner (80). Blomgran et al. (81) showed that virulent *Mtb* can influence adaptive immune response by the inhibition of neutrophil apoptosis *in vivo*. When compared to WT *Mtb*, mice infected with *nuoG* deletion mutant produced more apoptotic cells, had less bacilli per infected cell, quicker acquisition of bacteria by DCs and earlier trafficking to lymph nodes which led to faster activation of naïve T cells (81).

The *secA2* gene encodes for a component of the mycobacterial SecA2 protein secretion system. The deletion of *secA2* gene resulted in a mutant strain that was proapoptotic. Infection of THP-1 cells and BMDM with the deletion mutant showed increased apoptotic cells when compared to WT. Additionally, mice infected with the *SecA2* deletion mutant significantly enhanced the priming of $CD8^+$ T cells, linking apoptosis to adaptive immune response (82). The proapoptotic phenotype was due to the disruption of the SecA2 secretion system which prevented the secretion of SodA, an iron co-factored enzyme, superoxide dismutase, that allows for the conversion of superoxide anion to hydrogen peroxide (82). A SodA knockdown mutant showed attenuation in infected mice with less bacterial burden in the lungs and spleens compared to virulent control *Mtb*. In a long term infection study, when compared to the attenuated strain BCG, mice infected with SodA knockdown mutant showed to be more attenuated with less alveolar infiltration and less bacteria in the lungs and spleen (83).

A recent study revealed another proapoptotic *Mtb* mutant strain. The mycobacterial protein nucleoside diphosphate kinase (Ndk) interferes with host cell death pathways. Mutant strains that disrupted *Ndk* expression were used to infect SCID mice which resulted in reduced virulence with extended survival time and a decrease in bacterial loads in the lungs when compared to WT *Mtb*. *Ndk* knockdown mutants presented similar phenotype to *nuoG* deletion mutants, infected macrophages had increased ROS production in the phagosome along with higher levels of apoptotic cell death when compared to WT. Ndk was shown to disrupt NADPH oxidase assembly by interfering with the recruitment of $p67^{phox}$ subunit necessary for ROS production (84).

Another mycobacteria protein implicated in host cell death is early secreted antigenic target-6 (ESAT-6). ESAT-6 is a secreted protein that is dependent on the mycobacterial secretion system ESX-1. The gene is located in region of difference 1 (RD1) of the mycobacterial genome and its absence in BCG is considered the primary mechanism that contributes to its attenuated phenotype (85). ESAT-6 has been implicated to have cytolytic capacity as incubation of this purified protein with artificial lipid bi-layer resulted in the destruction of the membrane (85). Welin et al. (86) examined the effects of ESAT-6 in human monocyte-derived macrophages. When macrophages were infected with H37Rv at MOI 10 and cultured for two days, the infected cells died of necrosis. There was evidence of mitochondrial injury with the loss of transmembrane potential along with plasma membrane permeabilization with the release of IL-1β and a known DAMP, high mobility group box 1 (HMGB1). The cell death was also independent of caspase-1 and cathepsin B. These features of necrotic cell death were also dependent on ESAT-6. Macrophages infected with attenuated H37Ra or ESAT-6 or RD1 deletion mutants or H37Rv at a low MOI of 1 resulted in some of these features, but at significantly reduced levels (86). Simeone and colleagues (87) investigated the translocation of mycobacteria from the phagosome to the cytosol using fluorescence resonance energy transfer. Infected THP-1 macrophages at MOI of 1 were cultured for up to 10 days. Macrophages infected with BCG, RD1 deletion mutant or mutants that secreted truncated ESAT-6 showed no phagosomal rupture, even at 10 days p.i. When macrophages were infected with *Mtb* or *M. marinum*, phagosomal rupture occurred followed by necrotic cell death. At day 7 p.i. when differences between strains were most

evident, only 2-4% of cells infected with *Mtb* or RD1 complementation strains were viable (87).

Suppression of apoptosis supports an intracellular lifestyle and allows *Mtb* to replicate inside the macrophage. The bacillus encodes 11 serine/threonine protein kinases (STPK) which are signaling molecules that facilitate as environmental sensors. PknE, one of the STPKs, has been identified to suppress apoptosis. Infection of human macrophages with the PknE deletion mutant showed reduced intracellular growth with increased apoptosis. Microarray data from infected macrophages with the deletion mutant revealed increased expression of Bax, Bid and other components of intrinsic apoptotic pathway along with a decrease in the Mcl-1 expression. PknE was also shown to suppress apoptosis to support intracellular survival for *Mtb* in the presence of NO stress (88). MPT64 is a secreted protein of *Mtb* that suppresses apoptosis of the infected cell and preserves an intracellular environment for bacterial replication by upregulating the expression of the anti-apoptotic protein Bcl-2. Treating RAW264.7 macrophages with purified protein derivatives (PPD) from BCG induces apoptosis; however the addition of MPT64 inhibited apoptotic cell death (89).

1.6.2 Apoptosis versus Necrosis in TB

There are primarily two types of cell death that *Mtb* initiates in the infected macrophage: apoptosis or necrosis. In the context of *Mtb* infection, apoptotic cell death is antimicrobial in nature and serves to protect the host. Control in the spread of infection is accomplished by killing the bacteria in apoptotic vesicles through efferocytosis, thus protecting naïve phagocytes from becoming infected and reducing bacterial viability (73).

Additionally, the replication niche necessary for bacterial expansion is eliminated. Since apoptotic cells do not promote inflammation there is minimal damage to the tissue. And finally, apoptosis of infected macrophages allows for dendritic cells to acquire mycobacterial antigens for cross-priming. Apoptosis is a death mode strongly induced by attenuated strains of *Mtb* (90, 91). Conversely, necrosis serves to benefit the pathogen. Necrotic cell death liberates the once intracellular *Mtb* to the extracellular space due to the disintegration of the cellular and plasma membranes. This fosters dissemination of the pathogen as necrosis is proinflammatory, recruiting naïve cells to be available for the freed bacilli to invade. Macrophages infected with virulent strains of *Mtb* actively suppress apoptosis (79, 82, 92) and induce necrosis (91, 93, 94).

Apoptosis, whether induced by FasL or TNF-α, reduces the viability of intracellular *Mtb*. Virulent *Mtb* has strategies to inhibit host directed apoptosis of infected cells. One study showed that primary human macrophages infected with *Mtb* had reduced surface expression of Fas when compared to uninfected cells indicating that *Mtb* has the ability to modulate this receptor to reduce apoptotic killing mediated by FasL (95). In a study with human AMs, microarrays were used to compare the expression profile between macrophages infected with attenuated H37Ra and virulent H37Rv. The data revealed that in H37Rv-infected macrophages, several proapoptotic genes were downregulated and there was an increase in the expression of antiapoptotic gene Bcl-w compared to uninfected and H37Ra-infected macrophages. Infection with H37Ra showed a profile that favored apoptosis. This study revealed that virulent *Mtb* interferes with signals downstream of TNFR1signaling to inhibit TNF-α dependent apoptosis (96). In another

study that used human AMs, virulent *Mtb* blocked TNF-α dependent apoptosis by inactivating TNF-α. While both H37Ra- and H37Rv-infected macrophages produced comparable levels TNF-α, only virulent H37Rv was able to induce the production of IL-10 which led to the release of soluble TNFR2, thus binding to TNF-α and neutralizing the effects of the cytokine and preventing TNF-α mediated apoptosis (97).

In several studies that compared the effects of two mycobacterial strains, one attenuated and one virulent, H37Ra and H37Rv, respectively, the results consistently revealed that attenuated H37Ra induced apoptosis where virulent H37Rv promoted necrosis. Gan et al. showed the outcome of cell death from macrophages infected with H37Ra and H37Rv. In H37Ra-infected macrophages, the development of complete and stable apoptotic envelopes were formed by the translocation and exposure of phosphatidyl serine (PS) followed by annexin-1 which allowed for the crosslinking of annexin-1 by tissue transglutaminase thus stabilizing the membrane. In macrophages infected with H37Rv, the formation of apoptotic envelopes was blocked by an accumulation of proteolytically cleaved annexin-1. This event promoted plasma membrane disruption which led to necrosis. In both *in vitro* and *in vivo* experiments the virulent strain caused more necrosis where the attenuated strain caused apoptosis (90). Park et al. examined 4 clinical isolates of *Mtb* ranging in virulence. BMDM were challenged at low MOI of 5 and cultured for up to six days to allow for bacterial expansion. More virulent strains had faster growth rates with higher CFU and more bacilli per macrophage. More virulent strains also caused a higher percent of cell death and upon inspection with electron microscopy, infected cells died from necrosis. (93)

Damage to the mitochondria can lead to apoptosis or necrosis depending on the type of injury. Chen et al. showed that human monocyte-derived macrophages infected with attenuated H37Ra or H37Rv induced MOMP which led to the release of cytochrome c, two critical events upstream of intrinsic apoptosis. However, when comparing the apoptotic markers, PS and annexin-1, H37Ra-infected macrophages had significantly more cells with these markers than H37Rv-infected macrophages. Macrophages infected with H37Rv induced irreversible mitochondrial permeability transition (MPT) permitting the dissipation of the mitochondrial transmembrane potential which led to necrosis (91). Electron microscopic examination of infected cells showed H37Ra-infected macrophages had intact plasma membrane and condensed nuclei, two morphological features of apoptosis; whereas H37Rv-infected cells had complete destruction of the plasma membrane, indicative of necrotic cell death (91).

Studies have shown that *Mtb* can manipulate the host eicosanoid pathway and direct whether infected macrophages die a necrotic or apoptotic cell death by interfering with the repair mechanism of the plasma membrane or mitochondrial membrane (94, 98). Eicosanoids, products of arachidonic acid, have been associated with cell death and have roles in both anti- and proinflammatory responses. By tipping the balance one way or the other, two eicosanoids, prostaglandin E_2 (PGE_2) and lipoxin A_4 (LXA_4), determine the fate of the cell. Attenuated strains of *Mtb*, like H37Ra and BCG, activate the synthesis of PGE_2 and are weak inducers of LXA_4 production. In stark contrast, virulent strains of *Mtb*, like H37Rv or Erdman, are weak inducers of PGE_2 and strong at inducing the production of LXA_4 (99). Cyclooxygenase 2 (COX2) is an enzyme involved in the

biosynthesis of PGE_2. LXA_4 inhibits COX2 activity by blocking COX2 mRNA buildup, thus shutting down PGE_2 synthesis. In contrast, PGE_2 inhibits the production of LXA_4. Consequently, when there are high levels of LXA_4 there are inherently low levels of PGE_2 and vice versa (99). One of the protective effects of PGE_2, through its receptor EP2, is its suppression of mitochondrial inner membrane perturbation. Without PGE_2, MPT induced by H37Rv infection leads to necrosis (98). PGE_2 also protects the plasma membrane. Infection from *Mtb* produces small lesions in the plasma membrane of infected macrophages. Membrane lesions are repaired through the utilization, in part, by lysosomal trafficking and exocytosis. PGE_2 promotes lysosomal-dependent repair of plasma membrane which prevents necrosis (94). Thus, virulent *Mtb* facilitates low levels of PGE_2 by inducing LXA_4 which compromises the integrity of both the mitochondrial membrane and the plasma membrane leading to necrosis.

In vivo studies paralleled the protective versus detrimental effect in the balance between PGE_2 and LXA_4. In mice that are unable to produce LXA_4, 5-lipoxygenase knockout (*5 -lo*$^{-/-}$) mice, aerosol infection with virulent *Mtb* extended their survival time over WT mice and had less bacterial burden, less lung inflammation and higher expression levels of IL-12, IFN-γ and NOS2 mRNA (100). Furthermore, mice deficient in producing PGE, PGE synthase knockout ($PGES^{-/-}$) mice, died earlier than WT mice with significant increase in bacterial lung burden. WT mice infected with H37Ra resulted in more PGE_2 whereas virulent Erdman-infected mice had higher levels of LXA_4 (98). The role of lipoxin in *Mtb* infection was further supported by work in the zebrafish and *M. marinum* infection model as well as humans. Mutation in the locus that encodes

leukotriene A(4) hydrolases (*lta4h*) of the zebrafish led to an increase in lipoxin synthesis. These mutant zebrafish were hyper-susceptible to mycobacterial infection with increased bacterial burden and decreased TNF-α production. For humans, polymorphism in the *LTA4H* gene correlated to higher susceptibility to TB (101).

In a recent study investigating eicosanoids, Mayer-Barber et al. showed that during *Mtb* infection IL-1, interferon and the eicosanoid pathways are linked. Type I IFN promotes disease severity where PGE_2 and IL-1 counter its detrimental effects. Clinical data from two study cohorts revealed that there was a correlation between severity of disease, IL-1, type I IFN and eicosanoids in TB patients; disproportionately high type I IFN expression with or without decreased IL-1 responses in conjunction with decreased PGE_2/LXA_4 ratios were seen in patients with severe TB (102). Both *in vitro* and *in vivo* experiments revealed IL-1α or IL-1β can induce the production of PGE_2 and control bacterial replication during *Mtb* infection. Additionally, IL-1 and PGE_2 were found to inhibit type I IFN. In *Il1r*$^{-/-}$ mice infected with *Mtb*, there were elevated levels of IFN-β. The addition of exogenous IL-1α or IL-1β to *Mtb*-infected macrophages blocked IFN-β production and the addition of exogenous PGE_2 to infected macrophages curbed type I IFN production (102). Administering PGE_2 with a 5-LO inhibitor reduced lung bacterial burden, lessened lung pathology and extended the survival time of *Il1a,Il1b*$^{-/-}$ mice infected with *Mtb*. The therapeutic benefits of PGE_2 treatment of infected mice were directed towards disease exacerbation induced by type I IFN. Treating *Ifng*$^{-/-}$ or *Tnfa*$^{-/-}$ mice had zero effect on their survival indicating the treatment was exclusive to IL-1 mediated defense (102).

1.6.3 High MOI Cell Death

When lytic viruses complete its replication cycles and reach a "burst size" in the hijacked cell, it induces cytolysis to exit the cell. Comparable to lytic viruses, our lab demonstrated that *Mtb* is also capable of inducing cytolysis in the macrophage when the intracellular bacillary load reaches a threshold value. When BMDMs were challenged with virulent *Mtb* Erdman at MOI $\geq$ 25, they rapidly succumbed to cytolysis, death ensuing as early as 3 hours p.i. (103). This type of cell death was uniquely independent of conventional apoptosis and necrosis because it displayed characteristics of both death modalities. Macrophages that undergo high MOI cell death initially exhibited nuclear condensation and PS translocation, characteristic behavior of cells undergoing apoptosis, but quickly transitioned to necrosis with massive cell-wide membrane damage along with the disintegration of the plasma membrane (103). This necrotic cell death was also independent of TNF-α and caspases but was partially dependent on lysosomal proteases. The attenuated BCG also exhibited cytolytic ability at MOI 25 suggesting that high MOI cell death is also independent of the cytolytic capacity of ESAT-6. Unlike the antimycobacterial outcome of apoptosis, high MOI cell death did not reduce mycobacterial viability (103).

A successive study further investigated the mechanism behind high MOI cell death induced by *Mtb*. It was determined that necrosis was initiated by LMP. The injury to the lysosome released hydrolases that propagated damage to the outer and inner mitochondrial membrane resulting in loss of membrane potential. The mitochondrial injury was independent of Bax and Bak and MPT was not responsible for the loss of

membrane potential (104). SEM images of infected BMDM displayed massive membrane damage with exiting bacilli. Although LMP occurred, cell death was independent of cathepsins B, L and D thus the traditional lysosomal cell death was ruled out. Additionally caspse-1 was not involved which precluded pyroptosis and pyronecrosis. Examination of the lipid profile from dead cells revealed a significant reduction in certain phospholipids suggesting the work of lysosomal lipases. Infection with RD1/*espA* deletion mutants determined LMP, mitochondrial injury or cytolysis was not the work of ESAT-6. The mycobacterial PhoPR two-component system regulates mycobacterial gene expressions upon phagocytosis and its deletion reveals attenuated phenotype *in vivo* similar to RD1 deletion mutant. Infection with *phoPR* deletion mutant yielded significantly reduced LMP, mitochondrial injury and cell death indicating that one or more mycobacteria genes regulated by PhoPR were contributing to high MOI cell death (104).

The high MOI macrophage infection model bypasses the natural progression of *Mtb* growth within the macrophage and allows one to directly examine the outcome of infected macrophages with high intracellular bacillary loads. This model also allows one to dissect the cytolytic ability of mycobacterial strain versus its ability to infect a cell at a low MOI and survive long enough to expand its growth to a lethal point. A study by Park et al. (93) challenged BMDM with MOI 5 with a variety of *Mtb* strains and cultured them for 6 days. The strains that grew the quickest killed the host cell when bacterial load reached a threshold that was cytotoxic. From their data, that threshold was approximately 20 to 30 intracellular bacilli per macrophage, a value similar to our cytotoxic threshold

dose of MOI 25. Treating cells with IFN-γ protected the cells and inhibited bacterial replication indicating that the cytotoxicity was based on intracellular bacterial burden and not a trait of some virulent *Mtb* strains.

This study correlated high intracellular bacterial burden of macrophages with cytolytic activity of *Mtb*. The results from our studies and others suggest that virulent *Mtb* suppresses apoptosis and expands its growth until an intracellular threshold value, or a burst size, is reached upon which the replication niche becomes obsolete. Subsequently *Mtb* triggers a necrotic cell death to free itself from the confines of the intracellular domain. This mechanism serves as the exit strategy for the pathogen. Release into the extracellular space serves as the platform for new rounds of invasion into naïve phagocytic cells, replication and escape, propagating dissemination and spread of infection.

Although the cellular events in the mechanism of high MOI cell death were thoroughly investigated, that work and studies from others have focused on *in vitro* experiments. Therefore, we proposed the following burst size hypothesis as a model of the events that occur *in vivo* during *Mtb* infection (Fig. 1.1). The work presented in this dissertation investigates the relevance and the significance of necrotic cell death during the course of TB disease by using the murine low dose aerosol infection model for tuberculosis. Do the *in vitro* results of *Mtb*-infected macrophages translate to the cell fate of monocytic cells in the lungs? What is the pathological consequence of necrotic cell death to the host? The research presented in the following two chapters will answer these questions and enlighten this field of study to better understand the host-pathogen

interaction of TB in context of cell death and contribute to research toward improved therapies.

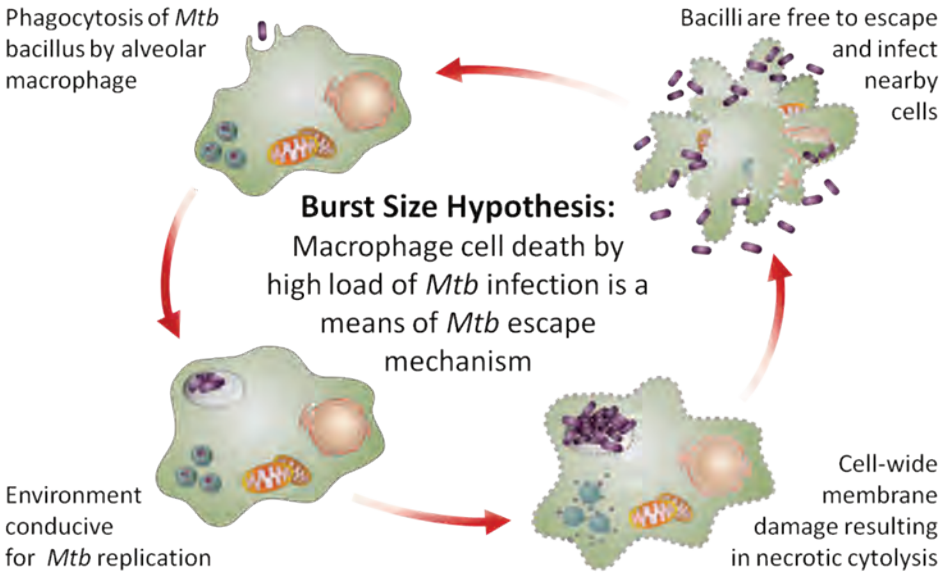

Figure 1.1. Burst size hypothesis model. Upon inhalation of an infectious droplet, *Mtb* is encountered by a small group of resident alveolar macrophages in the lungs. The macrophage engulfs the pathogen and initiates its killing program. However, *Mtb* countermeasures the host's defense mechanism and modulates the phagosome to hospitable conditions, allowing for replication to occur. Starting initially from a very small number of bacilli, once *Mtb* expansion reaches a burst size, cytolysis is triggered. The lysosome is damaged, followed by severe mitochondrial injury along with disintegration of the nuclear and plasma membrane. The cell lyses open spilling the intracellular content into the extracellular space. The liberated bacilli are free to invade neighboring cells, and repeat the cycle of invasion, replication and escape thus propagating the spread of infection.

Preface to Chapter II

A modified version of this chapter has been published.

Teresa Repasy[1], Jinhee Lee[1], Simeone Marino[2], Nuria Martinez[1], Denise E. Kirschner[2], Gregory Hendricks[3], Stephen Baker [4], Andrew A. Wilson[5], Darrell N. Kotton[5], Hardy Kornfeld[1*] (2013) *Intracellular bacillary burden reflects a burst size for Mycobacterium tuberculosis in vivo*. PLoS Pathog. 9(2): e1003190. doi:10.1371/journal.ppat.1003190

1 Department of Medicine, University of Massachusetts Medical School, Worcester, Massachusetts, United States of America

2 Department of Microbiology and Immunology, University of Michigan Medical School, Ann Arbor, Michigan, United States of America

3 Department of Cell Biology, University of Massachusetts Medical School, Worcester, Massachusetts, United States of America

4 Department of Quantitative Health Science, University of Massachusetts Medical School, Worcester, Massachusetts, United States of America

5 Pulmonary Center, Boston University School of Medicine, Boston, Massachusetts, United States of America

J.L. performed experiments for Fig. 2.1.
S.M. and D.E.K. performed the experiment for Fig. 2.14.
N.M. provided confocal images for Fig. 2.13B and C.
G.H. provided scanning electron micrographs for Fig. 2.10B & Fig. 2.13A.
S.B. performed the statistical analysis.
A.A.W. and D.N.K. provided the lentivirus for Fig. 2.1C.
T.R. performed all other experiments.
T.R. and H.K. prepared the manuscript.

CHAPTER II: Intracellular Bacillary Burden Reflects a Burst Size for *Mycobacterium tuberculosis In Vivo*

2.1 Abstract

We previously reported that *Mycobacterium tuberculosis* triggers macrophage necrosis *in vitro* at a threshold intracellular load of ~25 bacilli. This suggests a model for tuberculosis where bacilli invading lung macrophages at low multiplicity of infection proliferate to burst size and spread to naïve phagocytes for repeated cycles of replication and cytolysis. The current study evaluated that model *in vivo*, an environment significantly more complex than *in vitro* culture. In the lungs of mice infected with *M. tuberculosis* by aerosol we observed three distinct mononuclear leukocyte populations (alveolar macrophages, myeloid dendritic cells and recruited monocytes/macrophages) and neutrophils hosting bacilli. Four weeks after aerosol challenge, myeloid dendritic cells and neutrophils were the predominant hosts for *M. tuberculosis* while recruited monocytes/macrophages assumed that role by 10 weeks. Alveolar macrophages were a minority infected cell type at both time points. The burst size model predicts that individual lung phagocytes would harbor a range of bacillary loads with most containing few bacilli, a smaller proportion containing many bacilli, and few or none exceeding a burst size load. Bacterial load per cell was enumerated in lung monocytic cells and neutrophils at time points after aerosol challenge of wild type and interferon-γ null mice. The resulting data fulfilled those predictions, suggesting a median *in vivo* burst size in the

range of 20 to 40 bacilli for monocytic cells. Most heavily burdened monocytic cells were nonviable, with morphological features similar to those observed after high multiplicity challenge *in vitro*: nuclear condensation without fragmentation and disintegration of cell membranes without apoptotic vesicle formation. Neutrophils had a narrow range and lower peak bacillary burden than monocytic cells and some exhibited cell death with release of extracellular neutrophil traps. Our studies suggest that burst size cytolysis is a major cause of infection-induced mononuclear cell death in tuberculosis.

2.2 Introduction

Natural infection with *Mycobacterium tuberculosis* (*Mtb*) occurs by inhalation, followed by invasion of resident alveolar macrophages that provide the major initial replication niche for the pathogen. Macrophages infected with *Mtb in vitro* may die with primarily apoptotic or necrotic features (105); the cell death mode most relevant to TB disease *in vivo* remains undefined. A widely held paradigm is that macrophage apoptosis promotes host defense in TB while necrosis favors spreading infection. We previously reported that the cytolytic activity of *Mtb* correlates with intracellular bacillary burden in macrophages, increasing dramatically at a threshold load of ~25 bacilli per macrophage (103). At high intracellular burden, *Mtb* triggers a primarily necrotic death dependent on bacterial genes regulated by the PhoPR 2-component system (104). Our *in vitro* studies and data from other groups suggest that virulent *Mtb* strains suppress apoptosis of host macrophages (79, 82, 83, 92, 96) and grow to a threshold burden (93, 103) whereupon necrosis is triggered as an exit mechanism analogous to the burst size of lytic viruses.

In the present study, we investigated whether the necrotic death described for *Mtb*-infected macrophages *in vitro* is relevant to the fate of monocytic cells in the lung that become infected during the course of TB disease *in vivo*. Inhalation of *Mtb* is followed by the invasion of a small number of resident alveolar macrophages. We posit that within each infected macrophage, bacterial replication expands an initial low multiplicity of infection (MOI) to a burst size value. Once this threshold is exceeded, the liberated bacilli spread to naïve phagocytes. Successive rounds of invasion, replication and escape will result in a distribution of bacillary loads across the population of infected phagocytes. This model predicts that at any given time point after low dose aerosol challenge, phagocytes harboring 1-10 bacilli will outnumber those with higher bacillary loads, and that host cells containing $\geq$ 25 bacilli will be a distinct minority of infected cells. The model also predicts that with the induction of adaptive immunity (~3 weeks after aerosol challenge), inhibition of *Mtb* replication will rescue many infected cells with a low bacillary burden from progressing to burst size. This will increase the proportion of cells containing 1-10 bacilli while heavily infected cells will die and be replaced at a low rate thereby reducing the proportion of cells containing ≥ 25 bacilli.

To test those predictions we enumerated acid fast bacilli (AFB) per cell in whole lung leukocytes and bronchoalveolar lavage (BAL) cells harvested from mice after low dose aerosol infection with *Mtb* Erdman. The distribution of AFB burden in monocytic cells harvested from wild type (WT) C57BL/6 mice followed the predicted pattern. Analysis of interferon-γ knockout (GKO) mice with TB also conformed to the predicted effects of unrestricted *Mtb* replication on the distribution of bacillary loads per cell. The

morphology of heavily infected monocytic cells isolated from the lungs of mice with TB exhibited features similar to those seen after high MOI challenge *in vitro*: nuclear condensation without fragmentation and loss of cell membrane integrity without cell swelling or apoptotic vesicle formation. Taken together, these results support the burst size hypothesis for TB *in vivo*.

During the course of these experiments it became apparent that the diversity of cell types hosting *Mtb in vivo* adds an additional layer of complexity to TB pathogenesis. Neutrophils were major *Mtb* host cells 2-3 weeks post infection (p.i.) but rarely contained >10 AFB per cell. We also observed differences in the distribution of *Mtb* between three subpopulations of mononuclear leukocytes classified by CD11b and CD11c expression. The proportion of infected host cells differed between these subpopulations, and the proportions changed dynamically between 4 and 10 weeks p.i. The relative permissiveness or restriction of intracellular *Mtb* replication as well as the regulation of host cell fate may differ for each of these phagocytic cell types with implications for host defense, immune pathology and latent TB infection.

2.3 Materials and Methods

Ethics statement. Experiments with animals were conducted according to the National Institutes of Health guidelines for housing and care of laboratory animals and performed under protocols approved by the Institutional Animal Care and Use Committee and the Institutional Biosafety Committee at The University of Massachusetts Medical School (UMMS).

Mice. C57BL/6 WT, IFN-$\gamma^{-/-}$ (B6.129S7-Ifng^{tm1Ts}/J) knockout mice (#2287), and ApoE$^{-/-}$ were purchased from The Jackson Laboratory. Mice were housed in specific pathogen-free environment at Animal Medicine facility of UMMS.

Bacterial strain and *Mtb* infection. *Mtb* Erdman was used for *in vitro* and aerosol infections. Bacterial stocks for experiments were prepared as described previously (104). For *in vitro* infections, BMDM were generated as previously described (103) and plated in Lab-Tek tissue culture chamber slides (Nalge Nunc International) at a density of 2 x 10^5 cells per well, or in 24-well cell culture plates at 5 x 10^5 cells per well in complete DMEM. Cells were infected with *Mtb* Erdman (MOI 25, 3 h, 37°C), washed with PBS and then overlaid with fresh complete DMEM. For aerosol infections, mice were exposed to *Mtb* in a Glas-Col Inhalation Exposure System set to deliver ~100 CFU or ~300 CFU to the lung. For each experiment, 2 mice were sacrificed 24 hours p.i. to verify the delivered dose as described.

Cell preparation. Lung leukocytes were isolated as previously described (106). Briefly, mice were sacrificed and lungs were perfused through the heart with PBS. Excised lungs were minced and digested with 150 U/ml collagenase IV and 60 U/ml DNase (Sigma-Aldrich; 45 min, 37°C). Processed tissues were filtered using a 40 µm cell strainer and treated with Gey's Solution (Sigma-Aldrich). BAL cells were collected by flushing lungs three times with 0.75 ml PBS containing 0.2% BSA and 0.2 mM EGTA, and added to1.0 ml of 20% FBS in PBS and placed immediately on ice. BAL fluid was washed in PBS and treated with Gey's Solution. Whole lung leukocytes and BAL cells prepared in this manner were fixed in 1.5% paraformaldehyde for overnight at 4°C. Fixed

cell suspensions were washed, re-suspended in PBS and stored in 4°C. Cell counts were determined using a hemocytometer.

Intracellular bacterial enumeration. BAL cells and lung leukocytes were harvested from *Mtb* infected mice at predetermined time points. Slides were prepared using cytocentrifugation to immobilize 1×10^5 cells per slide (Thermo Electron Corporation). Cytospin slides were heat-fixed for Ziehl-Neelsen staining kit (TB Stain Kit ZN, BD Diagnostic Systems) following manufacturer's protocol. Stained slides were visualized using a Nikon Eclipse E400 Microscope and photomicrographs were obtained with a Nikon DS-Ri1 camera using NIS-Elements Microscope Imaging Software. Individual cells were interrogated for intracellular bacteria by counting AFB encased or surrounded by cellular membrane. Accurately counting intracellular AFB was reliable at low bacillary burden but became progressive more difficult in high burden cells with clumped bacilli. AFB counts were grouped into five bins: 1-5, 6-10, 11-15, 16-20, and ≥ 21. Cells were identified as monocytic cells (comprising AM, RM, mDC) or neutrophils based on nuclear morphology. AFB counts were tallied separately for these two categories.

Acid-fast, DAPI and immunostaining. To examine the nuclear morphology, cytospin slides were heat fixed and submerged in TB Carbolfuchsin ZN (BD Diagnostic Systems). Slides were heated in microwave oven for two consecutive intervals of 15 sec separated by 2 min at room temperature and then gently rinsed under running distilled water and decolorized with TB Decolorizer (BD Diagnostic Systems). Slides were rinsed again and then stained with 0.5 g/ml of 4',6'-diamidino-2-phenylindole, dihydrochloride

(DAPI) staining for 2 min. After a final rinse, slides were dried and cover slips mounted with ProLong Gold Antifade reagent (Invitrogen).

For immunostaining, BAL cells were affixed to Cell-Tak (BD Biosciences) treated cytospin slides and blocked with 3% BSA and 10% goat serum in PBS. Cells were stained with primary antibodies, 1:50 myeloperoxidase (LS Bio) and 1:50 histone H2B (Santa Cruz Biotechnology) or 1:50 neutrophil elastase (Calbiochem). Fluorescent anti-rabbit antibodies conjugated to Alexa Fluor 488, 568, 594 or 647 (Invitrogen) were used as secondary antibodies. Cells were mounted and stained with DAPI with Prolong Gold Antifade Reagent with DAPI (Invitrogen). Analysis of immunostained cells were performed with confocal scanning laser microscopy (SP2 AOBS Leica) and images were captured using LCS software.

Flow cytometry and analysis of lung cell population. BAL cells and lung leukocytes were washed and incubated with CD16/CD32 mAb (BD Biosciences) to block Fc binding. Cells were then stained with the following mAb purchased from eBioscience (San Diego, CA): eFluor450–anti-CD11b (M1/70); phycoerythrin–anti-CD11c (N418); allophycocyanin–anti-CD45 (30-F11); APC-eFluor780-anti-Ly-6G (RB6-8C5); and Live/Dead Fixable Dead Cell Stain Kit by Invitrogen. An LSRII flow cytometer (BD Biosciences) was used for acquisition and data were analyzed with FlowJo software (TreeStar). Unless otherwise stated, gating was set to exclude dead cells and lymphocyte populations in forward/side scatter graph and to include singlet cells in a dot plot of pulse area against pulse height. Gating on viable cells, we defined resident AM as $CD11b^{-}$ $CD11c^{+/hi}$ cells, RM as $CD11b^{+/lo}$ $CD11c^{lo/-}$ and mDC as $CD11b^{+/hi}$ $CD11c^{+/hi}$. Cells were

sorted utilizing BD FACSAria Cell Sorter (BD Biosciences) with the same gating strategies used for flow cytometry. Subsets of sorted cell populations were collected and affixed onto cytospin slides for Ziehl-Neelsen staining and enumeration of intracellular AFB by light microscopy.

GFP Labeling of Resident Alveolar Macrophages. A replication incompetent, VSVG-pseudotyped, lentivirus expressing GFP under the control of a CMV promoter (CMV-GFP-W) was used to transduce resident lung leukocytes. The vector was created using a 5-plasmid transfection method previously described (107, 108). Briefly, 293T cells were transfected with the pHAGE backbone lentiviral vector together with 4 expression vectors encoding the packaging proteins Gag-Pol, Rev, Tat, and the G protein of the vesicular stomatitis virus (VSV-G). To transduce lung cells, the viral titer was adjusted to 5×10^9/ml in DMEM with 10% FBS and mixed with lipofectamine 2000 (Invitrogen) at a ratio of 100:5 (v:v) on ice for 15-30 min. Mice were then infected by tracheal instillation of 5×10^7 virions in a volume of 50 ul.

Scanning electron microscopy. Samples of non-adherent cells infected with *Mtb* were processed by first preparing microscope slides with Cell-Tak (BD Biosciences). Cell suspensions were added to treated and dried slides by cytocentrifugation and allowed to bond to the Cell-Tak. The cells on the slides were fixed by immersion in 2% paraformaldehyde (v/v) / 2.5% glutaraldehyde (v/v) in 0.1 M Na cacodylate-HCl buffer (pH 7.2) overnight at 4°C. The next day the fixed samples were washed three times in 0.5 M Na cacodylate-HCl buffer (pH 7.0) and then post-fixed for 1 hr in 1% osmium tetroxide (w/v) in the same buffer. Following post-fixation, samples were dehydrated

through a graded series of ethanol to two changes of 100% ethanol and critical point dried in liquid CO_2. The microscope slides were cut to remove the excess glass, mounted onto aluminum stubs with silver conductive paste and then coated with carbon (1 nm) and then sputter coated with gold/palladium (4 nm). Specimens were then examined using an FEI Quanta 200 FEG MK II scanning electron microscope.

Computational model of TB infection in the lung. A 2-dimensional (2D) agent-based model (ABM) framework developed (109-111) for spatially characterizing the mechanisms of immunity in the lung during TB infection was used to test the burst size concept. The virtual environment reflects a 2 mm x 2 mm section of lung parenchyma represented as a 100 x 100 2D grid with micro-compartments scaled to the approximate size of a macrophage (~20 μm). A virtual low dose infection is triggered by one infected macrophage (M_I), with one intracellular *Mtb*. The ABM describes interactions between intracellular and extracellular *Mtb*, various states of macrophages (resting, infected, chronically infected and activated), T cell populations including $CD4^+$, $CD8^+$ and regulatory T cells along with major cytokines tumor necrosis factor-α and IFN-γ and chemokine effector molecules (e.g., CCL2, CCL5, CXCL9/10/11). Each immune cell's behavior adapts based on its environment and its interactions with other immune cells and *Mtb*. As infection progresses, *Mtb* is tracked continuously. Extracellular *Mtb* proliferation follows a logistic growth function (48 h doubling time) within a single micro-compartment with a given carrying capacity while intracellular *Mtb* follows an exponential growth curve with a doubling time of 24 h. Intracellular *Mtb* doubling time is set to 72 h after adaptive immunity appears at the infection site (i.e., 20 days p.i.).With

the current mechanisms already present in our model that can affect *Mtb* levels, we captured the process of burst size cytolysis by setting a maximum carrying capacity for a chronically infected macrophage. If the intracellular bacterial load exceeds this threshold, the macrophage bursts releasing viable bacteria into the extracellular space. The model allows a user defined parameter value for this threshold, labeled as *burst size*. For this study, we varied the burst sizes from 10 to 50 while maintaining fixed values for the remaining parameters to analyze affects of different burst sizes on the total lung bacterial burden.

Uncertainty and sensitivity analysis (U/SA) (112) has been used in this model to ensure that the selected parameter values influencing outcomes of infection (e.g. clearance, containment or dissemination) are in accordance with known dynamics. The results of U/SA analysis provide constructive evaluation of the critical processes and mechanisms suggesting strategies for model reduction, questions requiring additional *in vivo* experimentation, and to generate alternative hypotheses if burst size is not supported by model results (113).

Statistical Analysis. Unless otherwise stated, data from independent experiments are shown as mean ± SD or SEM. Comparisons between groups were evaluated with Student *t*-test using GraphPad Prism. Differences in the distribution of AFB load in frequency bins obtained from experiments with GKO and WT mice evaluated using analysis of variance for mixed model (114) with Restricted Maximum Likelihood (REML) algorithm (115) for fitting the model. Load data were transformed using natural logarithms to better approximate normally distributed errors, an assumption of the mixed model ANOVA.

The distributional characteristics of the data were evaluated using the Kolmogorov-Smirnov goodness of fit test (116) upon model residuals. A p value < 0.05 was regarded as statistically significant.

In the computational model, standard unidirectional *t*-test, with heteroscedasticity assumption (i.e., different variability between groups) was used to test statistically significant differences ($p<0.05$) between time course predictions with different burst sizes at different time points.

2.4 Results

Dynamic shifts of monocytic cells hosting *Mtb* in evolving pulmonary TB. Alveolar macrophages are the overwhelming majority of leukocytes in the normal alveolar space and they are considered the primary leukocyte type initially infected by inhaled *Mtb in vivo*. Any investigation of the burst size hypothesis for TB must consider the complexity of the *in vivo* environment and the potential for *Mtb* to invade a diverse spectrum of phagocytic cells in the lung (117, 118). To study the distribution of *Mtb* within subpopulations of monocytic cells, we harvested lungs of WT mice 4 and 10 weeks after aerosol challenge with *Mtb* Erdman. Whole lung $CD45^+$ leukocytes were sorted on the basis of CD11b and CD11c expression. Previous reports have extensively characterized subpopulations of leukocytes in lung tissues of mice with TB (118-125). In accordance with those studies, we classified alveolar macrophages (AM) as $CD11b^-$ $CD11c^{+/hi}$, recruited monocyte/macrophages (RM) as $CD11b^{+/lo}$ $CD11c^{lo/-}$ and myeloid dendritic cells (mDC) as $CD11b^{+/hi}$ $CD11c^{+/hi}$. For clarity we refer to AM, RM and mDC populations in this report based on CD11b and CD11c expression, recognizing that this

might not invariably correspond to functional identity. We evaluated additional cell surface markers including Ly-6G, CD115, F4/80 and MHC class II (not shown) but these provided no additional useful discriminatory information. Uninfected mice were sampled for comparison to the TB group at both time points (Table 2.1).

Mononuclear cells from uninfected lungs comprised a roughly equal proportion of AM and RM, with mDC a distinct minority at 1.6% (Fig. 2.1A). By 4 weeks p.i., the total number of mDC increased > 40-fold and they expanded proportionately from 1.6% to 18.5% of monocytic cells. The distribution of monocytic cells changed slightly at 10 weeks p.i., with a moderate expansion of RM and modest contraction of the AM and mDC populations. *Mtb*-infected monocytic cells were enumerated by microscopy on cytospin slides with Ziehl-Neelsen staining (Table 2.2). After 4 weeks of TB disease, mDC were the predominant *Mtb*-infected cell type, representing 78.2% of total AFB^+ monocytic cells (Fig. 2.1B). By 10 weeks p.i., the distribution of infected cells shifted, with RM becoming the primary *Mtb* host cells (60.4%), followed by mDC (31.2%). At both time points, AM represented approximately 10% of AFB^+ monocytic cells. The relative propensity for different mononuclear leukocyte cell types to harbor *Mtb* was estimated based their representation in the total and AFB^+ cells within the total population. On that basis, mDC were 13 and 18 times more likely to be infected with *Mtb* compared to AM or RM, respectively, at 4 weeks p.i.

Resident alveolar macrophages are a minor niche for *Mtb* replication. Resident AMs, by far the predominant leukocytes in the airspace of normal lungs, are the first phagocytes to become infected by *Mtb* following inhalation of droplet nuclei. In the

absence of infection or inflammation they are extremely long-lived, non-replicating cells with negligible replacement by bone marrow-derived leukocytes (107, 126). To investigate the impact of pulmonary TB on resident AM, we labeled these cells by tracheal instillation of a replication incompetent, VSVG-pseudotyped, GFP-expressing lentivirus (CMV-GFP-W) as previously described (107). Labeling efficiency is typically 30-40% of BAL cells, with no transduction of epithelial cells or parenchymal leukocytes. After an early loss of transduced cells in the first several weeks, the number of GFP^+ cells stabilizes at 20-30% of BAL cells for up to 2 years. To track the fate of resident AM in TB, mice were transduced with intratracheal CMV-GFP-W and rested for 8 weeks to allow the GFP^+ cell population to stabilize. One group of transduced mice was then infected with *Mtb* Erdman by aerosol while control transduced mice remained uninfected. Sets of *Mtb*-infected and control mice were sacrificed 4 weeks and 10 weeks after infection of the TB group and whole lung leukocytes were isolated for analysis by flow cytometry (Fig. 2.1C).

In uninfected mice, GFP^+ leukocytes comprised 97% AM, 2.8% mDC and < 0.3% RM or other cells (Table 2.3) reflecting the typical composition of leukocytes in airspace under basal conditions. After 4 weeks of TB disease, the total number of GFP^+ cells was little changed from baseline but the proportion AM among all GFP^+ cells fell to 68% while mDC increased to 27% of GFP^+ cells. Thus, ~22% of AM shifted their surface phenotype to one resembling mDC. Whether this represents induction of CD11b surface expression on cells that retain AM properties, or if these cells convert into functional mDC remains to be determined. The phenotypic shift of resident AM contributed only

~3% of the total increase in lung mDC at 4 weeks p.i., indicating increased mDC population mostly resulted from differentiation of monocytic cells newly recruited to the lung. Comparison of total GFP^+ cells counts between groups was limited by variation in labeling efficiency but the data suggest a trend after 10 weeks of TB for a modest loss of AM that were resident in the lung prior to infection. We found no GFP^+ leukocytes containing AFB at 4 or 10 weeks p.i., suggesting little or no horizontal spread of infection through the resident AM population present in the lung prior to infection. Most if not all of the AM accounting for ~10% of *Mtb*-infected monocytic cells at 4 and 10 weeks p.i. (Fig. 2.1B) were recruited to the lung after infection. We conclude that resident AM may be critical host cells for intracellular infection by inhaled *Mtb*, but only for the first round of bacillary replication to burst size. Subsequently, the rapidly expanding number of bacilli shifts to phagocytes newly recruited to the lung, most of which do not differentiate into AM.

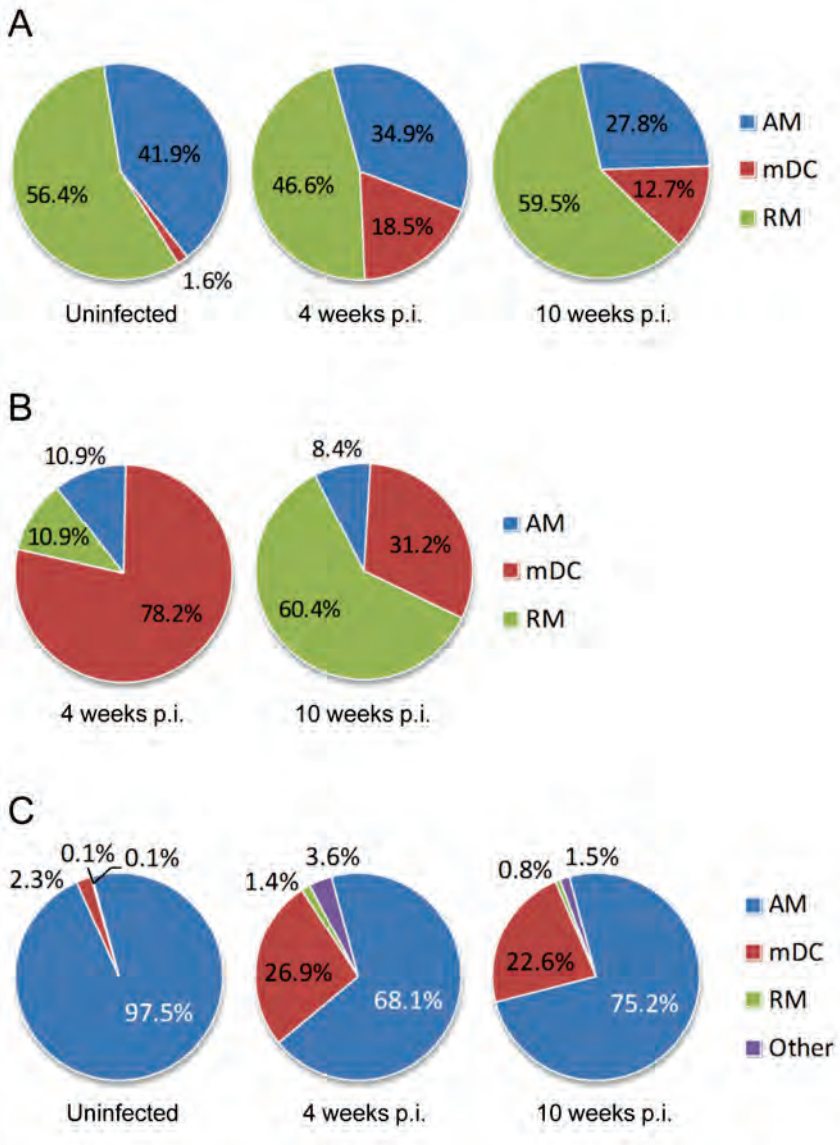

Figure 2.1. Distribution of *Mtb* infection within monocytic cell populations in the lung. Whole lung leukocytes were harvested from groups of mice with TB (4 and 10 weeks p.i.) and compared to uninfected controls. Monocytic cells were sorted into AM, RM and mDC as described in *Materials and Methods*. Ziehl-Neelsen staining was performed on cytospin preparations of sorted populations. (A) The proportion of AM, RM and mDC within the total lung monocytic cell population of uninfected mice and mice with pulmonary TB. (B) The proportion of AM, RM and mDC containing any AFB in mice with pulmonary TB. (C) The proportion of GFP-labeled lung leukocytes, GFP^+ AM, RM and mDC, in uninfected mice and mice with TB. Lung leukocytes within the airspace were transduced by tracheal instillation of WT mice with CMV-GFP-W. After 8 weeks, one group of GFP-transduced mice was challenged by aerosol with 300 CFU of *Mtb* Erdman delivered to the lung. The category *Other* comprised cells that could not be categorized as AM, RM or mDC based on light scatter characteristics and CD11b/CD11c staining. By light microscopy, cells in the *Other* category included a small number of neutrophils that may have acquired GFP by efferocytosis, as well of cells with monocytic appearance that had very high intracellular *Mtb* burden and features of cell death. Monocytic cell subsets were classified by surface immunostaining as alveolar macrophages (AM; $CD11b^-$ $CD11c^{+/hi}$), recruited monocyte/macrophages (RM; $CD11b^{+/lo}$ $CD11c^{lo/-}$) and myeloid dendritic cells (mDC; $CD11b^{+/hi}$ $CD11c^{+/hi}$).

Table 2.1. Percentage and total cell count of different cells from lung leukocytes.†

	Uninfected		4 weeks p.i.		Uninfected		10 weeks p.i.	
	Cells x 10^4	%	Cells x 10^4	%	Cells x 10^4	%	Cells x 10^4	%
AM	14.1 ± 3.4	41.9	47.8 ± 15.9*	34.9	16.6 ± 2.6	22.8	45.6 ± 9.4*	27.8
mDC	0.8 ± 0.4	1.6	25.3 ± 7.7*	18.5	0.4 ± 0.1	0.6	20.8 ± 6.8*	12.7
RM	15 ± 3.7	56.4	63.7 ± 5.8*	46.6	26.3 ± 6.5	36.2	97.5 ± 13.6*	59.5
Total	29.9		136.8		43.3		163.9	

†Results are presented as mean ± SD. *Indicates statistical significance.

Table 2.2. Distribution of AFB^+ cells for each cell type found in lung leukocytes.

	4 weeks p.i.				10 weeks p.i.			
	Cells x 10^4	%	AFB^+ cells	%	Cells x 10^4	%	AFB^+ cells	%
AM	47	23.5	0.02	10.9	45	19.9	0.1	8.4
mDC	25	12.5	0.14	78.2	20	8.8	0.37	31.2
RM	63	31.5	0.02	10.9	97	42.9	0.71	60.4
Total	135		0.71		162		1.46	

Table 2.3. Percentage and total cell count of different GFP^+ cells from lung leukocytes.†

	Uninfected		4 weeks p.i.		Uninfected		10 weeks p.i.	
	Cells x 10^4	%	Cells x 10^4	%	Cells x 10^4	%	Cells x 10^4	%
AM	3.5 ± 0.9	97	2.28 ± 1.4	68.1	4.1 ± 0.8	97.9	2 ± 0.6*	75.2
mDC	0.1 ± 0.1	2.8	0.9 ± 0.6*	26.9	0.08 ± 0.04	1.9	0.6 ± 0.08*	22.6
RM	0.003 ± 0.0	0.1	0.047 ± 0.0*	1.4	0.002 ± 0.0	0.05	0.02 ± 0.01*	0.8
Other	0.006 ± 0.0	0.2	0.12 ± 0.02*	3.6	0.005 ± 0.0	0.1	0.04 ± 0.02*	1.5
Total	3.7		3.3		4.2		2.6	

†Results are presented as mean ± SD. *Indicates statistical significance.

Enumeration of intracellular bacilli in pulmonary TB. To investigate the *in vivo* relevance of a burst size model for macrophage cell death in TB, we challenged C57BL/6 mice with virulent *Mtb* Erdman by aerosol set to deliver ~300 CFU to the lung. Lung cells were subsequently harvested in different sets of infected mice exclusively by BAL or by enzymatic digestion to isolate whole lung leukocytes. Cells were immobilized onto slides by cytocentrifugation and intracellular bacilli were visualized with Ziehl-Neelsen staining. The percent and total number of AFB^+ cells was enumerated at time points between 1 and 8 weeks p.i. In parallel with the characteristic kinetics of lung bacillary load in the aerosol TB model, the total number of AFB^+ cells increased logarithmically until reaching a plateau value between 2 and 3 weeks p.i. (Fig. 2.2A). When compared to whole lung leukocytes, the total number of AFB^+ BAL cells declined by 8 weeks p.i., likely reflecting a loss of airspace available to lavage. In contrast, the total number of AFB^+ lung leukocytes remained stable between 2 and 8 weeks p.i., reflecting the major site of TB disease more accurately than BAL at later time points. The proportion of BAL cells and lung leukocytes infected with *Mtb* peaked around 1.5% at 2 weeks p.i. and then declined, owing to the recruitment of naïve leukocytes to the infected lung (Fig. 2.2B). Light microscopy allowed reliable identification of neutrophils that were therefore counted separately from monocytic cells. Mononuclear leukocyte subsets, comprising AM, RM and mDC, are not visually distinguishable. AFB^+ neutrophils were not seen in BAL or lung leukocytes at 1 week p.i. but equaled monocytic cells as hosts for *Mtb* at weeks 2 and 3, the period of greatest bacillary expansion (Fig. 2.2C).

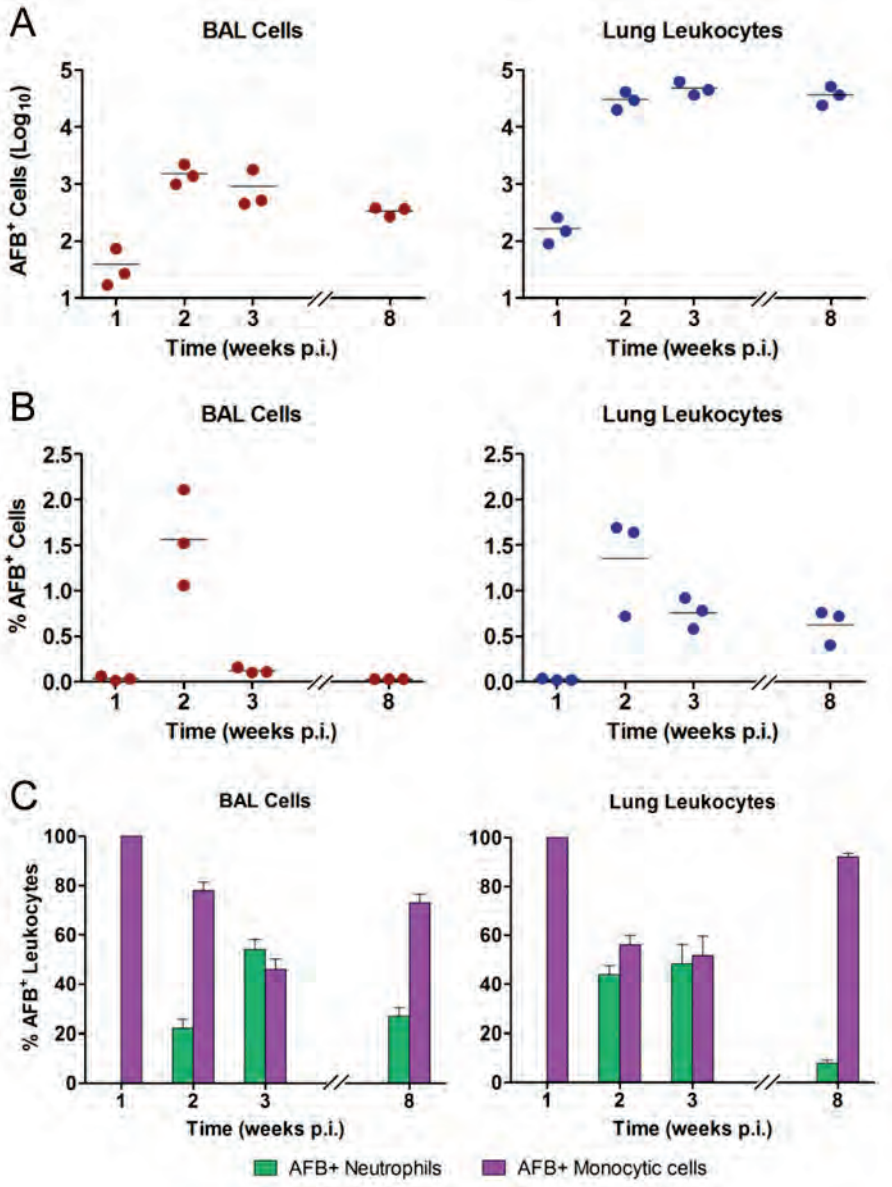

Figure 2.2. Kinetics of intracellular *Mtb* growth in vivo. BAL cells and whole lung leukocytes were harvested at 1, 2, 3 and 8 weeks after aerosol infection of mice with 300 CFU *Mtb* Erdman delivered to the lung. Cells from both sources were counted and cytospin preparations were made for Ziehl-Neelsen staining. (A) The total number of *Mtb*-infected (AFB^+) cells was derived by multiplying the % AFB^+ cells by the total number of cells in each sample. Results for individual mice are presented as $\log_{10}$ total AFB^+ cells, with the line representing the mean. (B) The proportion of *Mtb*-infected phagocytes within the total sample was counted at each time point and expressed as % AFB^+ cells. (C) Neutrophils infected with *Mtb* were identified by their typical nuclear morphology on Ziehl-Neelsen stained cytospin slides of BAL cells and whole lung leukocytes. The relative proportion of AFB in neutrophils versus monocytic phagocytes (AM, RM and mDC) is expressed as mean % AFB^+ leukocytes ± SD from one representative experiment. All in vivo experiments were repeated twice.

At each time point after aerosol challenge, AFB per neutrophil or monocytic cell was counted in individual cells. AFB counts were grouped into five bins (1-5, 6-10, 11-15, 16-20 and ≥ 21) with the top bin reflecting the highest burden that we could reliably count to ± 2 AFB (Fig. 2.3). Consistent with the distribution of intracellular bacillary loads predicted for a burst size model, the number of AFB^+ monocytic cells containing 1-5 AFB was greater than cells with higher bacillary loads at all time points (Fig. 2.4A).

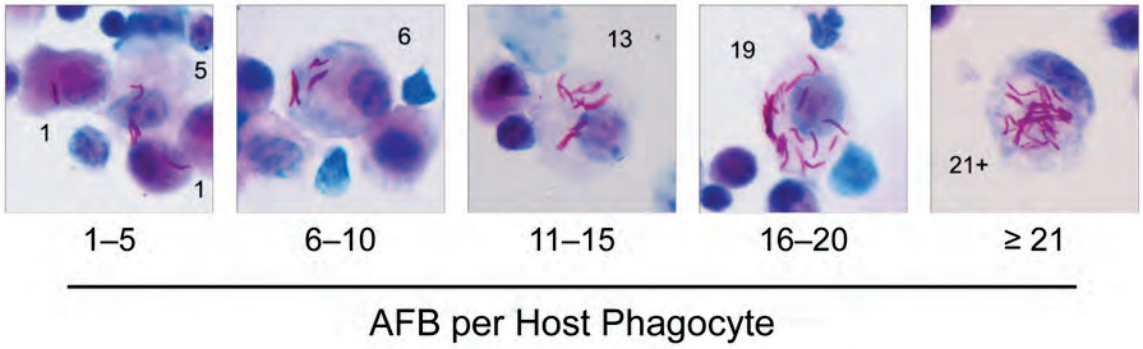

Figure 2.3. Enumeration of intracellular *Mtb* in lung phagocytes. BAL cells and whole lung leukocytes were isolated from C57BL/6 mice 2 weeks after aerosol challenge with *Mtb* Erdman. Ziehl-Neelsen stained cytospin preparations were used to visualize and count intracellular AFB by light microscopy. Representative photomicrographs show examples of infected cells along with AFB counts as indicated magnification, 400X).

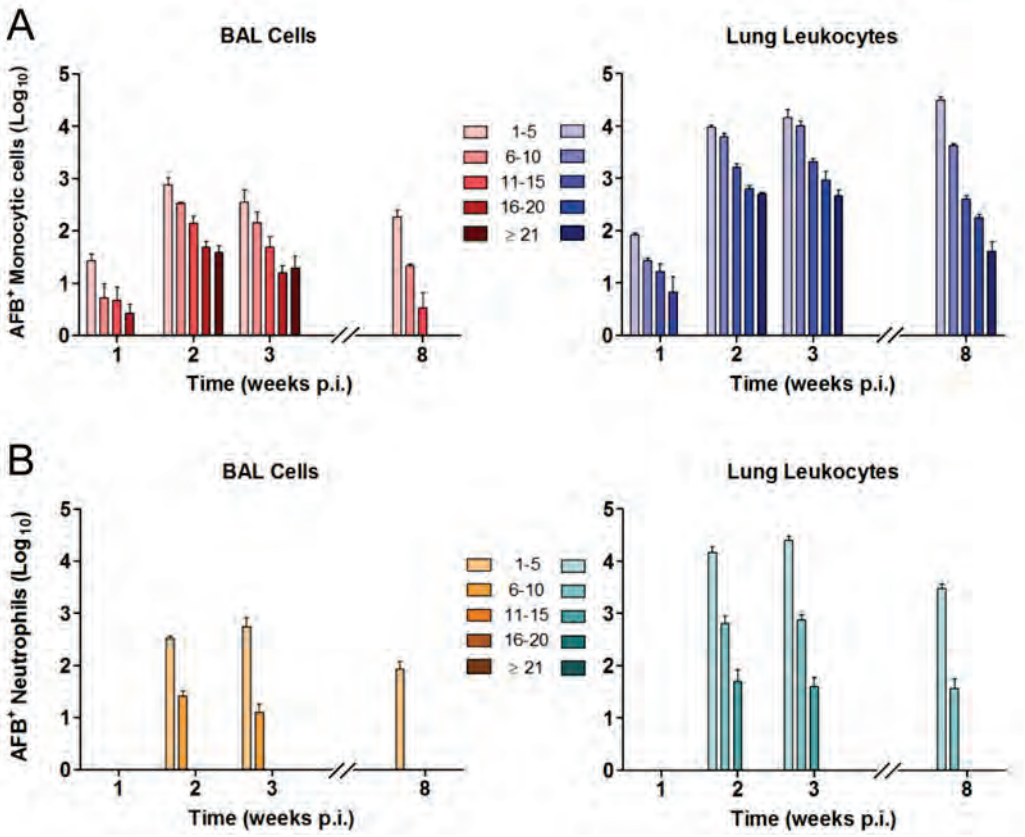

Figure 2.4. Distribution of intracellular bacillary load in lung phagocytes changes over time after aerogenic *Mtb* infection. The number of AFB per cell was counted in BAL cells and lung leukocytes harvested at the indicated times after aerosol challenge with *Mtb* Erdman. Across all time points, *Mtb* burden per cell was interrogated in a total 5.7 x 10^6 individual phagocytes, with counts grouped into bins of 1-5, 6-10, 11-15, 16-20, or≥ 21 AFB. Results are expressed as mean $\log_{10}$ AFB^+ monocytic cells (A) or neutrophils (B) ± SD within each bin, counted in BAL cells or in whole lung leukocytes as indicated. All bins were compared at each time point and between time points as described in *Materials and Methods*. Statistically significant differences ($p<0.05$) are not indicated on the figure for the sake of clarity. Among statistically significant differences, monocytic cells with 1-10 AFB outnumbered cells with > 10 AFB at all time points p.i., the proportion of monocytic cells containing > 15 AFB was lower at week 8 than earlier time points, and the distribution of AFB loads was significantly different in neutrophils compared to monocytic cells.

Also consistent with the burst size hypothesis, the proportion of AFB^+ monocytic cells harboring ≥ 21 bacilli peaked during the period of logarithmic *Mtb* replication at weeks 1 to 3 p.i. and then declined in parallel with induction of adaptive immunity. We previously reported an *in vitro* burst size of ~25 bacilli for *Mtb*-infected bone marrow derived

macrophages (BMDM) (103). In the present study, the bin of whole lung monocytic cells containing ≥ 21 AFB peaked at 2.8% of all AFB^+ monocytic cells by 2 weeks p.i. and then fell to 0.1% by 8 weeks p.i. (Fig. 2.5). We posit that cells with high burden reflect *Mtb* replication towards burst size, which dropped by a factor of 10 following the induction of adaptive immunity. The absolute number of heavily infected cells declined between 3 and 8 weeks p.i., indicating that cells dying after reaching burst size were being replaced at a reduced rate as host immunity limited *Mtb* replication. Monocytic cells estimated to contain up to 50 or more AFB were very rarely seen, representing 0.017% of AFB^+ cells at 3 weeks p.i. Most such cells appeared nonviable, with faintly stained cytoplasm and bacilli breaching the plasma membrane (Fig. 2.6A).

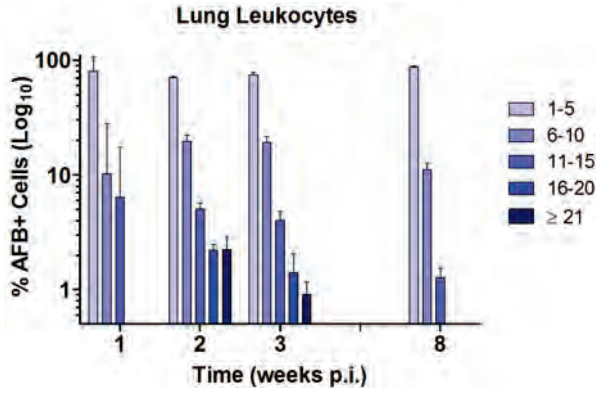

Figure 2.5. Change in the proportion of intracellular bacillary load in monocytic cells. AFB per cell was counted in cytospin samples of whole lung leukocytes harvested 1, 2, 3 and 8 weeks after aerosol challenge with *Mtb* Erdman. *Mtb* burden per monocytic cell (comprising AM, RM, mDC) was counted and stratified into the indicated bins of 1-5, 6-10, 11-15, 16-20, or ≥ 21. Results are expressed as mean % AFB^+ monocytic cells within each bin ± SD at the indicated time points. Statistical analysis described in *Materials and Methods* confirmed a significantly different distribution of AFB load in high bins at 8 weeks p.i. as compared to earlier time points.

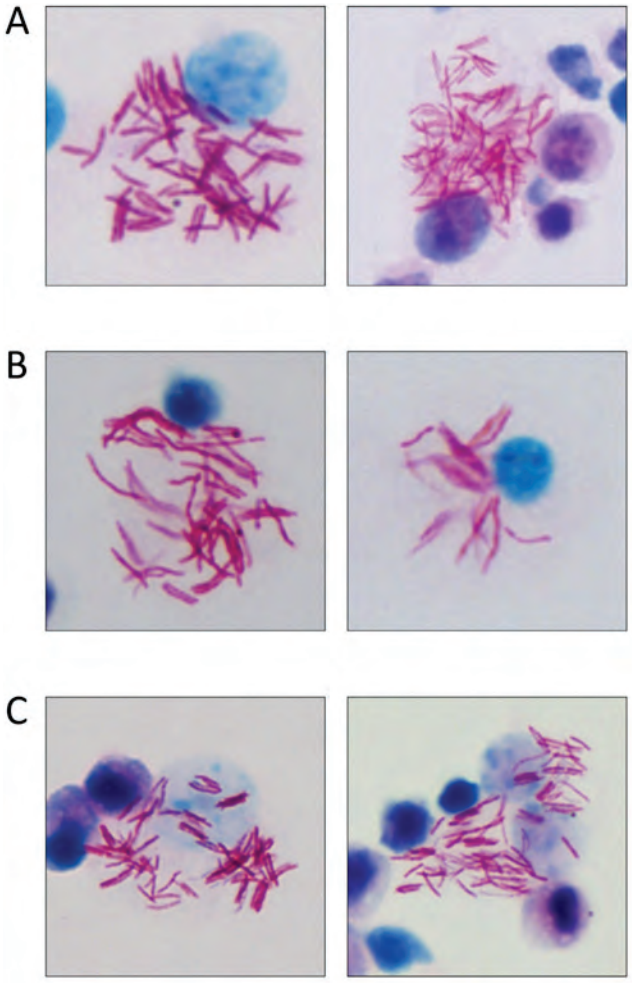

Figure 2.6. Cells heavily burdened with *Mtb* appear nonviable. (A) Lung leukocytes were isolated from WT mice 2 weeks after aerosol challenge with *Mtb* Erdman. Cytospin preparations were made and Ziehl-Neelsen stain was used to visualize and count intracellular AFB by light microscopy at 400X magnification. Photomicrographs show examples of heavily infected cells with ~50 intracellular AFB. (B) Whole lung leukocytes harvested 4 weeks after aerosol *Mtb* challenge were prepared for cell sorting. Cytospin preparations were made from the sorted population of "dead" cells defined by lower forward-scatter and higher side-scatter characteristics. AFB where visualized with Ziehl-Neelsen staining (magnification, X400). (C) Lung leukocytes from WT mice with 3 weeks of TB disease were processed by cytocentrifugation and Ziehl-Neelsen staining. The image shows clumps of AFB associated with dead cell remnants barely capable of retaining dye (magnification, X400).

We counted AFB per cell in cytospin preparations of flow-sorted monocytic cell types but found few cells containing > 10 AFB. This was inconsistent with results obtained with BAL cells or lung leukocytes that were cytocentrifuged directly onto the slides without further processing. Speculating that heavily burdened phagocytes progressing to necrosis were fragile and unable to withstand the stress of flow sorting, we examined the sorted population of non-viable cells defined by forward-scatter and side-scatter characteristics. Ziehl-Neelsen stained cytospins of those samples revealed much higher numbers of AFB in these dead and dying cells than in the sorted populations of viable cells (Fig. 2.6B). Collectively, these results support the concept of a mononuclear leukocyte burst size for virulent *Mtb in vivo* with a median value in the range of 20-40 bacilli. Of interest, while lung leukocytes with≥ 16 AFB declined by 84.5% between 3 and 8 weeks p.i., some high burden cells were still seen at the later time point, well after the induction of adaptive immunity when total lung bacillary load is held stable. Our findings in TB contrast with a report that viable macrophages isolated from the footpads of *M. leprae*-infected athymic *nu*/*nu* mice contained an average of 120 AFB per cell (127). Unlike *Mtb*, *M. leprae* is not cytolytic for macrophages *in vitro* even at MOI 100 (128).

In contrast to the distribution of *Mtb* in monocytic cells, neutrophils containing > 15 AFB were not seen at any time point, and neutrophils with 11-15 AFB were identified only at 2 and 3 weeks p.i. (Fig. 2.6B). This corresponds to the period of logarithmic *Mtb* expansion in the lung and the peak number of the most heavily infected monocytic cells. These results suggest that neutrophils are recruited to the vicinity of necrotic monocytic

cells and acquire bacilli at low to moderate MOI. The data also imply that neutrophils may be poor hosts for *Mtb* replication, presumably owing to their limited lifespan. Alternatively, neutrophils could be subject to burst size cytolysis with a lower threshold value or some other cell death mode in the context of TB.

***Mtb* replication dynamics in IFN-γ-deficient mice.** Interferon (IFN)-γ plays a critical role in protective immunity against *Mtb* by activating macrophages to limit bacterial replication (27). After aerosol challenge of GKO mice, lung *Mtb* burden increases logarithmically until death by 4-6 weeks p.i. We delivered 100 CFU of *Mtb* Erdman to WT and GKO mice and then harvested BAL cells for cytospin and Ziehl-Neelsen staining at five time points from 7 to 21 days. As expected, the total number of AFB^+ BAL cells increased progressively in GKO mice while in WT mice it was held to a plateau value after day 18 p.i. (Fig. 2.7). It was recently proposed that IFN-γ limits neutrophil recruitment to the lung in the transition from innate to adaptive immunity in TB (24). Consistent with that report, neutrophils represented a higher proportion of BAL cells in GKO compared to WT mice with TB (Fig. 2.8A). While neutrophils represented only 16% of BAL leukocytes in WT mice at 18 days p.i., they accounted for ~50% of AFB^+ cells at that time point (Fig. 2.8B). This suggests that despite the influence of IFN-γ on neutrophil trafficking, these cells are recruited to the immediate vicinity of *Mtb* infection where they may exert comparatively high phagocytic activity.

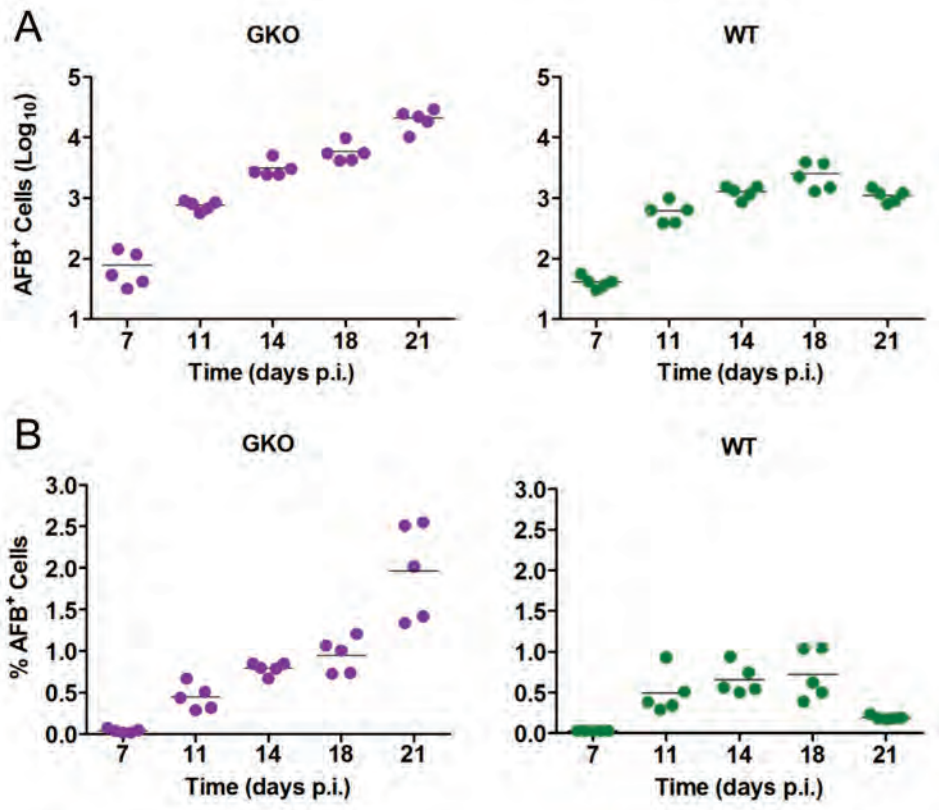

Figure 2.7. Kinetics of *Mtb* growth in IFN-γ-deficient mice. BAL cells were harvested from WT and GKO mice 7, 11, 14, 18 and 21 days after aerosol challenge with 100 CFU *Mtb* Erdman delivered to the lung. Total cells from both sources were counted and cytospin preparations were made for Ziehl-Neelsen staining. (A) The total number of *Mtb*-infected (AFB^+) cells was derived by multiplying the % AFB^+ cells by the total number of cells in each sample. Results for individual mice are presented as $\log_{10}$ total AFB^+ cells, with the line representing the mean. (B) The proportion of *Mtb*-infected phagocytes within the total sample was counted at each time point and expressed as % AFB^+ cells with the bar indicating the mean. Data were analyzed as detailed in *Materials and Methods*. The number of AFB^+ BAL cells from GKO mice was significantly different ($p<0.05$) from WT on days 14, 18 and 21 p.i. The % AFB^+ BAL cells from GKO mice were significantly different from WT on day 21 p.i. Data are representative from one experiment with five mice per group. In vivo experiments were repeated twice.

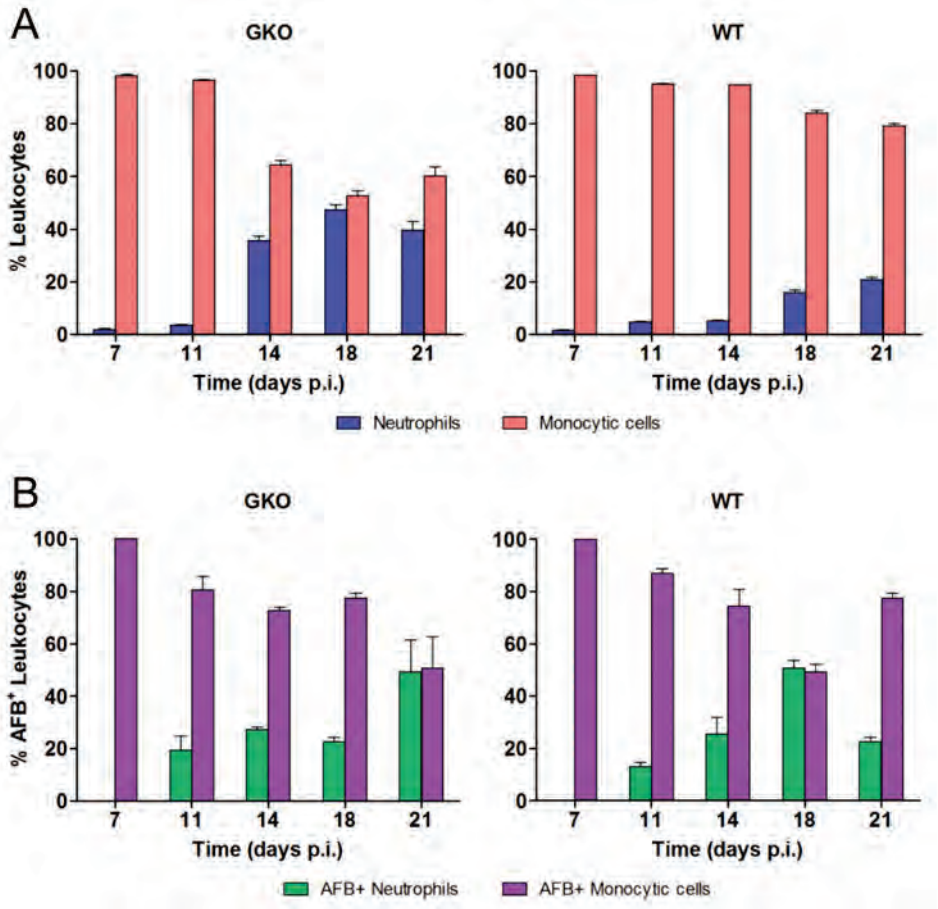

Figure 2.8. Lung leukocyte populations and distribution of intracellular *Mtb* in WT and GKO mice. (A) The relative proportion of neutrophils and monocytic cells in BAL from WT and GKO mice following aerogenic infection with *Mtb* Erdman was determined by light microscopy. Results are expressed as mean % cells of either type ± SD at the indicated time points. All groups were compared within and between all time points. GKO mice had a significantly higher proportion of neutrophils to monocytic cells compared to WT at 14, 18 and 21 days p.i. (B) The distribution of *Mtb* infection between neutrophils and monocytic cells was determined by counting AFB^+ cells of both types on Ziehl-Neelsen stained cytospins. Results are expressed as mean % AFB^+ ± SD. There was a statistically significant difference in the number of AFB^+ neutrophils between WT and GKO mice on day 18 p.i. There was also a significant increase in the number of AFB^+ neutrophils at day 21 p.i. for GKO mice compared to earlier time points.

Based on the burst size hypothesis, unrestricted intracellular *Mtb* replication in GKO mice is predicted to result in a persistently high proportion of heavily infected monocytic cells past the time point when WT mice start to restrict *Mtb* replication. Bacterial load per cell in BAL monocytic cells and neutrophils from GKO and WT mice was counted at each time point and tabulated in bins (Fig. 2.9). GKO mice had a higher proportion and total number of heavily infected cells on day 7 p.i. suggesting an innate IFN-γ response (20, 129) that limits *Mtb* replication before adaptive immunity is expressed. Prior to the full induction of adaptive immunity, *Mtb* replication in WT mice also proceeded at a rapid rate such that on day 14 p.i. the distribution of AFB loads was similar to that of GKO mice. As an effective IFN-γ-dominated adaptive immune response was expressed in WT mice, the proportion of heavily infected BAL cells declined. At day 21 p.i., the proportion AFB^+ cells in the top three bins were significantly higher in GKO compared to WT mice. AFB^+ cells containing 1-5 bacilli remained the most abundantly populated bin in GKO mice at all time points and cells containing > 50 AFB were very rarely seen, as was the case in WT mice. We interpret the distribution of AFB loads in GKO compared to WT mice as supporting the burst size hypothesis and also indicating that IFN-γ has little if any direct influence on the burst size value.

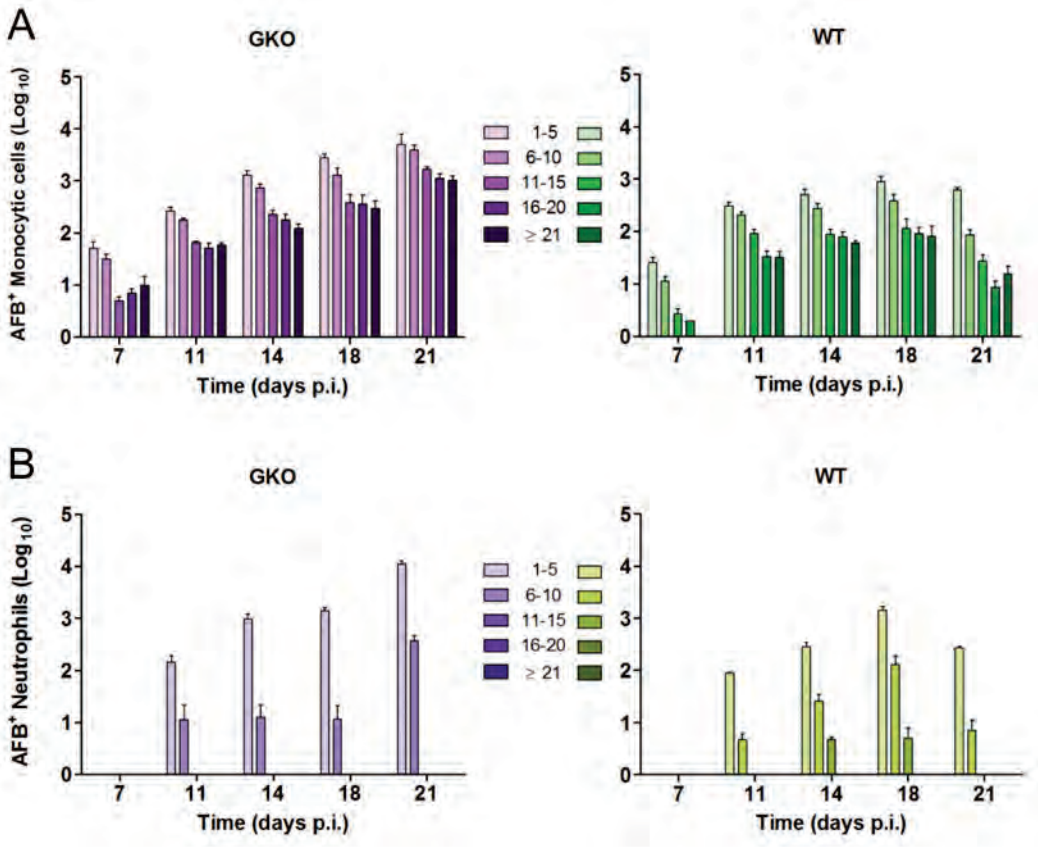

Figure 2.9. Distribution of AFB loads in lung monocytic cells and neutrophils from WT and GKO mice with TB. GKO and WT mice were challenged by aerosol with 100 CFU of *Mtb* Erdman delivered to the lung. BAL was performed 7, 11, 14, 18 and 21 days p.i. A total of 4.8 x 10^6 Ziehl-Neelsen stained cells were counted. Numbers of AFB per cell were grouped into 5 bins as indicated and counted separately in monocytic cells (A) and neutrophils (B) from GKO and WT mice. Results are presented as mean log_{10} AFB^+ cells in each bin ± SD. GKO mice had a greater number of AFB^+ monocytic cells in all bins at 7 days p.i. and a significantly higher proportion of cells with ≥ 11 AFB compared to WT mice at that time point. The proportion of cells within each bin was similar between WT and GKO mice on days 11-18 p.i. but by day 21 p.i. the proportion of cells with ≥ 11 AFB fell significantly in WT compared to GKO mice. On day 21 p.i. the number of AFB^+ neutrophils from GKO mice was significantly higher than earlier time points. In contrast, the number of AFB^+ neutrophils from WT mice was significantly lower on day 21 than day 18 p.i.

Cell death *in vivo* resembles high MOI necrosis *in vitro*. Macrophages challenged *in vitro* with *Mtb* at MOI≥ 25 rapidly undergo an atypical, caspase -independent cell death dominated by lipolytic attack on lipid membranes (104). This cell death mode has unique morphological features including nuclear condensation without fragmentation, and disintegration of lipid bilayers throughout the cell. In the present study, we compared the morphology of BAL cells harvested 3-4 weeks after low dose aerosol *Mtb* Erdman challenge to that of BMDM infected for 3 h *in vitro* with *Mtb* at MOI 25. Similar to the characteristic changes seen *in vitro*, monocytic cells from the lungs of mice with TB exhibited nuclear condensation and this was restricted to those cells with a high AFB burden (Fig. 2.10A). Nuclear fragmentation, a characteristic of caspase-mediated apoptosis, was not seen in > 5 x 10^5 DAPI-stained lung cells from mice with TB. The morphology of lung leukocytes having low numbers of intracellular bacilli was uniformly similar to the normal appearance of uninfected cells (Fig. 2.11).

Mtb-induced macrophage cytolysis *in vitro* is characterized by disintegration of mitochondrial, nuclear and plasma membranes without cell swelling or formation of apoptotic vesicles. To examine the ultra-structural features of infected lung leukocytes in the context of pulmonary TB, BAL cell cytospin preparations were visualized by scanning electron microscopy (EM) and compared to BMDM challenged with *Mtb* Erdman *in vitro* at MOI 25 (Fig. 2.10B). BAL cells isolated from mice with TB showed a similar pattern of injury to BMDM infected *in vitro*: plasma membrane damage and no evidence of budding vesicles or osmotic lysis. We also observed extrusion of chromatin through damaged nuclear membranes in dying BAL cells (Fig. 2.12), akin to results we

previously reported with *in vitro Mtb* infection (104). Taken together, these observations demonstrate consistent similarities between *Mtb*-induced cytolysis *in vitro* and *in vivo*.

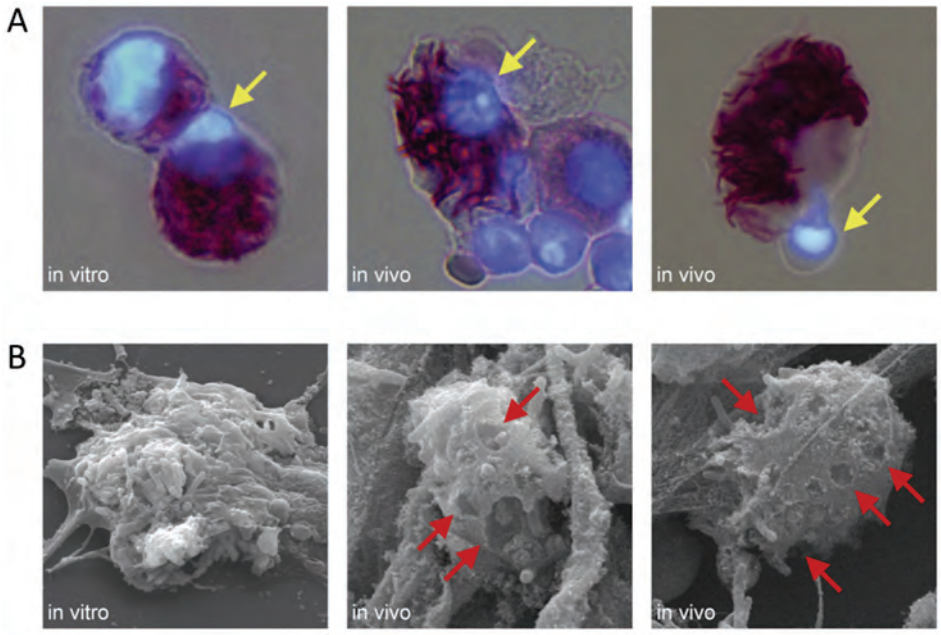

Figure 2.10. Morphology of macrophage cell death in pulmonary TB. (A) BMDM challenged with *Mtb* Erdman *in vitro* (MOI 25, 3 h) and BAL cells from WT mice challenged 3 weeks previously with a low aerosol dose of *Mtb* Erdman were stained with carbolfuchsin to visualize intracellular bacilli and stained with DAPI to visualize nuclear morphology (magnification, X400). Heavily infected cells in both cases exhibited nuclear condensation without fragmentation (*yellow arrows*). (B) Representative scanning electron micrographs of BMDM infected with *Mtb in vitro* and BAL macrophages isolated from mice after 4 weeks of TB disease (magnification, X5,000). Damaged cells in both cases exhibit disintegration of outer cell membranes (*red arrows*) with escape of intracellular bacilli. BAL cells were isolated from GKO mice 4 weeks after aerosol *Mtb* infection. Cytospin preparations were processed for Ziehl-Neelsen staining, immunostaining or scanning EM.

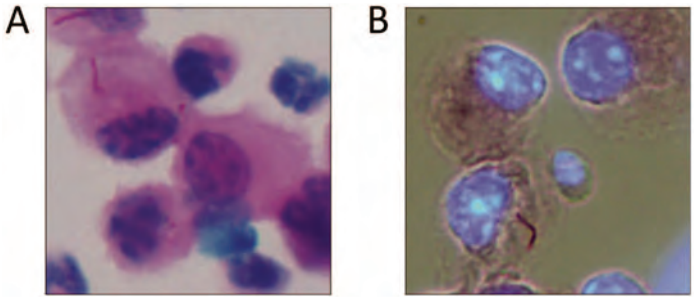

Figure 2.11. Cells with low intracellular *Mtb* appear like uninfected cells. BAL cells were isolated from WT mice 2 weeks p.i. and cytospin slides were prepared for (A) Ziehl-Neelsen or (B) DAPI plus carbolfuchsin staining. AFB were identified with light microscopy or fluorescence microscopy (magnification, 400X). Images of AFB^{+} cells with low intracellular *Mtb* appear similar in nuclear morphology with adjacent uninfected cells. Survey thousands of cells contain low number of bacilli identified none with the morphological features of necrosis that was typical of heavily infected cells.

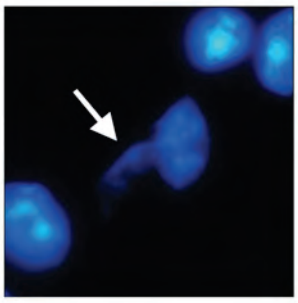

Figure 2.12. Chromatin extrusion from DAPI stained AFB^{+} cells. BAL cells from mice with aerogenic TB infected were harvested 3 weeks, p.i. Samples were prepared on cytospin slides and stained with DAPI. The image shows nuclear condensation and chromatin extruding through a damaged nuclear membrane into the cytoplasm (*white arrow*; magnification, X400).

***Mtb* infection is associated with release of neutrophil extracellular traps *in vivo*.** A high proportion of lung neutrophils were infected with *Mtb* after aerosol challenge and they were a significant host cell compartment for bacilli even after 8 weeks of TB disease. Compared to monocytic cells, neutrophils have a short lifespan in the lung in the absence of inflammation, which would seem to make them unproductive hosts for *Mtb* replication. Examining cytospin preparations of BAL cells from GKO mice, we observed large masses of amorphous extracellular material with numerous associated AFB (Fig. 2.13A). A combination of carbolfuchsin and DAPI stains indicated that these structures had a high content of extracellular DNA. Scanning EM revealed a network of extracellular fibrillar structures with adherent bacilli similar to the morphological features first described by Brinkmann and Zychlinsky (130). Furthermore, the thread-like structures were abundantly studded with globular domains. The composition of NETs includes characteristic components including myeloperoxidase (MPO), neutrophil elastase and cleaved histones (131, 132). Confocal scanning laser microscopy and immunostaining with antibodies against neutrophil elastase, MPO and histones showed co-localization of these molecules with extracellular DNA (Fig. 2.13B). Together, these data indicate the presence of neutrophil extracellular traps (NETs). We did not see NETs in cytospins from WT mice with TB. Release of NETs could be limited to conditions of uncontrolled *Mtb* replication in GKO mice but more likely occurs at a low frequency in WT mice that is undetectable by the methods we used. Furthermore, we observed *Mtb*-induced NETs in BAL from hypercholesterolemic ApoE null mice with TB (Fig. 2.13C). At the time of sampling p.i., these mice express comparable levels of IFN-γ with WT, but

are unable to control bacterial replication and they develop severe neutrophilic lung inflammation (133). Ramos-Kichik et al. (134) reported that *Mtb* induces NET release *in vitro* and that NETs trap the bacilli but are unable to kill them, in contrast to microbicidal activity of NETs against *Listeria monocytogenes*. We believe that our data from GKO and ApoE null mice are the first evidence for NET release in the context of TB disease *in vivo* and indicate that an extracellular population of bacilli may be adherent to NETs in the lung.

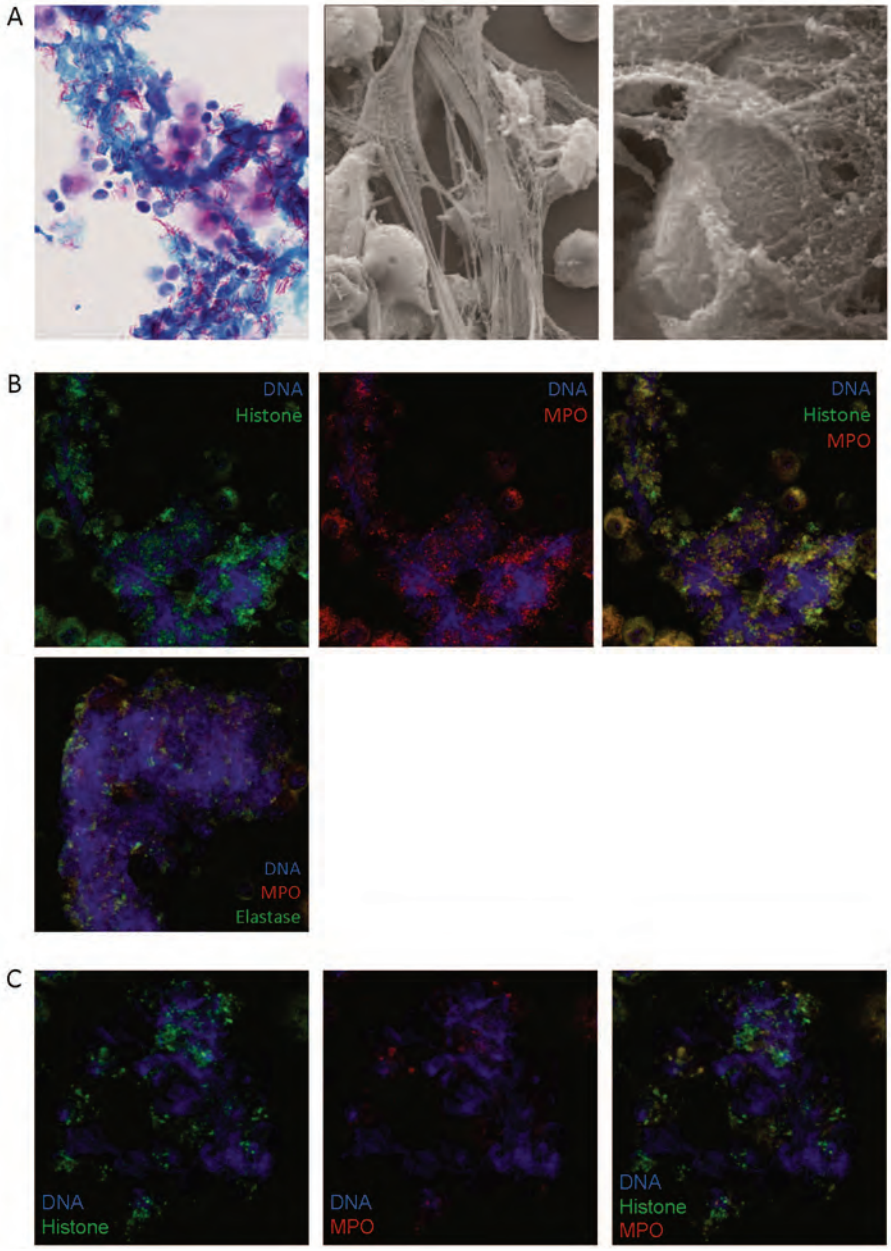

Figure 2.13. Morphology of neutrophil cell death in pulmonary TB. (A) Ziehl-Neelsen staining (*left panel*) identified amorphous extracellular material with associated AFB (magnification, X400). Scanning EM (*middle panel*) demonstrated the presence of cell-associated extracellular fibers consistent with NETs (magnification, X5,000). High resolution of SEM image (*right panel*) revealed globular domains decorating the extracellular fibrous structures (magnification, X25,000). (B) NETs were identified by immunostaining using DAPI to stain DNA (*blue*) and antibodies against histone H2B (*green*) and MPO (*red*) or neutrophil elastase (*green*) and MPO (red). Stained cells were analyzed using confocal scanning laser microscopy (magnification, 63X objective). (C) BAL cells from ApoE null mice 4 weeks p.i. were stained for DNA (*blue*), histone H2B (*green*) and MPO (*red*) and visualized with confocal scanning laser microscopy.

2.5 Discussion

We examined leukocytes from the lungs of mice infected with *Mtb* by aerosol to test a model of burst size cytolysis suggested by prior *in vitro* studies. The distribution of *Mtb* load in monocytic cells was skewed such that most AFB^+ cells contained few bacilli while a minority had a high bacillary load. The morphology of heavily infected cells mirrored that seen with *Mtb*-induced necrosis *in vitro*; they appeared nonviable, with condensed nuclei and disrupted plasma and nuclear membranes. We interpret these findings as consistent with burst size cytolysis at median threshold in the range of 20-40 AFB. That value is close to the burst size reported for *in vitro* infection of BMDM (104). The comparison of WT and GKO mice demonstrated that by limiting *Mtb* replication to burst size, IFN-γ promotes the survival of monocytic host cells with a sublethal bacillary burden. A similar phenomenon was reported for BMDM *in vitro*, where virulent *Mtb* strains introduced at low MOI grew rapidly and caused necrosis but cytolysis was prevented when *Mtb* replication was inhibited by exogenous IFN-γ (93). Despite an effective immune response in WT mice, some monocytic cells with > 15 AFB were present at 8 weeks p.i., accounting for 0.6% of all AFB^+ cells at that time. This implies ongoing *Mtb* replication in a limited population of monocytic cells balanced by microbicidal activity in as yet unknown compartments during the period of "stationary persistence" that is not reflected by an increase in total lung CFU. A similar conclusion was reached by Gill et al. (135) in a study that employed in silico modeling and *in vivo* experiments using *Mtb* transformed with an unstable plasmid replication clock.

Virulent *Mtb* strains inhibit host-protective apoptotic death of infected macrophages (79, 82, 83, 92, 96), permitting optimal replication before spreading to other cells. Transit between replication niches requires time and incurs risk for bacilli that may be trapped in the extracellular environment, subjected to antimicrobial activities, or taken up by phagocytes that do not support replication. Delaying host cell death for 3-5 *Mtb* doublings should accelerate the increase in total lung bacillary load in the critical period prior to the induction of adaptive immunity. Lacking any means to manipulate burst size in biological experiments, we took advantage of an existing computational model to test the effects of different burst size values on *Mtb* accumulation in the lung. This in silico agent-based model replicates the interplay between host and pathogen, taking multiple variables into account over three biological scales: molecular, cellular and tissue in a 2 mm x 2 mm section of lung. The model captures burst size by setting a value to the maximum carrying capacity of *Mtb* per macrophage, above which the macrophage bursts, releasing viable bacilli to infect naïve cells. We varied burst size values in the computational model to 10, 20, 30, 40, and 50, keeping all other parameter values fixed in order to analyze the effects of this isolated change. To account for stochastic variability, each experiment was run 20 times (equivalent to using 20 mice for each time point).

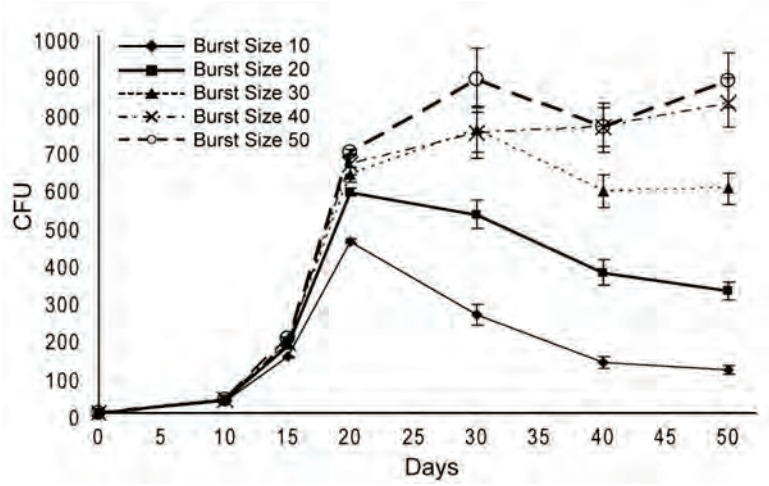

Figure 2.14. Higher burst size parameter values result in higher total bacterial counts in computational simulation of *Mtb* replication in the lung. A multiscale computational model described in *Materials and Methods* was used to generate values for total bacterial counts over time in a 2 mm x 2 mm virtual section of lung starting with a single macrophage infected with a single bacillus at time zero. The different curves correspond to different burst size parameter values for the number of *Mtb* bacilli within a macrophage that induce cytolysis. All the other parameters in the computational model capturing immune mechanisms are identical for each curve and are calibrated to reproduce a typical chronic *Mtb* infection in a mouse. The x-axis shows days after time zero, while the y-axis shows mean total *Mtb* counts ± SD for 20 individual program runs at each burst size value. For ease of illustration, significant differences ($p<0.05$) are not shown on the graph. Overall, *t*-test results show that higher burst size values favor higher total lung bacterial load. Scaling to the whole lung can be done by multiplying the prediction by a factor of ~10^4, assuming a mouse lung volume of ~1 cm^3. The scaling returns CFU in the whole lung in the range of 1-10 x 10^6.

Figure 2.14 shows five time courses of total bacterial counts for each burst size assumption. By day 20, a burst size >20 resulted in a significantly greater increase in total bacteria as compared to smaller burst sizes. For burst sizes 10 and 20, a peak is reached at day 20 and a lower steady state is achieved as adaptive immunity is expressed in the lung. For burst sizes > 20, the *Mtb* count either stabilizes at the peak (burst size 30) or trends up at a slower rate (burst sizes 40 and 50). Overall, increasing the burst size resulted in higher bacterial loads, consistent with advantage for the pathogen with burst size > 20. While providing independent support for the burst size hypothesis, the model has several limitations. In its current iteration, only macrophages are considered as hosts for *Mtb* and

it assumes that every bacillus liberated from a dying macrophage invades a different new host cell at MOI 1. Our animal data show that AM, RM, mDC and neutrophils all harbor *Mtb* and these cell types likely differ in their capacity to support or inhibit bacillary replication. The biological data also suggest that the efficiency of *Mtb* escape and re-infection of new host cells is lower than the model assumes since we saw neutrophils (cells unlikely to support multiple rounds of *Mtb* replication) harboring up to 15 AFB. We also frequently observed *Mtb* in clumps that would deliver multiple bacilli if ingested by a single phagocyte (Fig. 2.6C). Insights from the *in vivo* TB study presented here will be applied to future refinements of the agent-based model.

We identified three discrete monocytic cell populations hosting *Mtb*, in general agreement with prior reports (117-119). We recognize that monocytic cells hosting *Mtb* in the lung may be even further sub-classified (121), and that functional heterogeneity between individual cells of the same surface phenotype is likely. Cells classified as mDC were increased in number and proportion by 4 weeks p.i. and were favored hosts for *Mtb* at that time. This increase was due mostly to recruitment, with a minor contribution from phenotypic shift of AM resident in the lung prior to aerosol *Mtb* challenge as demonstrated by lentiviral GFP labeling. By 10 weeks p.i., the predominant AFB^{+} monocytic cells were RM. The basis for that switch is presently unknown but might relate to the reported increase of GM-CSF and decrease of M-CSF in the lung over time after aerosol *Mtb* infection, which correlates with reduced DC-like cell surface markers and increased foamy macrophages (120). The extent to which mDC and RM defined by surface phenotype differ at a functional level is unknown. They might differentially

restrict or permit *Mtb* replication, differ in their response to IFN-γ, or differ in susceptibility to cytolysis. Ryan et al. (136) reported that *Mtb* induces non-apoptotic death of human peripheral blood-derived DC, with some features similar to those of murine BMDM challenged at high MOI *in vitro*. Our *in vivo* data imply that tissue mDC are subject to burst size cytolysis, but this has not been directly tested *in vitro*. IFN-γ-activated BMDM restrict *Mtb* replication *in vitro* more effectively than activated bone marrow-derived DC (137). If that difference holds *in vivo*, it would favor RM survival with a sub-lethal *Mtb* load and the preferential accumulation of these cells in the lung over time p.i. Loss of heavily infected monocytic cells during the process of flow sorting prevented us from comparing the distribution of AFB loads within purified populations of mDC, RM and AM. We are exploring alternative approaches to generate such data.

We confirmed that neutrophils are also major *Mtb* host cells *in vivo*, albeit with a narrower range of AFB load than monocytic cells. As a proportion of all AFB^+ cells, neutrophils were major *Mtb* hosts in the period of logarithmic increase of total lung bacillary load. The proportion of neutrophils with relatively high burden (6-15 AFB) also peaked at 2-3 weeks p.i. in WT mice. In GKO mice, total lung *Mtb* burden and infected neutrophils increased logarithmically until death. Cytokines play a major role in the positive and negative regulation of neutrophil trafficking to the lung in TB. Nandi and Behar reported that coincident with the induction of adaptive immunity, IFN-γ inhibits neutrophil accumulation in part by reducing Th17 differentiation (24). We found that neutrophils accounted for half of all AFB^+ leukocytes on day 18 p.i. in WT mice, despite being a distinct minority of total lung leukocytes at that time. This indicates that

neutrophils are recruited to the proximity of necrotic cells at foci of *Mtb* infection in the lung. We propose that death-associated molecular patterns (DAMPs) released from monocytic cells undergoing *Mtb*-induced necrosis contribute to neutrophil recruitment and activation in TB. In that regard, we previously described neutrophil-rich inflammation and a high frequency of cell death in pulmonary TB lesions of diabetic and hypercholesterolemic mice that express IFN-γ to an equal or greater extent than mice without metabolic disorders (106, 133, 138), and we showed that HMGB1 is released in the course of *Mtb* burst size cytolysis (139). Despite their recruitment to TB lesions and phagocytosis of bacilli, neutrophils are unlikely to host multiple rounds of *Mtb* replication before dying by spontaneous apoptosis or by NETosis.

In summary, our data support a burst size model for *Mtb* cytolysis *in vivo*. The features of this atypical necrotic death that we characterized *in vitro* are favorable for an exit mechanism *in vivo*. *Mtb*-induced cell death occurs at a threshold intracellular burden, it liberates the bacilli free of apoptotic vesicles, and it has little impact on *Mtb* viability. We did not find any DAPI-stained cells with fragmented nuclei or signs of apoptotic vesicle formation by scanning EM of BAL or lung leukocytes in the present study. While classical apoptosis has clearly been demonstrated in TB, our data suggest that burst size necrosis is a common fate for *Mtb*-infected monocytic cells *in vivo*. The burst size model logically fits into the pathogenesis of TB but our results highlight complex host-pathogen interactions. Resident AM are a transient niche for *Mtb* immediately after inhalation, but bacilli rapidly move into cells with surface phenotypes of mDC or RM, preferentially infecting the former early in disease and then shifting to the latter during stationary

persistence. Neutrophils avidly acquire bacilli in the 3 week interval of logarithmic increase in total lung bacterial load. Their trafficking may be regulated in part by DAMPs released through burst size cytolysis of *Mtb*-infected cells. Neutrophils may promote host defense in the transition from innate to adaptive immunity(25, 140), but play a detrimental role if they accumulate in excess, as occurs with poorly controlled TB in mice and in humans (22, 138, 141). NETs lack antimicrobial activity against *Mtb in vitro* (134). Their potential to reduce *Mtb* viability *in vivo* is presently unknown. In neutrophilic TB lesions, NETs might promote lung injury as they were shown to do in a mouse influenza model (142). It is interesting to consider what role NETs could play in forming a milieu that supports extracellular persistence of *Mtb* in necrotic lung lesions. A refined understanding of host-pathogen interactions in TB will require analysis of unique *Mtb* interactions with each of these phagocyte types *in vivo*, using cells isolated from the tuberculous lung.

Preface to Chapter III

A modified version of this chapter has been submitted for publication.

Teresa Repasy[a], Nuria Martinez[a], Jinhee Lee[a], Kim West[a], Wenjun Li[b], Hardy Kornfeld[a]# *Neutrophil Recruitment and Infection is Associated with Bacterial Replication in Tuberculosis*

Department of Medicine, University of Massachusetts Medical School, Worcester, Massachusetts, USA[a]

Division of Preventive and Behavioral Medicine, University of Massachusetts Medical School, Worcester, Massachusetts, USA[b]

N.M. assisted in experiment for Fig. 3.8.
J.L. assisted in experiments for Fig. 3.6.
K.W. assisted in experiments for Fig. 3.7 and 3.8.
W.L. performed the statistical analysis for Fig. 3.1D.
T.R. performed all other experiments.
T.R. and H.K. prepared the manuscript.

CHAPTER III: Neutrophil Recruitment and Infection is Associated with Bacterial Replication in Tuberculosis

3.1 Abstract

We previously reported that burst size necrosis is the chief mode of mononuclear cell death in the lungs of mice infected with *Mycobacterium tuberculosis* and that neutrophils are major host cells for *M. tuberculosis* in the period of logarithmic bacterial growth before adaptive immunity is expressed. The present study explored the link between burst size necrosis and neutrophil accumulation in the lungs of wild-type C57BL/6 mice infected with one of four *M. tuberculosis* strains of increasing virulence (Rv*ΔphoPR* mutant, H37Ra, H37Rv and Erdman). At every time point studied, Erdman produced the highest bacterial load and the highest proportion and number of *M. tuberculosis*-infected neutrophils despite total lung neutrophil counts similar to H37Rv. These parameters, along with the proportion of TUNEL-positive cells, tracked with virulence across all strains tested. Differences in neutrophil infection were not reflected by levels of chemoattractant cytokines in bronchoalveolar lavage fluid, while interferon-γ (reported to suppress neutrophil trafficking to the lung in tuberculosis) was highest in Erdman-infected mice. Treating Erdman-infected mice with ethambutol resulted in a dose-dependent decrease in proportion of mononuclear cells with high bacterial burden and a dose-dependent decrease in the ratio of infected neutrophils to infected mononuclear cells. We conclude that faster replicating *M. tuberculosis* strains produce more burst size

necrosis that in turn drives neutrophil recruitment, overriding cytokine counter-regulation. Neutrophils infected with *M. tuberculosis* constitute a biomarker for poorly controlled bacterial replication, high rates of infection-induced mononuclear cell death, and increased severity of pulmonary immune pathology in tuberculosis.

3.2 Introduction

We previously reported that necrotic cell death of mononuclear phagocytes (MPs) infected with *Mycobacterium tuberculosis* Erdman is associated with high intracellular bacterial burden and is the predominant form of cell death in tuberculosis (TB) disease *in vivo* (143). Our data from *in vivo* and *in vitro* experiments support the concept of burst size cytolysis in MPs containing 20-40 bacilli (103, 104, 143). This necrotic cell death mode relies on mycobacterial genes regulated by the PhoPR 2-component system but it is independent of Esx-1 (104). Neutrophils comprised roughly half of all *M. tuberculosis*-infected lung leukocytes 3 weeks after aerosol challenge with Erdman. Bacterial burden increases logarithmically at this early stage of TB disease, prior to the full expression of adaptive immunity in the lung (143). At later time points, when total lung bacillary load is constrained to a plateau level by host immunity, the proportion of neutrophils amongst all *M. tuberculosis*-infected phagocytes fell to ~10%. Mice lacking interferon (IFN)-γ failed to restrict Erdman replication and had a rising proportion of infected neutrophils until death. These results suggested the hypothesis that neutrophils are recruited to TB lesions in response to signals associated with burst size necrosis of MPs.

In the present study, we investigated the impact of *M. tuberculosis* replication rate on neutrophil recruitment to the lung and its influence on the pathology of TB disease. To

test the hypothesis that bacillary replication drives MP necrosis and consequently neutrophil recruitment to TB lesions, wild-type C57BL/6 mice were challenged with one of four *M. tuberculosis* strains differing in virulence: Erdman, H37Rv, H37Ra, or an H37Rv mutant lacking the *phoPR* coding region (RvΔ*phoPR*). Results confirmed that bacterial replication during the innate phase of the host response correlated with the total number of lung leukocytes infected with acid-fast bacilli (AFB), the proportion of *M. tuberculosis*-infected (AFB^+) leukocytes that were neutrophils and the distribution of AFB burden per cell in MPs and neutrophils. There was no biologically significant difference in the levels of IL-1α, IL-1β, IL-17, KC (CXCL1) or MIP-2 (CXCL2) in bronchoalveolar lavage (BAL) fluid at 2 weeks post-infection with any of the four strains despite presenting dramatic differences in AFB^+ neutrophils. At the same time point, IFN-γ was 15-fold higher in BAL from Erdman-infected mice compared to the other strains. Terminal deoxynucleotidyl transferase dUTP nick end labeling (TUNEL) staining of lung sections showed that Erdman induced the most cell death, followed by H37Rv and then H37Ra. By light and fluorescence microscopy, neutrophils were identified adjacent to $TUNEL^+$ cells. Finally, treating Erdman-infected mice with ethambutol resulted in a dose-dependent reduction in the proportion of monocytic cells with high intracellular AFB load, a shift to lower AFB load in infected neutrophils and a drop in the proportion of neutrophils amongst all AFB^+ phagocytes. These results support a model where the rate of *M. tuberculosis* replication and consequent burst size necrosis of MPs drives neutrophil recruitment to TB lesions despite potentially counter-regulatory cytokine signals.

3.3 Materials and Methods

Mice. C57BL/6 mice were purchased from The Jackson Laboratory and housed in pathogen-free environment at Animal Medicine facility at The University of Massachusetts Medical School (UMMS). Experiments using mice were conducted in accordance with the guidelines set by the National Institutes of Health regarding the housing and care of laboratory animals. All animal experiments were performed under protocols approved by the Institutional Animal Care and Use Committee and the Institutional Biosafety Committee at UMMS.

Bacterial strains and *M. tuberculosis* infection. *M. tuberculosis* Erdman, H37Rv, H37Ra (provided by H. Remold) and Rv∆*phoPR* mutant (provided by K. Papavinasasundaram) (2) were used in this study. Infections were performed by delivering ~100 CFU of *M. tuberculosis* Erdman, H37Rv or H37Ra by aerosol route using Glas-Col Inhalation Exposure System or ~400 CFU for Rv∆*phoPR*. For every experiment, the delivered dose was verified by sacrificing two mice 24 h after exposure and plating lung lysates for CFU.

Bacterial culture. Bacterial burden was determined by counting CFU of infected lung homogenates. At indicated time points, lungs were harvested and homogenized in 1 ml of PBS with 0.05% Tween 80 using a Bullet Blender (Next Advance) tissue homogenizer. Lung homogenates were serially diluted 10-fold and 100 µL of three consecutive dilutions, depending on the strain, were plated in duplicate on Middlebrook 7H11 agar plates supplemented with Middlebrook OADC Enrichment. Plates were incubated at 37°C and CFU were counted 2, 3 and 4 weeks after plating.

Cell preparation. Whole lung leukocytes were isolated by sacrificing infected mice and perfusing the heart with PBS. Lungs were excised, minced and then incubated with 150 U/ml collagenase IV (Sigma-Aldrich) and 60 U/ml DNase (Sigma-Aldrich) for 45 min at 37°C with constant agitation. Lung tissues were filtered through a 40 μm cell strainer and treated with Gey's Solution (Sigma-Aldrich). Single lung cell suspensions were used for flow cytometry and cytospin preparation.

Enumeration of intracellular bacteria. Isolated whole lung leukocytes at a density of 1 x 10^5 cells per slide were immobilized onto cytospin slides by cytocentrifugation. Cytospin slides were heat fixed and processed for Ziehl-Neelsen staining (TB Stain Kit, BD Diagnostic Systems). Using light microscopy, each cell was examined for intracellular AFB and AFB counts were grouped into five bins: 1-5, 6-10, 11-15, 16-20 and ≥21. Based on nuclear morphology, infected cells were identified as neutrophils or MPs (comprising alveolar macrophages, recruited monocytes/macrophages, myeloid dendritic cells). AFB counts were tallied separately according to the cell type.

Flow cytometry. Single lung cell suspensions were incubated in CD16/CD32 mAb (BD Biosciences) to block Fc binding. The following mAb purchased from eBioscience (San Diego, CA) were used for staining cell surface markers: CD11b-PerCP-Cyanine5.5 (M1/70), CD45-APC (30-F11), Ly-6G-Alexa Fluor 700 (RB6-8C5). Live/Dead Fixable Dead Cell Stain Kit was purchased from Invitrogen. Data was acquired using LSRII flow cytometer (BD Biosciences) and analyzed with FlowJo software (TreeStar). The gating strategy excluded dead cells and lymphocytes by forward and side scatter. Gating on $CD45^+$ cells, neutrophils were defined as Ly-$6G^{hi}$ $CD11b^{hi}$ cells.

Histology, TUNEL assay and immunostaining. *M. tuberculosis*-infected lungs were inflated with 10% buffered formalin and fixed for 24 h. Paraffin embedded sections were stained with hematoxylin and eosin (H&E) for histopathology. The In Situ Cell Death Detection Kit (Roche) was used for TUNEL assay. For immunostaining of lung sections, primary Ab against myeloperoxidase (MPO; LS Bio) and secondary Ab Alexa 555 (Invitrogen) were used. The In Situ Cell Death Detection Kit (Roche) with fluorescein-dUTP was used to detect $TUNEL^+$ cells. All histology work was performed by the DERC Morphology Core facility at UMMS. Lung sections were analyzed using Nikon Eclipse E400 Microscope equipped with a Nikon DS-Ri1 camera using NIS-Elements Microscope Imaging Software or Spot Advance Software.

Cytokine measurement. BAL fluid was obtained by flushing infected lungs with lavage fluid (0.2% BSA 0.2mM EGTA in PBS) three times. BAL fluid was filter-sterilized and stored at-80°C until ready for use. Cell-free lung lysates were prepared by adding equal volumes of homogenized lung tissue in PBS with 0.05% Tween 80 to T-PER tissue protein extraction reagent (Thermo Scientific). The mixture was incubated (20 min, 4°C) then centrifuged (10 min, 12,000 x *g*) and the supernatant was filter sterilized and stored at -80°C until used. BAL fluid and lung lysates were individually assayed for IFN-γ, IL-1α, IL-1β, IL-17, JE (CCL2), KC, MIP-2, (R&D Systems), HMGB1 (IBL International) and S100A8/A9 (CusaBio) by ELISA following the manufacturers' protocols. Absorbance was measured using Thermo-Multiskan Ascent ELISA reader (Thermo Scientific).

Ethambutol treatment. Four days after mice were challenged with ~100 CFU of *M. tuberculosis* Erdman via aerosol route, ethambutol (EMB; Sigma-Aldrich) was provided to the infected mice *ad libitum* in drinking water at concentrations of 67, 200 and 600 μg/ml. Water bottles containing EMB were replaced weekly and drug therapy continued for 11 days until the 2 week post-infection time point.

Statistical analysis. For Figure 1D, the data followed an approximate Poisson distribution; therefore we compared the median values by strain at each time point and bin using a Poisson regression model, and expressed the differences as ratios to a reference group and tested their statistical significance. For all other data, statistical analysis was performed using SigmaPlot v11.0 (Systat Software, Inc.). One-way ANOVA with Tukey or Holm-Sidak post-test was used for comparison with more than two groups and Student's *t*-test was used when comparing two groups. A P value <0.05 was considered statistically significant.

3.4 Results

Lung bacterial burden and leukocyte infection reflect *M. tuberculosis* virulence. To investigate the influence of virulence on the distribution of intracellular *M. tuberculosis* infection among lung leukocyte populations, wild-type C57BL/6 mice were challenged by aerosol with one of four *M. tuberculosis* strains. The panel of bacteria included two commonly used virulent laboratory strains (Erdman and H37Rv) and two strains of reduced virulence (H37Ra and RvΔ*phoPR*). Based on the association of mycobacterial virulence with faster *in vivo* doubling times (144) and a burst size model of horizontal transmission within the host, we predicted that *M. tuberculosis* virulence

would also be reflected in the distribution of bacilli between MPs and neutrophils and the distribution of AFB loads within individual leukocytes of both types.

Aerosol conditions were set to deliver ~100 CFU of Erdman, H37Rv or H37Ra and ~400 CFU of Rv∆*phoPR* to the lung. Total lung burden of each strain was measured at 2, 4 and 24 weeks post-infection (p.i.) by counting CFU of plated lung homogenates (Fig. 3.1A). All four strains exhibited logarithmic growth during the predominantly innate phase of host defense in the first 2 weeks p.i. Erdman had the highest replication rate in this interval, achieving 2 logs greater mean CFU than H37Rv which had the second highest number. Of the attenuated strains, mean CFU for Rv∆*phoPR* was ~0.5 logs lower than H37Rv while H37Ra was a further ~0.5 logs lower than Rv∆*phoPR*. Mean lung CFU for Erdman, H37Rv and H37Ra increased by 4 weeks p.i., while Rv∆*phoPR* dropped by nearly 0.5 logs and was at least 2 logs lower than the other strains. At 24 weeks p.i., Erdman and H37Rv declined slightly while H37Ra dropped more than 1 log from its 4 week p.i. high point.

The *M. tuberculosis* growth curves reflected the hierarchy of bacterial virulence. Results confirmed the substantially faster doubling time for Erdman compared to H37Rv noted by North and Izzo in CB-17 mice infected intravenously with 2×10^5 bacilli (144). The earlier control of Erdman could reflect accelerated kinetics of immune priming due to faster dissemination from lung to lymph node as proposed by Chackerian et al. (145). The early control of Rv∆*phoPR* more likely reflects susceptibility of the pathogen to the effector mechanisms of host immunity.

To investigate the correlation between total lung bacterial burden and infection of phagocytic cells, whole lung leukocytes were isolated by enzymatic digestion and immobilized by cytocentrifugation onto slides for Ziehl-Neelsen staining. Leukocytes containing any AFB were counted for each *M. tuberculosis* strain at each time point (Fig. 3.1B). The total number of AFB^+ leukocytes for all strains increased logarithmically in the first 2 weeks p.i. Between 2 weeks and 4 weeks p.i., total AFB^+ cells from mice infected with Erdman, H37Rv and H37Ra continued rising logarithmically but at a lower rate. In mice infected with Rv∆*phoPR*, total AFB^+ lung leukocytes were confined to a plateau level nearly 3 logs lower than the Erdman group. Between 4 weeks and 24 weeks p.i., there was a slight trend for increased total AFB^+ cells in mice infected with Erdman, H37Rv and H37Ra but at a much slower rate than in the first 4 weeks p.i. The slight increase of AFB^+ leukocytes for all three strains occurred despite a decline in total lung bacterial burden that was modest for Erdman and H37Rv but >1 log for H37Ra.

The relative proportion of *M. tuberculosis*-infected neutrophils at 2 weeks p.i. was much greater in mice infected with Erdman than the other bacterial strains (Fig. 3.1C). No AFB^+ neutrophils were identified in lung leukocytes from mice infected with Rv∆*phoPR*. We interpreted these results as demonstrating a correlation between bacterial doubling time and horizontal spread of infection within the population of phagocytes recruited to the lung during the innate phase of host immunity, and a correlation of bacterial replication rate with burst size necrosis and neutrophil recruitment to the site of infection. These dynamics are curtailed when adaptive immunity reduces the proportion of MPs that remain permissive for *M. tuberculosis* replication, which in turn reduces the

rate of burst size necrosis. Total AFB^+ lung leukocytes remained elevated at 24 weeks p.i. as control of *M. tuberculosis* replication prevented burst size necrosis in a high proportion of infected MPs, extending their survival with a sub-lethal intracellular *M. tuberculosis* load.

Phagocyte bacterial burden reflects *M. tuberculosis* replication rate and host immunity. To evaluate the distribution of *M. tuberculosis* burden on a per cell basis over the course of pulmonary TB disease, AFB per cell were counted in individual MPs and neutrophils as we previously described (143). Counts were grouped into five bins comprising cells with 1-5, 6-10, 11-15, 16-20 or ≥21 AFB per cell (Fig. 3.1D, E). The top bin reflected the fact that 20 AFB was the highest number that could be reliably counted within an infected cell by light microscopy. This number also approaches the estimated burst size range for *M. tuberculosis* Erdman *in vivo* (143). In the present study, the distribution of bacillary loads within MPs at 2 weeks p.i. largely matched the prediction for a burst size model with the majority of infected cells containing 1-5 bacilli and fewer than 10% containing≥21 AFB (Fig. 3. 2). An exception was H37Ra where no MPs containing >15 bacilli were identified at that early time point. This might reflect random variation or methodological limitations but the data could reflect the induction of apoptosis by H37Ra at low MOI as was reported after *in vitro* infection of macrophages with this attenuated strain (146). A similar finding of fewer bacteria per infected phagocyte was also observed in mice challenged by aerosol with a pro-apoptotic (Δ*nuoG*) mutant of H37Rv (81).

Control of bacterial replication in TB is only achieved with the expression of adaptive immunity at the site of disease (26). By 4 weeks p.i., the proportion of MPs with high AFB loads was reduced by a factor of 10 or more (Figs. 3.1D, S1). This was consistent with immune-mediated enhancement of antimicrobial activity that is effective in most but not all *M. tuberculosis*-infected MPs with the greatest impact on the less virulent strains. By 24 weeks p.i., Erdman was the only strain where cells with $\geq$21 AFB could be detected. In H37Rv-infected mice, MPs had $\leq$20 AFB, and MPs from H37Ra-infected mice contained $\leq$10 AFB. We interpreted the persistence of cells heavily infected with Erdman and to a lesser extent H37Rv as evidence of ongoing *M. tuberculosis* replication in a reduced proportion of MPs that was balanced by elimination so that total lung CFU was held to a plateau value. This model is consistent with evidence for ongoing *M. tuberculosis* replication during the plateau phase of TB disease in mice that was detected using an unstable plasmid replication clock (135). The capacity for persistent growth under immune pressure was greatest for Erdman, less so for H37Rv and nil for H37Ra.

The infection rate and distribution of AFB load in neutrophils from mice infected with Erdman was consistent with our earlier report (143). The maximum neutrophil AFB load with Erdman was 11-15 at 2 weeks p.i., falling to 6-10 at 4 weeks and 1-5 at 24 weeks (Fig. 3.1E). At 2 weeks p.i., lungs of mice challenged with H37Rv or H37Ra had a lower proportion and total number of AFB^+ neutrophils than the Erdman group. The distribution of bacterial loads in neutrophils was limited to $\leq$10 AFB for H37Rv at 2 weeks p.i. falling to $\leq$5 by 4 weeks p.i. Neutrophils from H37Ra-infected mice contained $\leq$5 AFB at 2 weeks and 4 weeks p.i. No AFB^+ neutrophils were identified in lung

leukocytes from mice infected with Rv∆*phoPR* and by 24 weeks p.i. none were seen in H3Ra-infected mice. The temporal pattern of neutrophil infection was consistent with a model where these cells are recruited to sites of burst size necrosis, which are fewer as adaptive immunity restricts *M. tuberculosis* replication. We previously reported that Rv∆*phoPR* is attenuated for the capacity to cause macrophage necrosis, even when delivered at high MOI *in vitro* (104). That phenotype would be predicted to result in a reduced capacity to escape macrophages through cytolysis in an *M. tuberculosis* strain that retains the virulence-associated phenotype of apoptosis suppression (92, 96). This would account for its restricted horizontal spread of infection amongst recruited lung leukocytes *in vivo* and in particular for the absence of detectable uptake by neutrophils.

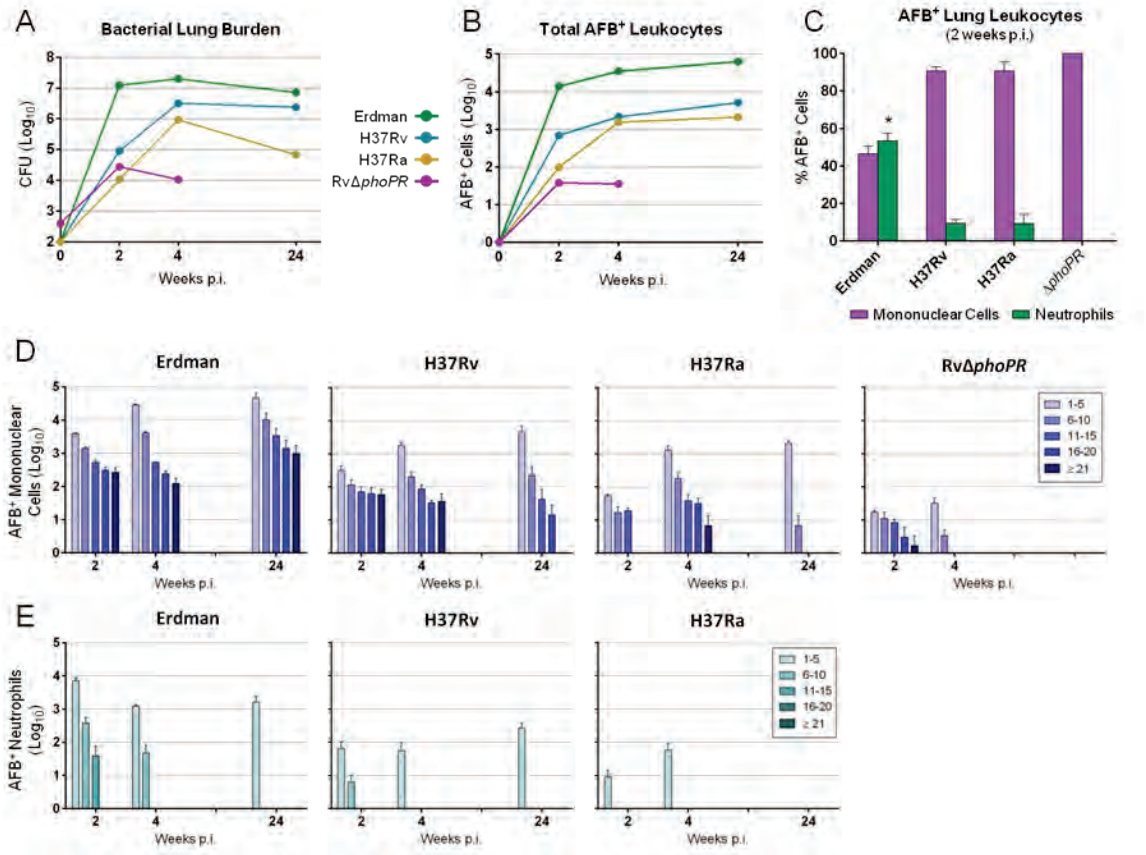

Figure 3.1 Growth and distribution of *M. tuberculosis* strains in murine host.(A) Total lung CFU of *M. tuberculosis* Erdman, H37Rv, H37Ra at 2, 4 and 24 weeks after aerosol infection (RvΔ*phoPR* at 2 and 4 weeks only). The values are presented as mean $\log_{10}$ CFU (n=4). Mice infected with Erdman had significantly higher CFU than the other mycobacterial strains, $P<0.001$ for all strains at 2 and 4 weeks p.i. and $P<0.01$ for H37Rv at 24 weeks p.i. Total lung CFU of H37Rv was significantly higher than H37Ra or RvΔ*phoPR*, $P<0.001$ at 2 and 4 weeks p.i. and $P<0.001$at 24 weeks p.i. (B) Whole lung leukocytes were isolated and cytospin preparations were made for acid-fast staining. The total number of *M. tuberculosis*-infected (AFB^+) lung leukocytes was calculated by multiplying the percent of enumerated AFB^+ cells by the total number of leukocytes in each sample. The data represent the mean $\log_{10}$ AFB^+ cells (n=3). Erdman-infected mice had the greatest number of AFB^+ leukocytes, $P<0.001$ for 2 and 4 weeks p.i. and $P<0.01$ for 24 weeks p.i. H37Rv-infected mice had significantly more AFB^+ leukocytes than mice infected with H37Ra or RvΔ*phoPR* at 2 weeks p.i., $P<0.01$. At 4 weeks p.i., both H37Rv and H37Ra infected mice had significantly more AFB^+ leukocytes than RvΔ*phoPR*-infected mice, $P<0.001$. (C) The distribution of infection between neutrophils and mononuclear phagocytes was determined by counting AFB^+ leukocytes from lungs harvested at 2 weeks p.i. Results are expressed as mean % AFB^+ cells ± SD (n=3). * $P<0.001$. Intracellular AFB loads of *M. tuberculosis* Erdman, H37Rv, H37Ra and RvΔ*phoPR* in mononuclear phagocytes (D) and neutrophils (E) at indicated time points were enumerated by microscopy. The number of AFB per cell was counted at the indicated time points with counts grouped into five bins of 1-5, 6-10, 11-15, 16-20, or ≥21 AFB. Data are presented as $\log_{10}$ AFB^+ cells in each bin ± SD. Statistically significant differences ($P<0.05$) are not shown for sake of clarity. All strains, bins and time points were compared using a Poisson regression model. Among significant differences, Erdman-infected mice yielded more AFB^+ mononuclear phagocytes and more AFB^+ neutrophils for all bins at all time points compared to the other *M. tuberculosis* strains.

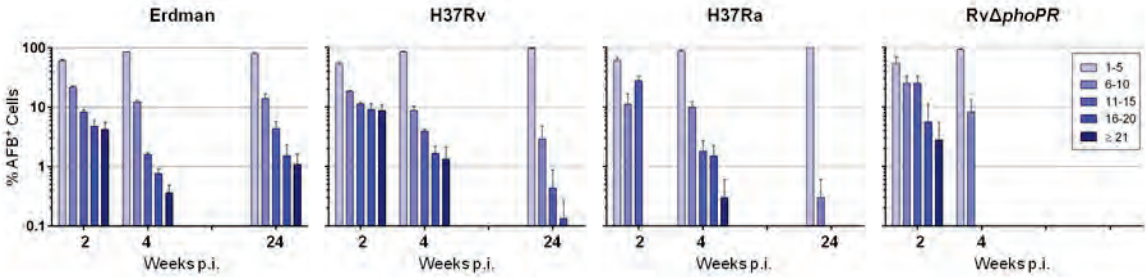

Figure 3.2. Proportion of bacillary loads in mononuclear phagocytes. Wild-type mice were challenged with *M. tuberculosis* Erdman, H37Rv, H37Ra or Rv*ΔphoPR* by aerosol. Lung leukocytes were harvested 2, 4 and 24 weeks p.i.(only 2 and 4 weeks for Rv*ΔphoPR*-infected mice) and cytospin slides were processed for Ziehl-Neelsen staining. AFB per mononuclear phagocyte were counted on cytospin samples and stratified into indicated bins. Results are expressed as mean % AFB^+ mononuclear cells within each bin ± SD.

Progressive lung pathology correlates with *M. tuberculosis* virulence. To compare pulmonary immune pathology in mice infected with Erdman, H37Rv or H37Ra, we examined H&E stained lung sections from mice challenged with a low aerosol dose of each *M. tuberculosis* strain (Fig. 3.3A). Inflammation was quantified by morphometric analysis of H&E stained sections, measuring the combined area of all the inflammatory lesions expressed as the % of total lung area examined at x20 magnification (Fig. 3.3B). At 2 weeks p.i., an average of 35 lesions per mouse was identified in the Erdman-challenged group and this inflammation occupied ~2% of total lung area. In contrast, only one lung lesion per mouse was visible in the H37Rv-infected group (0.03% of total lung area) and no lesions were visible at this magnification in lungs from mice infected with H37Ra. Inflammation in Erdman-infected mice occupied 12.5% of total lung by 4 weeks p.i. with values of 1.5% and 0.4% in mice infected with H37Rv or H37Ra, respectively. At the 24 week p.i. time point, lung architecture was extensively damaged in the Erdman group with 40% of total lung area involved. Inflammation progressed to

involve 22.6% of lung area in H37Rv-infected mice and 1.3% of total lung area in the H37Ra group. In the phase of murine TB disease following the expression of adaptive immunity (4 and 24 weeks p.i.) total AFB^+ leukocytes were nearly equal in mice infected with H37Rv vs. H37Ra group (Fig. 3.1B), yet the area of inflammation was much lower in H37Ra-infected lungs (Fig. 3.3B). Bacterial replication (reflected by high AFB per cell in MPs; Fig. 3.1D) appeared to be a more significant driver of immune pathology than total number of *M. tuberculosis*-infected leukocytes. Notably, the inflammatory infiltrates in the lungs of H37Ra-infected mice were nearly devoid of neutrophils, whereas neutrophils were common in the pulmonary immune pathology of mice infected with Erdman and, to a lesser extent, H37Rv (Fig. 3.3C). We examined 4-week p.i. lung sections immunostained for myeloperoxidase (MPO) to detect neutrophils, finding no MPO signals from H37Ra-infected mice (data not shown) whereas MPO^+ neutrophils were present in mice infected with Erdman and H37Rv.

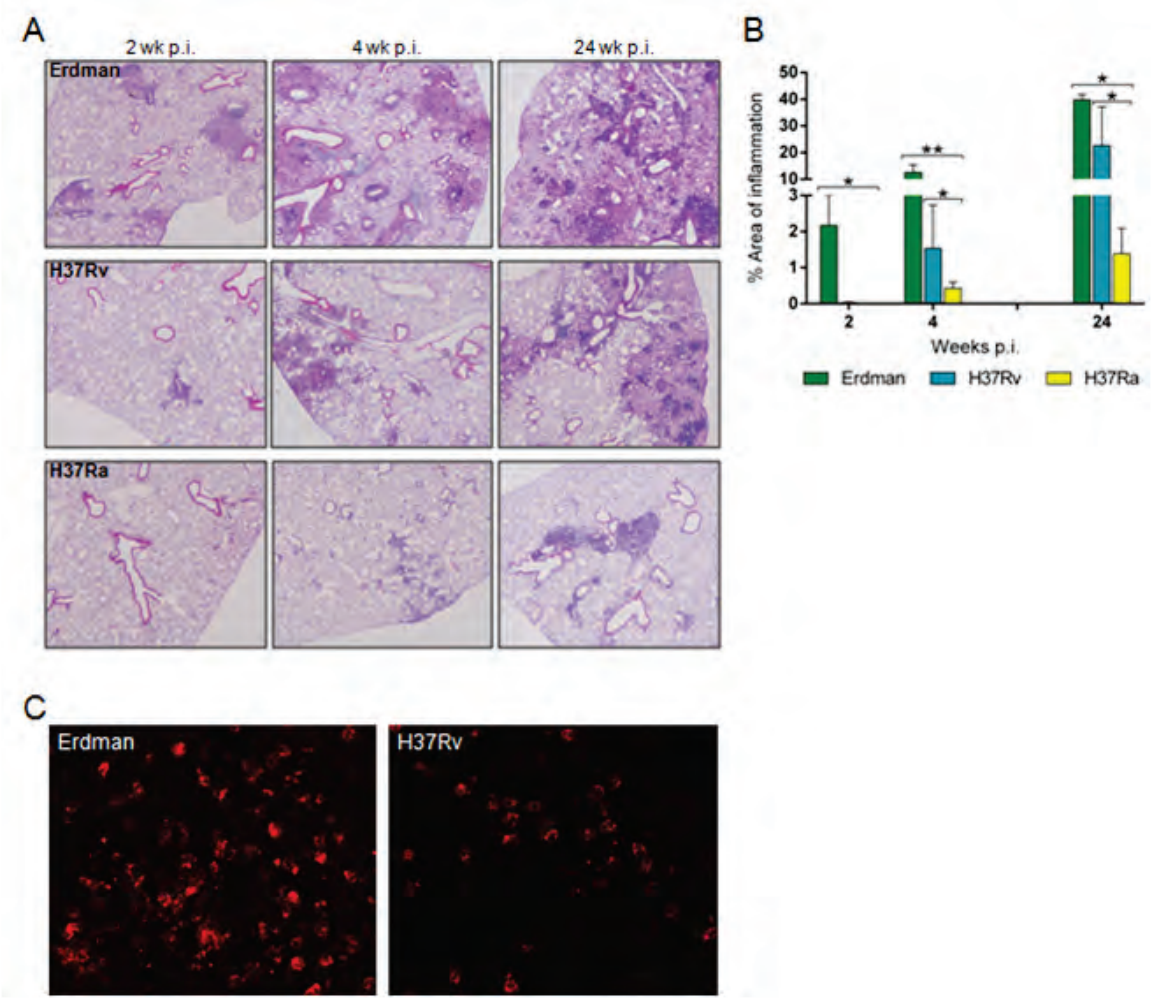

Figure 3.3 Histopathology of *M. tuberculosis*-infected lungs. Wild-type mice were challenged with ~100 CFU of *M. tuberculosis* Erdman, H37Rv or H37Ra via aerosol route. Infected lungs were harvested at indicated time points and processed for H&E staining. (A) Representative photomicrographs at 2, 4 and 24 weeks p.i. (magnification x20). (B) Cross-sectional areas of all lung tissue sections were examined by light microscopy and measured for total lung area and areas of inflammation. Calculation for the percent of area of inflammation was derived from ((cumulative summation of inflamed areas)/(total lung area surveyed) x 100). Values are mean ± SD (n=3). * P<0.05 , ** P<0.001. (C) Representative images of MPO^{+} neutrophils in red fluorescence from lung sections of Erdman- and H37Rv-infected mice at 4 weeks p.i. (magnification x400).

Increased cell death in lung lesions of *M. tuberculosis* Erdman-infected mice. To compare the extent of cell death at the tissue level in mice infected with each of the four *M. tuberculosis* strains, lungs were harvested for TUNEL assay. Lung sections from 2 and 4 weeks p.i. were examined at x20 magnification to identify five fields of inflammatory infiltrates having the most abundant $TUNEL^+$ cells in each section. In the selected fields, all $TUNEL^+$ and $TUNEL^-$ cells were counted (Fig. 3.4A). At 2 weeks p.i., Erdman yielded an average of 7.6% $TUNEL^+$ cells, which was nearly 6 fold higher than the other three strains. At this time point, the proportion of $TUNEL^+$ cells was comparable in mice infected with H37Rv, H37Ra or Rv*ΔphoPR*. At 4 weeks p.i., lesions from Erdman-infected mice contained a mean of 11.1% $TUNEL^+$ cells, while 5.0% and 2.3% of cells were $TUNEL^+$ in mice infected with H37Rv and H37Ra, respectively. At this time point, no $TUNEL^+$ cells were identified in lung sections from mice infected with Rv*ΔphoPR*. At 24 weeks p.i., extensive lung tissue damage made it unfeasible to enumerate individual $TUNEL^+$ cells, particularly in Erdman-infected mice (Fig. 3.4B). Areas of TUNEL staining were exclusively confined to necrotic lesions with densely packed leukocytes having both nuclear and cytoplasmic TUNEL staining. In these areas, cellular borders were mostly indistinguishable. The size of $TUNEL^+$ regions paralleled the area of lung inflammation observed in H&E stained lung sections.

If neutrophils are recruited to the site of TB disease by damage-associated molecular pattern molecules (DAMPs) released from MPs undergoing infection-induced necrosis, then they should be found in proximity to dying cells. To further test that prediction, we processed lung sections from 4 weeks p.i. for combined MPO immunostaining and

TUNEL assay (Fig. 3.4C). By fluorescence microscopy we observed that neutrophils predominantly accumulated in lesions where $TUNEL^+$ cells were also present. Virtually all of the $TUNEL^+$ cells identified were MPO^-, suggesting that the dead cells were predominantly MPs (147, 148). This impression was further supported by light microscopy of slides processed for colorimetric TUNEL assay (Fig. 3.4D). Although we were unable to count individual $TUNEL^+$ cells at 24 weeks p.i., we did observe clusters of neutrophils positioned in areas of abundant TUNEL signals (Fig. 3.5). Altogether, these findings demonstrate that neutrophils are recruited to the immediate vicinity of macrophages undergoing infection-induced cytolysis where they engulf bacilli released into the extracellular space.

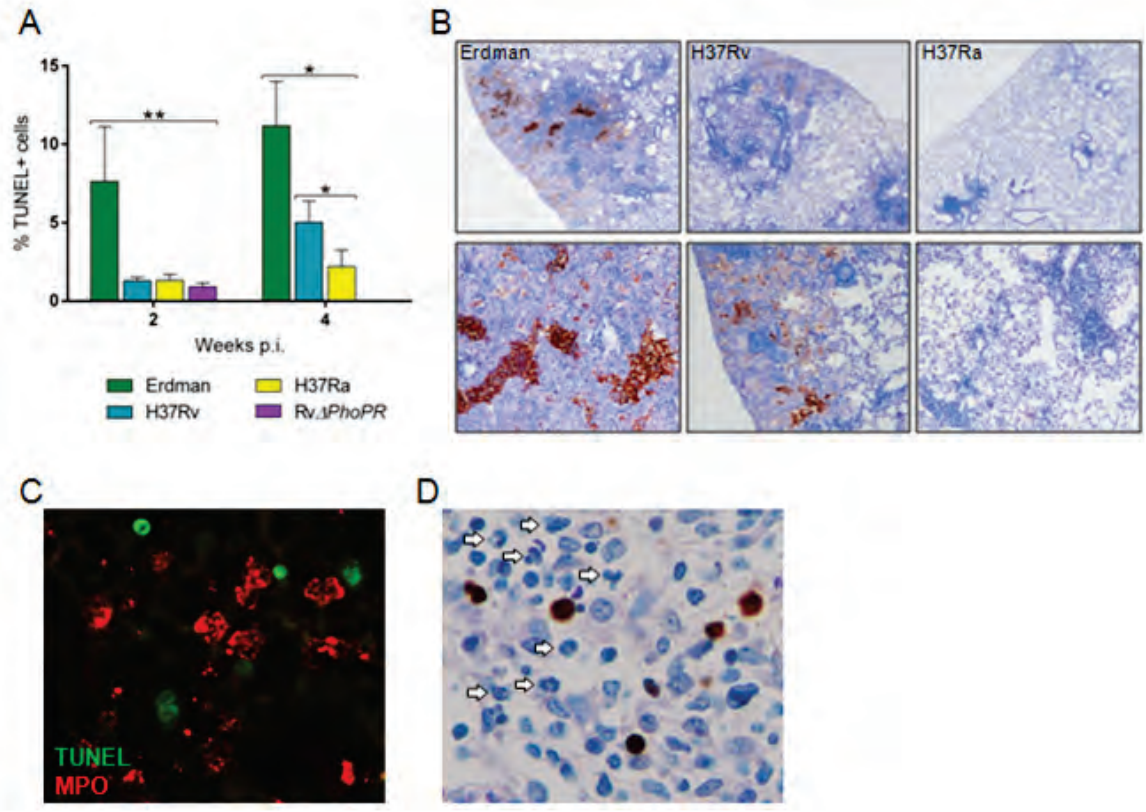

Figure 3.4 Cell death in lung lesions correlates with *M. tuberculosis* virulence. (A) Mice were infected with *M. tuberculosis* Erdman, H37Rv, H37Ra or RvΔ*phoPR* by aerosol. Lung sections were processed for colorimetric TUNEL assay and TUNEL$^+$ cells were enumerated by examining all cross-sectional areas of lung tissue sections and selecting 5 fields with the most TUNEL$^+$ signals. For each field, individual TUNEL$^+$ and TUNEL$^-$cells were counted and all 5 fields were tallied. Percent TUNEL$^+$ cells was calculated as ((total TUNEL$^+$ cells)/(total cells)x100). Values are mean ± SD (n=3). * P<0.01, ** P<0.001. (B) Representative images of highest TUNEL signals from lung tissue sections at 24 weeks p.i. (*upper panels*, magnification x20; *lower panels*, magnification x200). (C) Representative immunofluorescent image of a lung section from an Erdman-infected mouse at 4 weeks p.i. TUNEL$^+$ cells are identified by green fluorescence and MPO$^+$ neutrophils are identified by red fluorescence (magnification x400). (D) Colorimetric TUNEL assay on a representative lung section from an Erdman-infected mouse 4 weeks p.i. revealing neutrophils (*arrows*) in the vicinity of TUNEL$^+$ cells (*brown*) (magnification x400).

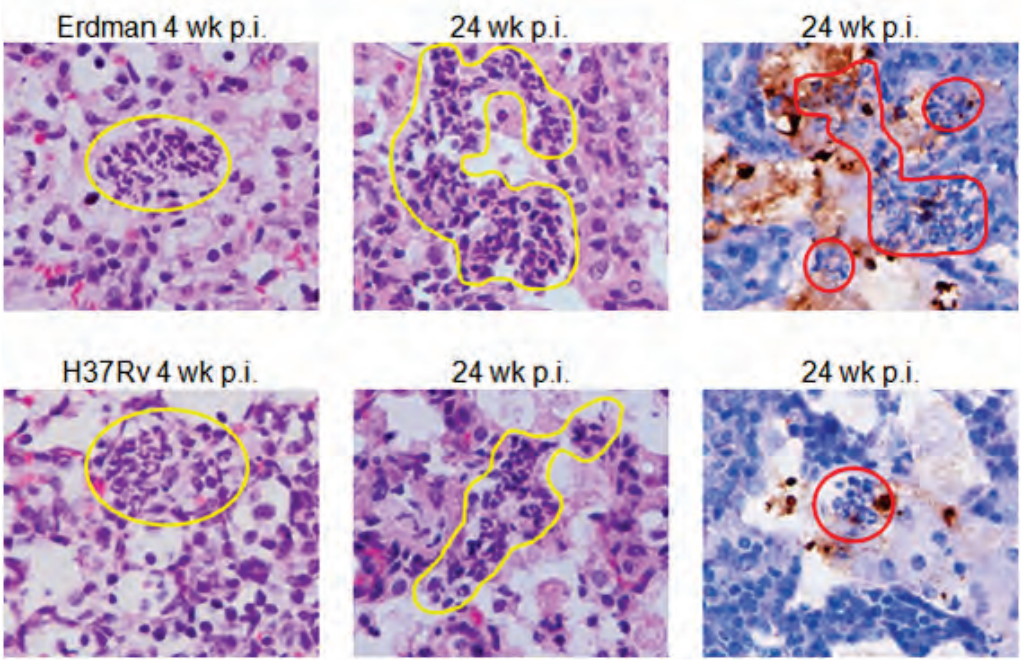

Figure 3.5. Neutrophil clusters in lung TB lesions. Lung sections from mice infected with *M. tuberculosis* Erdman or H37Rvwere processed for H&E staining or colorimetric TUNEL assay. At 4 and 24 weeks p.i. clusters of neutrophils were observed predominantly in the vicinity of macrophages (H&E staining) and TUNEL signals (brown staining).

Neutrophil infiltration in the lungs correlates with bacterial virulence. The dynamics of neutrophil recruitment and intracellular infection was strikingly different in mice infected with an *M. tuberculosis* strain of high (Erdman) vs. intermediate (H37Rv) virulence. Between 2 weeks and 4 weeks p.i., total lung neutrophils increased 4.5 fold in mice infected with Erdman and 3.5 fold with H37Rv but dropped more than 1 log by the 24 week time point (Fig. 3.6A). As a proportion of all $CD45^+$ lung leukocytes, neutrophils peaked at 4 weeks p.i. (58% and 37% for mice infected with Erdman or H37Rv, respectively) and then fell to <3% at 24 weeks (Fig. 3.6B). At each time point, total lung neutrophils recovered from mice infected with either *M. tuberculosis* strain were not significantly different but the total number and proportion of *M. tuberculosis*-

infected (AFB^+) neutrophils were significantly higher in mice infected with Erdman compared to H37Rv (Fig. 3.6A). At the 2 week p.i. time point, AFB were detected in 3.84% of total lung neutrophils from the Erdman group but in only 0.06% of neutrophils from mice infected with H37Rv. These distributions fell to 0.15% and 0.01% at 4weeks p.i. and then rebounded to 6.65% for Erdman and 3.22% for H37Rv at 24 weeks. The disproportionate number of AFB^+ neutrophils in Erdman-infected mice, despite relatively similar total lung neutrophils in H37Rv-infected mice, suggested an association between macrophage burst size necrosis with the faster replicating *M. tuberculosis* strain along with neutrophil recruitment directly to the site of infection where bacilli are engulfed. The late rise in the proportion of AFB^+ neutrophils in both groups of mice reflected a persistent population of infected cells within a shrinking pool of total lung neutrophils.

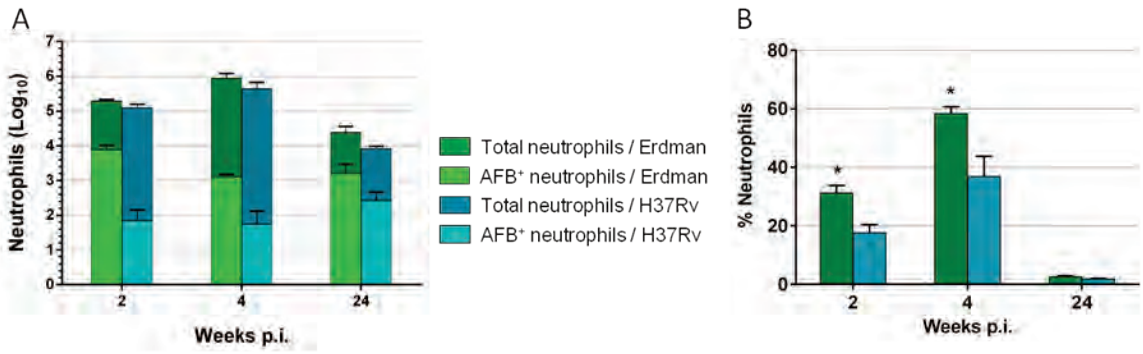

Figure 3.6 Neutrophil accumulation in the lungs of mice with TB. Mice were infected with *M. tuberculosis* Erdman or H37Rv by aerosol. At 2, 4 and 24 weeks p.i. isolated lung leukocytes were analyzed by flow cytometry. Neutrophils were defined as Ly-$6G^{hi}$ $CD11b^{hi}$cells. For AFB^+ neutrophils, lung leukocytes were harvested and cytospin slides were processed for Ziehl-Neelsen staining. AFB^+ neutrophils were identified based on nuclear morphology and acid-fast bacilli. (A) Total lung neutrophil counts and AFB^+ neutrophil counts in mice infected with *M. tuberculosis* Erdman (*green bars*) or H37Rv (*blue bars*). AFB^+ neutrophil counts in both groups (*light green and light blue bars*). Total neutrophil counts in Erdman-infected and H37Rv-infected mice were not significantly different at any time point but the number of AFB^+ neutrophils was significantly greater in Erdman-infected mice at 2 and 4 weeks p.i. $P<0.001$. (B) The proportion $CD45^+$ Ly-$6G^{hi}$ $CD11b^{hi}$ neutrophils among all $CD45^+$ lung leukocytes was higher in Erdman-infected mice (*green bars*) at 2 and 4 weeks p.i. compared to H37Rv-infected mice (*blue bars*). Data are presented as the mean ± SD (n=3)* $P<0.01$.

Cytokine profile of tuberculous lung. We considered that DAMPs might provide dominant signals for neutrophil recruitment to TB lesions, at least during the period of logarithmic increase in lung bacterial load and peak levels of burst size necrosis. An alternative explanation is that neutrophil recruitment is mainly controlled by regulated cytokine signaling networks stimulated by the infecting microbes. In that case, the uniquely high level of neutrophil recruitment and neutrophil infection in TB lesions caused by *M. tuberculosis* Erdman should be reflected by high levels of candidate chemoattractant factors and low levels of factors associated with the resolution of neutrophilic inflammation. To test that prediction, we measured eight proinflammatory cytokines in BAL fluid from mice challenged with Erdman, H37Rv, H37Ra or RvΔ*phoPR* at 2, 4 and 24 weeks p.i. (Fig. 3.7A). At 2 weeks, the levels of IL-1α, IL-1β, IL-17, JE, KC and MIP-2 were comparable in mice infected with any of the four *M. tuberculosis* strains. At 4 and 24 weeks p.i., the levels of IL-17, JE and KC in BAL fluid of Erdman-infected mice were by a statistically significant degree compared with the other two *M. tuberculosis* strains tested. The functional significance of those differences was uncertain and might reflect a result rather than a cause of greater leukocyte accumulation in the Erdman group at those time points. The BAL fluid of Erdman-infected mice also had higher levels of IL-1α and IL-1β at 24 weeks.

In contrast to the other cytokines measured, the level of IFN-γ in BAL fluid from Erdman-infected mice at 2 weeks p.i. was 14 times higher than in mice infected with H37Rv or the attenuated *M. tuberculosis* strains. Over the following two time points there was a rise and then a fall in IFN-γ levels for all *M. tuberculosis* strains but it remained

substantially higher in the Erdman-infected mice. Consistent with the BAL fluid results, the level of IFN-γ was also higher in whole lung lysate of mice infected with Erdman compared to H37Rv despite dilution with uninvolved tissue using that approach (Fig. 3.7B). The elevated levels of IL-1α and IL-1β in BAL fluid of Erdman-infected mice at 24 weeks p.i. indicated a persistent inflammatory response despite higher levels of IFN-γ in the mice infected with the most virulent strain of *M. tuberculosis* tested.

The calgranulins S100A8 and S100A9 as homodimeric or heterodimeric complexes are present constitutively at high levels in neutrophils (149). In addition to their intracellular functions, these S100 proteins are recognized as DAMPs released at high amounts at sites of infectious and non-infectious inflammatory disorders (150). Recently, Gopal et al. (151) linked S100A8/A9 proteins to neutrophil accumulation and damaging lung pathology in TB. Serum S100A8/A9 in human pulmonary TB patients was shown to directly correlate with severity of disease. We measured the S100A8/A9 protein complex in BAL fluid from mice infected with Erdman, H37Rv, H37Ra or RvΔ*phoPR* (Fig. 3.7C). The levels were comparable at 2 weeks p.i. in mice infected with any of these four *M. tuberculosis* strains but at 4 and 24 weeks, the level in BAL fluid of Erdman-infected mice was significantly higher than in mice infected with H37Rv or H37Ra. The high levels of S100A8/A9 at the later time points in Erdman-infected mice may have been both a cause and effect of greater neutrophil accumulation in that group but there was no indication that these S100 proteins were a determining factor accounting for the predominance of AFB^+ neutrophils in the Erdman group at 2 weeks p.i.

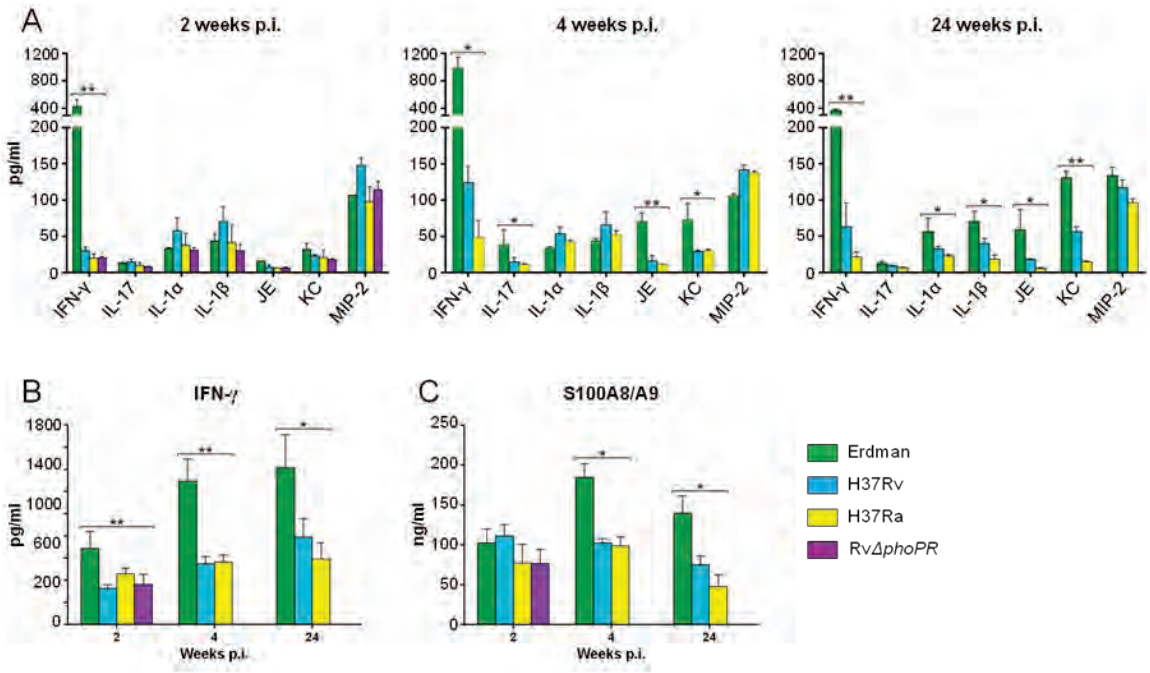

Figure 3.7 Lung cytokine levels during TB disease. The indicated cytokines were measured by ELISA of BAL fluid (A, C) and cell-free lung homogenates (B) from mice infected with indicated *M. tuberculosis* strains. Data are presented as the mean concentration± SD (n=3 or 4). * $P<0.05$, ** $P<0.001$.

Mycobacterial replication drives neutrophil recruitment in TB. It is conceivable that some property of *M. tuberculosis* Erdman other than its high replication rate and resultant burst size macrophage necrosis was responsible for the high rate of neutrophil infection in pulmonary TB lesions. To address that question, mice were challenged with 100 CFU of Erdman delivered to the lungs and then treated for 11 days with the bacteriostatic drug ethambutol (EMB) at doses of 67, 200 or 600 μg/ml in drinking water, starting on day 4 p.i. A control group received plain water. All mice were sacrificed on day 14 p.i. for determination of lung bacterial load, total AFB^+ leukocytes and the distribution of AFB load per phagocyte in MPs and in neutrophils. The 2 week time point was selected as the period of peak bacterial replication before the full expression of

adaptive immunity. Compared to untreated mice, there was a dose dependent decrease in lung CFU with EMB treatment of ~0.5 logs at 67 μg/ml and a further ~0.5 logs at 200 μg/ml (Fig. 3.8A). Lung CFU in mice treated with EMB at 600 μg/ml was ~4 logs lower than untreated controls. The total number of AFB^+ leukocytes mirrored the CFU counts (Fig. 3.8B). Treatment with EMB had a significant, dose dependent impact on the distribution of intracellular AFB loads in MPs, consistent with inhibition of bacterial replication (Fig. 3.8C). In untreated control mice, the total number of MPs containing 1-5 AFB was 1.0 log greater than the number of cells with ≥21 AFB. This spread increased to 1.7 logs and 2.3 logs in mice treated with EMB at 67 μg/ml and 200 μg/ml, respectively. No MPs containing >6 AFB were identified in mice given EMB at 600 μg/ml. There was a disproportionate reduction of AFB^+ neutrophils compared to AFB^+ MPs in mice treated with EMB (Fig. 3.8D). The ratio of AFB^+ neutrophils to AFB^+ MPs was 0.36 in control mice, falling to 0.19 and 0.17 in mice treated with at 67 μg/ml and 200 μg/ml, respectively. We interpreted these results as evidence that bacterial replication rate, reflected by the proportion of MPs with high AFB loads, drives burst size necrosis that in turn promotes neutrophil recruitment to sites of active TB disease in the lung.

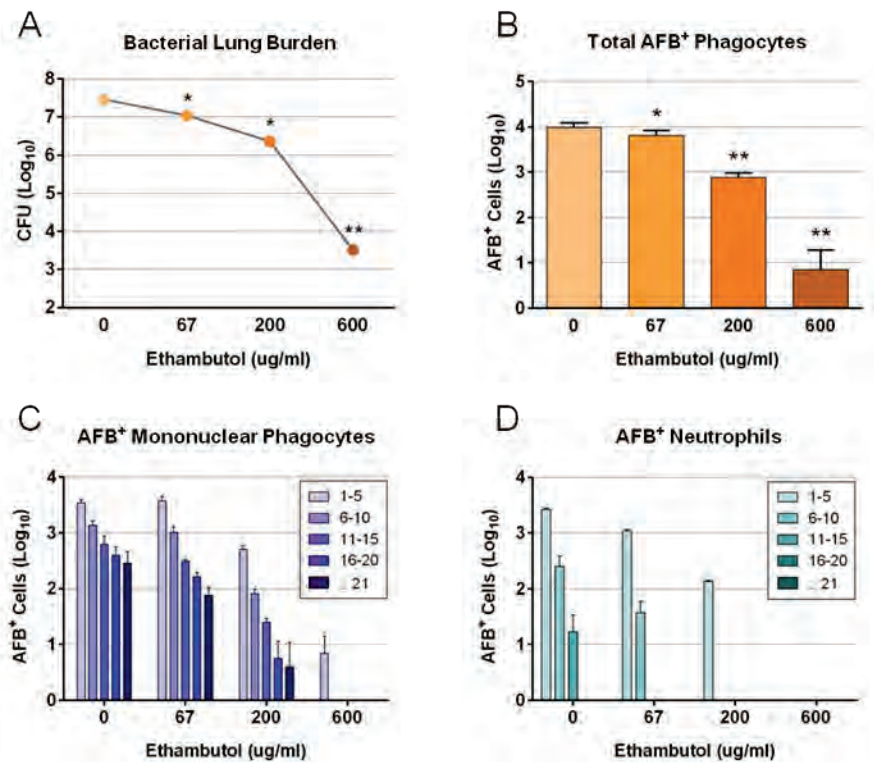

Figure 3.8 Ethambutol (EMB) treatment of mice with TB. Mice were infected with *M. tuberculosis* Erdman by aerosol and treated with ethambutol at 67, 200 or 600 µg/ml for 11 days, beginning on day 4 p.i. At 2 weeks p.i. infected lungs were harvested and plated for CFU (A) or enumerated for AFB^+ cells from cytospin slides with Ziehl-Neelsen staining (B-D). (A) Compared to untreated mice, there was a dose-dependent reduction of lung CFU in EMB-treated mice. Data represent mean (n=4). * P<0.01, ** P<0.001. (B) Total AFB^+ phagocytes also fell with increasing dosages of EMB. * P<0.01, ** P<0.001 compared to untreated mice. (C) EMB treatment resulted in a dose-dependent reduction of total AFB^+ MPs and a progressively lower proportion of mononuclear cells with high AFB loads. (D) EMB treatment resulted in a dose-dependent reduction of total AFB^+ neutrophils and a lower proportion of neutrophils with high AFB loads at each dose increment. Only untreated mice had neutrophil AFB loads of 11-15 per cell while mice treated with 600 µg/ml EMB had no detectable AFB^+ neutrophils. (B-D) Data represent mean ± SD (n=3).

3.5 Discussion

We previously reported data supporting a model of burst size necrosis for *M. tuberculosis* infected macrophages *in vitro* and *in vivo* (103, 104, 143). Following aerosol challenge, horizontal spread of *M. tuberculosis* Erdman, particularly into neutrophils, was curtailed by an effective adaptive immune response in wild-type C57BL/6 mice whereas infected neutrophils increased until death in IFN-$\gamma^{-/-}$ mice that

were incapable of limiting bacterial replication in MPs (143). The present study extended that investigation by challenging wild-type mice with four *M. tuberculosis* strains of graded virulence as a complementary approach to study the effects mycobacterial replication on intracellular bacillary load, burst size necrosis and neutrophilic inflammation.

Whether classified on the basis of replication rate, total lung bacterial load or the extent of immune pathology, Erdman was clearly the most virulent of the four *M. tuberculosis* strains tested, followed by H37Rv and then H37Ra. As expected, the mutant RvΔ*phoPR* was the most attenuated strain. The steep growth curve of Erdman between inhalation of ~100 CFU and the 2 week p.i. time point was matched by highest rate of horizontal transmission into neutrophils in that phase of TB disease. Resident alveolar macrophages are by far the predominant phagocytes in the normal alveolar airspace and therefore the most likely host cells for the first round of *M. tuberculosis* replication. Only single bacilli can be conveyed by inhalation of infectious aerosols to the alveolar airspaces, so the initial infection of alveolar macrophages begins at an MOI of one bacillus per macrophage. Our data unexpectedly demonstrate that RvΔ*phoPR* was capable of limited replication *in vivo*, exceeding 5 AFB per cell in 50% of infected MPs and reaching≥21 AFB in 3% (Fig. 3.2). The total number of RvΔ*phoPR* bacilli in the lung increased by 4-5 doublings from the initial aerosol dose. Despite this replicative capacity there was no evidence for horizontal spread of RvΔ*phoPR* to recruited leukocytes (Fig. 3.1B). That conclusion fits with the attenuated capacity for burst size

macrophage necrosis *in vitro* that we originally reported for this strain (104) along with the absence of neutrophil infection *in vivo* identified in the current study.

The disparities between H37Rv and Erdman were striking, as were some similarities between H37Rv and H37Ra. The H37Rv isolate used for our experiments was fully virulent in terms of reaching a plateau lung burden of ~10^6 CFU that persisted for 24 weeks, along with a progressive increase in pulmonary immune pathology. It is known that H37Rv can spontaneously lose the expression of the cell wall lipid phthiocerol dimycocerosate (PDIM), resulting in its attenuation (152, 153). Although the H37Rv isolate used in our study retained PDIM (data not shown), it exhibited a slower *in vivo* growth rate compared to Erdman and substantially less horizontal spread into neutrophils. At 2 weeks p.i., the proportion of AFB^+ neutrophils among all AFB^+ phagocytes was 7 fold lower in mice infected with H37Rv than in Erdman-infected mice and the proportion of *M. tuberculosis*-infected neutrophils within the total lung neutrophil population was 65 fold lower.

The initial growth curve of H37Rv in the lung was steeper than H37Ra and it maintained a high plateau burden at 24 weeks p.i., by which time the total lung CFU of H37Ra declined more than 1 log. Despite these differences, the total number of AFB^+ leukocytes in the lungs of mice infected with H37Rv or H37Ra was surprisingly close at the 4 and 24 week time points. At the last time point, the maximum intracellular bacillary burden in MPs had shifted towards lower values for H37Ra (≤10 AFB) compared to H37Rv (≤20 AFB). Among the factors that may contribute to these dynamics, we note that the survival of macrophages challenged *in vitro* with *M. tuberculosis* at MOI=1 is

prolonged by IFN-γ activation, which prevents bacilli from growing to a burst size load (93). We previously reported that IFN-γ exerts the opposite effect in macrophages with a high intracellular bacillary load (MOI=25) by accelerating necrosis (139). These effects of IFN-γ could explain the elimination of MPs containing >10 AFB at 24 weeks after infection with H37Ra that has limited or no replicative capacity at that late phase of TB disease and therefore does continuously drive some host cells to high AFB loads. Survival of MPs with a low burden intracellular AFB load would be extended while the most heavily infected cells would be eliminated.

Macrophage infection with *M. tuberculosis* has been linked to a diverse range of apoptotic and necrotic cell death modes, based mostly on evidence from *in vitro* experiments (154). Macrophages may respond to attenuated mycobacterial strains, including H37Ra, by undergoing caspase-mediated apoptosis that is believed to provide host-protective effects (74, 146). The slower growth rate of H37Ra in the first 4 weeks p.i. along with the scarcity of cells harboring >15 AFB could at least in part reflect macrophage apoptosis and the delivery of bacilli to acidified vacuoles following efferocytosis by naïve macrophages (73). Efferocytosis also provides a mechanism for spreading infection to naïve MP (81, 155), which might explain the ability of H37Ra to inhabit nearly as many lung leukocytes as H37Rv in our study. In contrast to H37Ra and some other attenuated strains, virulent *M. tuberculosis* strains suppress macrophage apoptosis to preserve a protected replication niche which they ultimately escape by triggering necrosis (103, 104, 143). This necrotic death mode shows a threshold dose effect at MOI 25 *in vitro* while evidence from mice with TB disease suggests an *in vivo*

burst size in the range of 20-40 AFB. The mechanistic basis for this bacterial load-dependent cytolysis is presently unknown but appears to be a catastrophic event following lysosomal rupture that requires an intact *M. tuberculosis* PhoPR 2-component system. Under *in vivo* conditions it is likely that additional factors play a role in cytolysis but the majority of non-viable lung leukocytes in mice with TB contain >10 bacilli (143).

Neutrophils are increasingly recognized as major hosts for intracellular infection by *M. tuberculosis* in mice and in humans (22, 118, 143). They play a complex role in TB pathogenesis with host protective effects in the initiation of adaptive immunity (25, 140) but they promote damage when present in excess at later stages of disease (138, 141, 156, 157). The determinants of neutrophil recruitment to sites of TB disease therefore assume importance as possible drug targets for host-directed therapies to limit tissue damage in TB. In the present study, infection with Erdman was associated with disproportionately high spread into neutrophils despite no significant difference in total lung neutrophil numbers compared to mice infected with H37Rv. The presence of AFB^+ neutrophils unambiguously places those cells at the site of TB disease where they must, at least initially, engulf bacilli released from necrotic MPs.

Neutrophils are recruited to sites of necrotic cell death *in vivo*, swarming to sites of sterile or infectious injury (158). In contrast, apoptotic cells release lactoferrin which acts as a "stay away" signal specifically inhibiting neutrophil but not MP migration in response to "find me" signals, thereby facilitating the non-inflammatory clearance of apoptotic cells (159). In our experiments AFB^+ neutrophils correlated with *M. tuberculosis* virulence and with time points after aerosol challenge when bacteria were

replicating at high rates and consequently triggering high rates of MP necrosis. Infection with Erdman resulted in the highest number and proportion of AFB^+ neutrophils among total neutrophils and among total AFB^+ lung leukocytes despite being the strongest inducer of IFN-γ, which was shown by Nandi et al. (24) to limit neutrophil recruitment and retention in the lungs of *M. tuberculosis*-infected mice. Neutrophil recruitment in Erdman-infected mice was not explained by the levels of several other chemoattractant factors in BAL fluid, suggesting that other signals perhaps in concert with DAMPs may override other regulatory influences. A range of neutrophil chemoattractant factors and pathways have been linked to DAMPs and neutrophil recruitment in TB and other settings, including S100A8/A9 proteins, leukotriene B4, formyl peptide receptor-2 ligands, HMGB1, purine metabolites, MIP-2 and ENA-78 among others (151, 160-162). This redundancy complicates the identification of pathways. In the present study we were unable to link the enhanced neutrophil accumulation in Erdman-infected mice with levels of MIP-2, S100A8/A9 or HMGB1 in BAL fluid. We speculate that the higher level of S100A8/A9 at later time points in Erdman-infected mice was an effect rather than a cause of neutrophil accumulation.

In summary, the data presented here and the results from our published studies (103, 104, 143) are consistent with a model of TB pathogenesis where bacterial replication in MPs reaches threshold lethal burden enabling bacilli to escape and spread infection to recruited phagocytes, including neutrophils, that respond to signals associated with necrotic cell death. The high proportion of neutrophils in TB lesions at the 24 week time point when areas of TUNEL-positivity were greatest (Fig. 3.4B) yet *M. tuberculosis*

replication even for Erdman was relatively low compared to 2 weeks p.i. (Fig. 3.1A) suggests that a feed-forward mechanism might perpetuate inflammation in more severe TB lesions. Neutrophils have relatively short half-lives *in vivo*, although there is contrasting evidence that their lifespan might be prolonged in TB or curtailed by *M. tuberculosis*-induced NETosis (81, 143). The high rate of burst size necrosis that occurs early in TB caused by fast-replicating virulent *M .tuberculosis* strains might cause neutrophils to accumulate in lesions in excess of the capacity to clear their corpses. This in turn would result in sustained release of DAMPs and other signals even as bacterial replication is restricted by IFN-γ to a limited number of permissive macrophages. Such dynamics could be a factor in the equilibrium between stable, expanding and contracting TB lesions revealed by positron emission tomography (163). Targeting pathways of neutrophil trafficking to sites of infection-induced necrosis might shift this equilibrium towards stability and contraction, thus limiting the tissue injury that is responsible for most morbidity and mortality in TB.

Chapter IV: Conclusion

4.1 Summary

As an intracellular pathogen, *Mtb* must be able to survive and establish a replication niche within the host cell. However, to spread infection, it must also be able to exit the current cell in order to invade another. Many studies have shown that virulent *Mtb* prevents apoptosis and induces necrosis which supports this lifestyle. The work from Lee et al. (103, 104) correlated necrotic death of macrophages and high intracellular mycobacterial load proposing the escape mechanism of virulent *Mtb* is to trigger cytolysis when it reaches a threshold value. One of the goals of this thesis was to determine if *in vitro* high MOI induced cell death was applicable to the fate of *Mtb*-infected MPs in the lungs during TB disease *in vivo*. The results presented in this thesis confirmed the *in vitro* observations and conformed to the predictions made by the burst size hypothesis. We presented a model of tuberculosis where infection was initiated by mycobacterial invasion of a few alveolar macrophages which progressed to the burst size value inducing cytolysis and facilitating dissemination. The freed bacilli infect naïve phagocytes and the cycle of invasion, replication and escape repeats.

Data from enumerating intracellular bacilli of infected MPs and neutrophils exhibited the predictions made based on the burst size hypothesis. Infected phagocytes displayed a diverse range of intracellular loads, but the proportion of cells with the lowest number of bacilli greatly outnumbered those with higher intracellular burden and infected cells at

burst size bacillary loads at were a minority. The median burst size was determined to be in the range of 20-40 bacilli. The percent of heavily infected cells were the highest during period of logarithmic bacterial expansion and then decreased significantly following the expression of adaptive immunity. This indicated that as heavily infected cells died they were replaced at a lower rate due to the host response limiting bacterial replication. It also greatly broadened the range between heavily infected cells and those with only a few bacilli. Examination of infected cells from *Mtb*-infected IFN-$\gamma^{-/-}$ mice revealed that in the absence of IFN-γ, unrestricted bacterial replication yielded progressive increase in heavily infected cells indicating IFN-γ rescued many infected cells from progressing to burst size in WT mice. Inspection of heavily infected cells from mice reflected morphological features from *in vitro* studies, substantial membrane damage and condensed nuclei without fragmentation. Taken together, the data supported the concept that bacterial replication in MPs reached a lethal cytolytic threshold (or burst size) which freed the bacilli to spread infection.

During the course of disease the primary host cell that harbored the pathogen shifted from one cell type to another. In the early stage of infection MPs were the only infected leukocytes, most likely represented by resident alveolar macrophages, the first cells to encounter the bacilli. After adaptive immunity, mDCs were the primary host cells, followed by RMs by 10 weeks p.i. AMs were a minority throughout the infection from all time points studied. During week 2-3 p.i. when bacterial population was expanding logarithmically, neutrophils were the primary host cells even though the proportion of neutrophils in the airspace never exceeded 20% of the total phagocytes. This indicated

that neutrophils were being recruited directly to the sites of necrotic MPs. The proportion of highest burdened neutrophils peaked during log growth of *Mtb*. In IFN-$\gamma^{-/-}$ mice, the number of infected neutrophils progressively increased until their death. Neutrophils from IFN-$\gamma^{-/-}$ mice exhibited formation of NETs and their current role in TB disease is unknown. The burst size hypothesis was revised to reflect the observation that four different phagocytes served as the primary host cell for *Mtb* (Fig. 4.1). A better understanding is needed in the interactions between each of these cell types and *Mtb*.

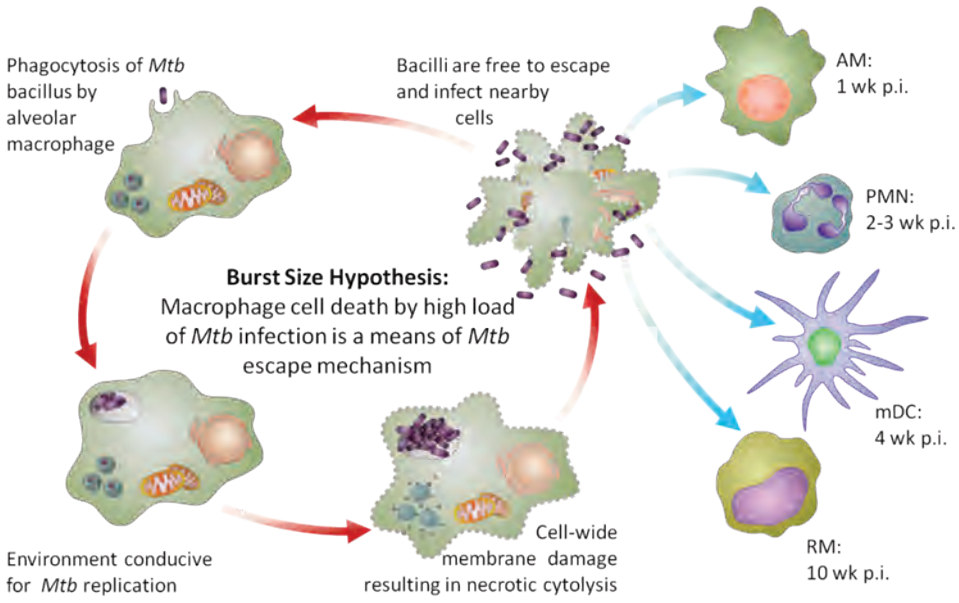

Figure 4.1. Revised burst size model. After burst size necrosis the liberated bacilli are free to invade neighboring cells. Based on the time course of infection, the primary host cell will shift from one type to another. Resident alveolar macrophages will be the first cells to encounter the pathogen, during logarithmic bacterial replication, neutrophils are the primary host. After the expression of adaptive immunity, myeloid dendritic cells will be the major host cell, then during persistent phase of infection, recruited monocytes/macrophages will take the role.

The rationale behind the second part of this thesis was based on noteworthy observations from the first part of this study. When bacterial replication increased logarithmically at early stage of TB disease, between week two and three p.i., neutrophils were the dominant host comprising roughly 50% of all infected cells although disproportionately, they were a minority of all phagocytes in the airspace. After the expression of adaptive immunity bacterial replication was constrained and infected neutrophils decreased to about 10% of all infected phagocytes. When bacterial replication was unrestricted, as seen in INF-$\gamma^{-/-}$ mice, the proportion of infected neutrophils progressively increased along with heavily infected MPs until death (143). This data indicated there is a link between burst size necrosis of MPs and infected neutrophils. The second part of this thesis described the continued study of burst size necrosis and the investigation into the impact of mycobacterial replication on burst size necrosis and the effect of neutrophil accumulation in the lungs. Based on the data from the first study, our hypothesis states that mycobacterial replication drives burst size necrosis of MPs which recruits neutrophils to the sites of infection (Fig. 4.2).

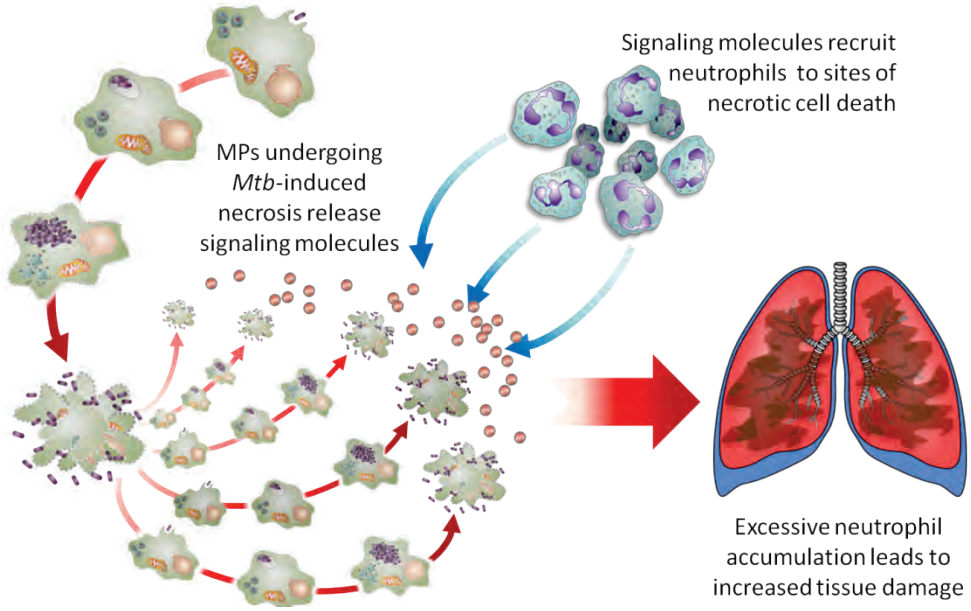

Figure 4.2. Burst size necrosis of MPs drives neutrophil recruitment. MPs infected with virulent *Mtb* undergo burst size necrosis when bacterial replication reaches a threshold value. Cell lysis of MPs release bacteria along with signaling molecules, such as DAMPs, that recruit neutrophils to sites of infection. Faster replicating *Mtb* will promote more burst size necrosis causing more neutrophils to traffic to the lung resulting in severe lung pathology.

To test that theory, four different strains of *Mtb* were selected, graded in virulence and ranked from the most virulent to the most attenuated: Erdman, H37Rv, H37Ra, mutant lacking *phoPR* coding region (RvΔ*phoPR*). WT mice were infected with one of four strains and the infection outcome of each strain on the host was characterized by evaluating the lung bacterial burden, the distribution of bacillary loads of infected MPs and neutrophils, cell death rates, lung inflammation and immune response. The data from this study showed amongst all strains, Erdman proved to be consistently the most virulent. With the fastest replication rate, Erdman-infected mice yielded the highest lung bacterial load paired with the largest pool of infected cells. Heavily infected MPs and largest number of infected neutrophils were also seen in Erdman-infected mice. This was

the case for all times points tested. Erdman-infected mice produced the greatest amount of pulmonary inflammation with the most lesions and highest rates of cell death from TUNEL assays. Immunofluorescent images of MPO^+ neutrophils from Erdman-infected mice had the highest signals compared to zero signals from H37Ra-infected mice at 4 weeks p.i. MPO^+ signals were also seen in proximity to $TUNEL^+$ cells for Erdman-infected mice. TUNEL stained lung section showed clusters of neutrophils localized in areas of TUNEL signals for both Erdman and H37Rv-infected lungs. Upon comparing the outcome of Erdman and H37Rv infections, while both groups had comparable amounts of lung neutrophils, Erdman-infected neutrophils were over 2 logs higher than H37Rv-infected neutrophils at 2 weeks p.i. and remained over a log at 4 weeks. This indicates that neutrophils are being recruited directly to the sites of MP necrosis. Evaluation of the cytokines from BAL at 2 weeks p.i. proved nothing significant from all strains tested, except for the high level of IFN-γ from Erdman-infected mice. When Erdman-infected mice were treated with Ethambutol, a bacteriostatic agent, in a dose-dependent manner, the bacterial lung burden, total number of infected cells including heavily infected MPs and infected neutrophils all decreased.

The data from this study showed that none of the chemoattractant cytokines examined were responsible for the neutrophil recruitment in Erdman-infected mice. Erdman infection was a strong inducer of IFN-γ. Although IFN-γ has been shown to reduce neutrophil recruitment in the lungs during TB disease (24), our data suggests that some other signal possesses a stronger chemoattractant capacity to override the regulation of known cytokines. The possible candidate could be a DAMP. Studies have shown DAMPs

are released when *Mtb*-infected cells die via necrosis and many have been identified with neutrophil recruitment activity (13, 151, 160). In the presence of leukotriene B4 (LTB4), neutrophils at sites of infection could increase their accumulation by amplifying the cell death signal to distant neutrophils through intracellular signaling mediated by LTB4 (158). LTB4 has also been shown to be elevated in the plasma from pulmonary TB patients and patients with advanced lesions had the highest values (164). This could be due to excess neutrophil accumulation.

In summary, the work presented in this thesis provides some insight to our understanding of the interaction between *Mtb* and the host in context of the cell death. This study showed that MPs infected with *Mtb* undergo necrotic cell death related to the high intracellular bacterial burden and this is a common fate for *Mtb*-infected MPs in TB disease *in vivo*. The primary host cell harboring *Mtb* during the course of TB disease shifted from one type to another. Lastly, work presented in this study revealed faster replicating *Mtb* strains promoted high rates of burst size necrosis recruiting more neutrophils to necrotic sites regardless of cytokine regulations increasing their infection rate and lung inflammation. Collectively, infected neutrophils can serve as biomarkers for poorly controlled *Mtb* infection.

4.2 Discussion

The onset of adaptive immunity in the host dramatically changes the interaction between the host and the pathogen. In the context of *Mtb* infection, the induction of IFN-γ has a profound impact on bacterial replication as reflected by the distribution of bacterial load per MP as demonstrated in this study between IFN-$\gamma^{-/-}$ and WT mice at 21

days p.i. (Fig. 2.9). This data shows the effect of IFN-γ in altering the bacterial loads, thus increasing the spread between the heaviest infected cells and least infected cells. The difference in the bacterial loads between these two groups may indicate that IFN-γ is involved in modifying the burst size of mononuclear phagocytes. A lower burst size is advantageous for the host as demonstrated from the in silico model (Fig. 2.14). A once sub-lethal load during innate phase of infection may be the new burst size after adaptive immunity thus significantly reducing the number of heavily infected cells.

This study demonstrated the association between bacterial replication and increased neutrophil accumulation and infection. It is possible that there is no preferential recruitment of neutrophils to sites of infection and rather *Mtb*-infected MPs and those dying from burst size necrosis release inflammatory signals to recruit any and all myeloid cells to these necrotic lesions. The peak of infected neutrophils during logarithmic period of bacterial replication may be more representative of their ability to arrive at these sites faster than other leukocytes. Neutrophils can move at speeds at least twice that of macrophages (165), allowing them to arrive at necrotic sites and engulf extracellular bacteria prior to the arrival of macrophages. Additionally, neutrophils have been shown to engulf bacteria faster than macrophages (166) which could also account for the higher proportion of infected neutrophils during this time. Although this study was unable to link neutrophil-specific signaling molecules to its enhanced recruitment, the very fact that DAMPs are passively released from necrotic cells and certain DAMPs are potent at recruiting neutrophils should be further investigated. The ability to target pathways of neutrophil migration to necrotic sites may lead to reduced lung injury in patients with TB.

One of the highlights from this work revealed that during the course of TB disease, a diverse set of phagocytic cells harbors *Mtb* (AM, RM mDC and neutrophils) and that infected AM only accounted for approximately 10% of infected MPs. We also identified a population of resident AM that phenotypically shifted to resemble mDC. It is not known if these cells are functionally mDC and in what capacity they serve either the host or the pathogen. While the interaction between *Mtb* and macrophages has been studied extensively, it is clear that further analysis is needed in the interaction between *Mtb* and the other host phagocytes. Determining whether these cells provide a permissive or restrictive replication environment, response to IFN-γ and regulation of host cell fate are just some of the factors that need to be identified in order to enhance our understanding of host-pathogen interactions during *Mtb* infection.

Cell death and *Mtb* infection are intricately entwined as death of the host cell is an essential part of the pathogen's life cycle. In this study we demonstrated that during TB disease, necrosis is a common form of cell death for infected MPs and this death modality is a means for horizontal spread of infection. Although we were able to correlate internalized bacterial numbers with cell lysis, the bacterial factor(s) involved in triggering necrosis is yet unknown. Several studies have shown that ESAT-6, a secreted mycobacterial protein, is capable of cytolysis, damaging phagosomal membranes and involved in macrophage and neutrophil necrosis (86, 87, 167, 168). However, *in vitro* studies of *Mtb* infection-induced cytolysis revealed that necrotic cell death occurred when BMDM were challenged with BCG and an *Mtb* deletion mutant lacking both RD1 and EspA indicating this type of death was independent of ESAT-6 (103, 104). Perhaps

mycobacterial gene(s) under the control of PhoPR signaling system could be involved since macrophages infected with high MOI of Rv*ΔphoPR* failed to cause cytolysis (104).

Previous *in vitro* work also characterized the cellular events of lysosomal rupture and lethal mitochondrial damage preceding necrosis (104), but the mechanism behind the initiation of these critical events are yet to be discovered. Perhaps these unknown factors are also involved in the microdisruptions of the plasma membrane that was observed by Divangahi et al. during *Mtb* infection (94). Studies have linked necrosis triggered by *Mtb* to the production of host eicosanoid LXA_4 induced by virulent strains of *Mtb* which simultaneously inhibits PGE_2 production thereby preventing plasma membrane repair. Additionally, the suppression of PGE_2 diminished its protective effect on the mitochondrial membrane compromising the stability of its inner membrane resulting in necrosis (94, 98, 99). It is unclear how *Mtb* influences the inhibition or production of these host eicosanoids. Future investigation into these areas will hopefully provide answers that will yield successful drug targets for therapies that will inhibit *Mtb*-induced cytolysis and/or block the pathways that cause necrotic cell death of MPs by host-derived therapies.

References

1. Philips, J. A., and J. D. Ernst. 2012. Tuberculosis pathogenesis and immunity. *Annual review of pathology* 7: 353-384.
2. Russell, D. G., C. E. Barry, 3rd, and J. L. Flynn. 2010. Tuberculosis: what we don't know can, and does, hurt us. *Science* 328: 852-856.
3. Cosma, C. L., D. R. Sherman, and L. Ramakrishnan. 2003. The secret lives of the pathogenic mycobacteria. *Annual review of microbiology* 57: 641-676.
4. Russell, D. G., P. J. Cardona, M. J. Kim, S. Allain, and F. Altare. 2009. Foamy macrophages and the progression of the human tuberculosis granuloma. *Nature immunology* 10: 943-948.
5. O'Garra, A., P. S. Redford, F. W. McNab, C. I. Bloom, R. J. Wilkinson, and M. P. Berry. 2013. The immune response in tuberculosis. *Annual review of immunology* 31: 475-527.
6. Russell, D. G. 2007. Who puts the tubercle in tuberculosis? *Nature reviews. Microbiology* 5: 39-47.
7. Glickman, M. S., and W. R. Jacobs, Jr. 2001. Microbial pathogenesis of Mycobacterium tuberculosis: dawn of a discipline. *Cell* 104: 477-485.
8. Barry, C. E., 3rd, H. I. Boshoff, V. Dartois, T. Dick, S. Ehrt, J. Flynn, D. Schnappinger, R. J. Wilkinson, and D. Young. 2009. The spectrum of latent tuberculosis: rethinking the biology and intervention strategies. *Nature reviews. Microbiology* 7: 845-855.
9. Ernst, J. D. 1998. Macrophage receptors for Mycobacterium tuberculosis. *Infection and immunity* 66: 1277-1281.
10. Kleinnijenhuis, J., M. Oosting, L. A. Joosten, M. G. Netea, and R. Van Crevel. 2011. Innate immune recognition of Mycobacterium tuberculosis. *Clinical & developmental immunology* 2011: 405310.
11. Saraav, I., S. Singh, and S. Sharma. 2014. Outcome of Mycobacterium tuberculosis and Toll-like receptor interaction: immune response or immune evasion? *Immunology and cell biology*.
12. Fremond, C. M., D. Togbe, E. Doz, S. Rose, V. Vasseur, I. Maillet, M. Jacobs, B. Ryffel, and V. F. Quesniaux. 2007. IL-1 receptor-mediated signal is an essential component of MyD88-dependent innate response to Mycobacterium tuberculosis infection. *J Immunol* 179: 1178-1189.
13. Mayer-Barber, K. D., D. L. Barber, K. Shenderov, S. D. White, M. S. Wilson, A. Cheever, D. Kugler, S. Hieny, P. Caspar, G. Nunez, D. Schlueter, R. A. Flavell, F. S. Sutterwala, and A. Sher. 2010. Caspase-1 independent IL-1beta production is critical for host resistance to mycobacterium tuberculosis and does not require TLR signaling in vivo. *J Immunol* 184: 3326-3330.

14. Scanga, C. A., A. Bafica, C. G. Feng, A. W. Cheever, S. Hieny, and A. Sher. 2004. MyD88-deficient mice display a profound loss in resistance to Mycobacterium tuberculosis associated with partially impaired Th1 cytokine and nitric oxide synthase 2 expression. *Infection and immunity* 72: 2400-2404.
15. Liu, P. T., S. Stenger, H. Li, L. Wenzel, B. H. Tan, S. R. Krutzik, M. T. Ochoa, J. Schauber, K. Wu, C. Meinken, D. L. Kamen, M. Wagner, R. Bals, A. Steinmeyer, U. Zugel, R. L. Gallo, D. Eisenberg, M. Hewison, B. W. Hollis, J. S. Adams, B. R. Bloom, and R. L. Modlin. 2006. Toll-like receptor triggering of a vitamin D-mediated human antimicrobial response. *Science* 311: 1770-1773.
16. Yuk, J. M., D. M. Shin, H. M. Lee, C. S. Yang, H. S. Jin, K. K. Kim, Z. W. Lee, S. H. Lee, J. M. Kim, and E. K. Jo. 2009. Vitamin D3 induces autophagy in human monocytes/macrophages via cathelicidin. *Cell host & microbe* 6: 231-243.
17. Gandotra, S., S. Jang, P. J. Murray, P. Salgame, and S. Ehrt. 2007. Nucleotide-binding oligomerization domain protein 2-deficient mice control infection with Mycobacterium tuberculosis. *Infection and immunity* 75: 5127-5134.
18. Divangahi, M., S. Mostowy, F. Coulombe, R. Kozak, L. Guillot, F. Veyrier, K. S. Kobayashi, R. A. Flavell, P. Gros, and M. A. Behr. 2008. NOD2-deficient mice have impaired resistance to Mycobacterium tuberculosis infection through defective innate and adaptive immunity. *J Immunol* 181: 7157-7165.
19. Bhatt, K., and P. Salgame. 2007. Host innate immune response to Mycobacterium tuberculosis. *Journal of clinical immunology* 27: 347-362.
20. Sada-Ovalle, I., A. Chiba, A. Gonzales, M. B. Brenner, and S. M. Behar. 2008. Innate invariant NKT cells recognize Mycobacterium tuberculosis-infected macrophages, produce interferon-gamma, and kill intracellular bacteria. *PLoS pathogens* 4: e1000239.
21. Singh, A., A. B. Dey, A. Mohan, and D. K. Mitra. 2014. Programmed death-1 receptor suppresses gamma-IFN producing NKT cells in human tuberculosis. *Tuberculosis (Edinb)* 94: 197-206.
22. Eum, S. Y., J. H. Kong, M. S. Hong, Y. J. Lee, J. H. Kim, S. H. Hwang, S. N. Cho, L. E. Via, and C. E. Barry, 3rd. 2010. Neutrophils are the predominant infected phagocytic cells in the airways of patients with active pulmonary TB. *Chest* 137: 122-128.
23. Lowe, D. M., P. S. Redford, R. J. Wilkinson, A. O'Garra, and A. R. Martineau. 2012. Neutrophils in tuberculosis: friend or foe? *Trends in immunology* 33: 14-25.
24. Nandi, B., and S. M. Behar. 2011. Regulation of neutrophils by interferon-gamma limits lung inflammation during tuberculosis infection. *The Journal of experimental medicine* 208: 2251-2262.

25. Blomgran, R., and J. D. Ernst. 2011. Lung neutrophils facilitate activation of naive antigen-specific CD4+ T cells during Mycobacterium tuberculosis infection. *J Immunol* 186: 7110-7119.
26. North, R. J., and Y. J. Jung. 2004. Immunity to tuberculosis. *Annual review of immunology* 22: 599-623.
27. Cooper, A. M., D. K. Dalton, T. A. Stewart, J. P. Griffin, D. G. Russell, and I. M. Orme. 1993. Disseminated tuberculosis in interferon gamma gene-disrupted mice. *The Journal of experimental medicine* 178: 2243-2247.
28. Cooper, A. M., J. Magram, J. Ferrante, and I. M. Orme. 1997. Interleukin 12 (IL-12) is crucial to the development of protective immunity in mice intravenously infected with mycobacterium tuberculosis. *The Journal of experimental medicine* 186: 39-45.
29. Casanova, J. L., and L. Abel. 2002. Genetic dissection of immunity to mycobacteria: the human model. *Annual review of immunology* 20: 581-620.
30. MacMicking, J. D., R. J. North, R. LaCourse, J. S. Mudgett, S. K. Shah, and C. F. Nathan. 1997. Identification of nitric oxide synthase as a protective locus against tuberculosis. *Proceedings of the National Academy of Sciences of the United States of America* 94: 5243-5248.
31. Gupta, A., A. Kaul, A. G. Tsolaki, U. Kishore, and S. Bhakta. 2012. Mycobacterium tuberculosis: immune evasion, latency and reactivation. *Immunobiology* 217: 363-374.
32. Chen, C. Y., D. Huang, R. C. Wang, L. Shen, G. Zeng, S. Yao, Y. Shen, L. Halliday, J. Fortman, M. McAllister, J. Estep, R. Hunt, D. Vasconcelos, G. Du, S. A. Porcelli, M. H. Larsen, W. R. Jacobs, Jr., B. F. Haynes, N. L. Letvin, and Z. W. Chen. 2009. A critical role for CD8 T cells in a nonhuman primate model of tuberculosis. *PLoS pathogens* 5: e1000392.
33. Kozakiewicz, L., Y. Chen, J. Xu, Y. Wang, K. Dunussi-Joannopoulos, Q. Ou, J. L. Flynn, S. A. Porcelli, W. R. Jacobs, Jr., and J. Chan. 2013. B cells regulate neutrophilia during Mycobacterium tuberculosis infection and BCG vaccination by modulating the interleukin-17 response. *PLoS pathogens* 9: e1003472.
34. Torrado, E., J. J. Fountain, R. T. Robinson, C. A. Martino, J. E. Pearl, J. Rangel-Moreno, M. Tighe, R. Dunn, and A. M. Cooper. 2013. Differential and site specific impact of B cells in the protective immune response to Mycobacterium tuberculosis in the mouse. *PloS one* 8: e61681.
35. Cooper, A. M., K. D. Mayer-Barber, and A. Sher. 2011. Role of innate cytokines in mycobacterial infection. *Mucosal immunology* 4: 252-260.
36. van Crevel, R., T. H. Ottenhoff, and J. W. van der Meer. 2002. Innate immunity to Mycobacterium tuberculosis. *Clinical microbiology reviews* 15: 294-309.

37. Todde, V., M. Veenhuis, and I. J. van der Klei. 2009. Autophagy: principles and significance in health and disease. *Biochimica et biophysica acta* 1792: 3-13.
38. Ni Cheallaigh, C., J. Keane, E. C. Lavelle, J. C. Hope, and J. Harris. 2011. Autophagy in the immune response to tuberculosis: clinical perspectives. *Clinical and experimental immunology* 164: 291-300.
39. Gutierrez, M. G., S. S. Master, S. B. Singh, G. A. Taylor, M. I. Colombo, and V. Deretic. 2004. Autophagy is a defense mechanism inhibiting BCG and Mycobacterium tuberculosis survival in infected macrophages. *Cell* 119: 753-766.
40. Singh, S. B., A. S. Davis, G. A. Taylor, and V. Deretic. 2006. Human IRGM induces autophagy to eliminate intracellular mycobacteria. *Science* 313: 1438-1441.
41. Shin, D. M., J. M. Yuk, H. M. Lee, S. H. Lee, J. W. Son, C. V. Harding, J. M. Kim, R. L. Modlin, and E. K. Jo. 2010. Mycobacterial lipoprotein activates autophagy via TLR2/1/CD14 and a functional vitamin D receptor signalling. *Cellular microbiology* 12: 1648-1665.
42. Shi, C. S., and J. H. Kehrl. 2008. MyD88 and Trif target Beclin 1 to trigger autophagy in macrophages. *The Journal of biological chemistry* 283: 33175-33182.
43. Watson, R. O., P. S. Manzanillo, and J. S. Cox. 2012. Extracellular M. tuberculosis DNA targets bacteria for autophagy by activating the host DNA-sensing pathway. *Cell* 150: 803-815.
44. Harris, J., S. A. De Haro, S. S. Master, J. Keane, E. A. Roberts, M. Delgado, and V. Deretic. 2007. T helper 2 cytokines inhibit autophagic control of intracellular Mycobacterium tuberculosis. *Immunity* 27: 505-517.
45. Kumar, D., L. Nath, M. A. Kamal, A. Varshney, A. Jain, S. Singh, and K. V. Rao. 2010. Genome-wide analysis of the host intracellular network that regulates survival of Mycobacterium tuberculosis. *Cell* 140: 731-743.
46. Romagnoli, A., M. P. Etna, E. Giacomini, M. Pardini, M. E. Remoli, M. Corazzari, L. Falasca, D. Goletti, V. Gafa, R. Simeone, G. Delogu, M. Piacentini, R. Brosch, G. M. Fimia, and E. M. Coccia. 2012. ESX-1 dependent impairment of autophagic flux by Mycobacterium tuberculosis in human dendritic cells. *Autophagy* 8: 1357-1370.
47. Shin, D. M., B. Y. Jeon, H. M. Lee, H. S. Jin, J. M. Yuk, C. H. Song, S. H. Lee, Z. W. Lee, S. N. Cho, J. M. Kim, R. L. Friedman, and E. K. Jo. 2010. Mycobacterium tuberculosis eis regulates autophagy, inflammation, and cell death through redox-dependent signaling. *PLoS pathogens* 6: e1001230.
48. Shui, W., C. J. Petzold, A. Redding, J. Liu, A. Pitcher, L. Sheu, T. Y. Hsieh, J. D. Keasling, and C. R. Bertozzi. 2011. Organelle membrane proteomics reveals differential influence of mycobacterial lipoglycans on

macrophage phagosome maturation and autophagosome accumulation. *Journal of proteome research* 10: 339-348.

49. Russell, D. G., B. C. Vanderven, S. Glennie, H. Mwandumba, and R. S. Heyderman. 2009. The macrophage marches on its phagosome: dynamic assays of phagosome function. *Nature reviews. Immunology* 9: 594-600.
50. Fratti, R. A., J. M. Backer, J. Gruenberg, S. Corvera, and V. Deretic. 2001. Role of phosphatidylinositol 3-kinase and Rab5 effectors in phagosomal biogenesis and mycobacterial phagosome maturation arrest. *The Journal of cell biology* 154: 631-644.
51. Fratti, R. A., J. Chua, I. Vergne, and V. Deretic. 2003. Mycobacterium tuberculosis glycosylated phosphatidylinositol causes phagosome maturation arrest. *Proceedings of the National Academy of Sciences of the United States of America* 100: 5437-5442.
52. Scherr, N., P. Muller, D. Perisa, B. Combaluzier, P. Jeno, and J. Pieters. 2009. Survival of pathogenic mycobacteria in macrophages is mediated through autophosphorylation of protein kinase G. *Journal of bacteriology* 191: 4546-4554.
53. Rohde, K., R. M. Yates, G. E. Purdy, and D. G. Russell. 2007. Mycobacterium tuberculosis and the environment within the phagosome. *Immunological reviews* 219: 37-54.
54. Sturgill-Koszycki, S., P. H. Schlesinger, P. Chakraborty, P. L. Haddix, H. L. Collins, A. K. Fok, R. D. Allen, S. L. Gluck, J. Heuser, and D. G. Russell. 1994. Lack of acidification in Mycobacterium phagosomes produced by exclusion of the vesicular proton-ATPase. *Science* 263: 678-681.
55. Davis, A. S., I. Vergne, S. S. Master, G. B. Kyei, J. Chua, and V. Deretic. 2007. Mechanism of inducible nitric oxide synthase exclusion from mycobacterial phagosomes. *PLoS pathogens* 3: e186.
56. Bryk, R., C. D. Lima, H. Erdjument-Bromage, P. Tempst, and C. Nathan. 2002. Metabolic enzymes of mycobacteria linked to antioxidant defense by a thioredoxin-like protein. *Science* 295: 1073-1077.
57. Flynn, J. L., and J. Chan. 2003. Immune evasion by Mycobacterium tuberculosis: living with the enemy. *Current opinion in immunology* 15: 450-455.
58. Ruan, J., G. St John, S. Ehrt, L. Riley, and C. Nathan. 1999. noxR3, a novel gene from Mycobacterium tuberculosis, protects Salmonella typhimurium from nitrosative and oxidative stress. *Infection and immunity* 67: 3276-3283.
59. Ehrt, S., M. U. Shiloh, J. Ruan, M. Choi, S. Gunzburg, C. Nathan, Q. Xie, and L. W. Riley. 1997. A novel antioxidant gene from Mycobacterium tuberculosis. *The Journal of experimental medicine* 186: 1885-1896.
60. Piddington, D. L., F. C. Fang, T. Laessig, A. M. Cooper, I. M. Orme, and N. A. Buchmeier. 2001. Cu,Zn superoxide dismutase of Mycobacterium

tuberculosis contributes to survival in activated macrophages that are generating an oxidative burst. *Infection and immunity* 69: 4980-4987.

61. Ng, V. H., J. S. Cox, A. O. Sousa, J. D. MacMicking, and J. D. McKinney. 2004. Role of KatG catalase-peroxidase in mycobacterial pathogenesis: countering the phagocyte oxidative burst. *Molecular microbiology* 52: 1291-1302.
62. Hmama, Z., R. Gabathuler, W. A. Jefferies, G. de Jong, and N. E. Reiner. 1998. Attenuation of HLA-DR expression by mononuclear phagocytes infected with Mycobacterium tuberculosis is related to intracellular sequestration of immature class II heterodimers. *J Immunol* 161: 4882-4893.
63. Wojciechowski, W., J. DeSanctis, E. Skamene, and D. Radzioch. 1999. Attenuation of MHC class II expression in macrophages infected with Mycobacterium bovis bacillus Calmette-Guerin involves class II transactivator and depends on the Nramp1 gene. *J Immunol* 163: 2688-2696.
64. Noss, E. H., C. V. Harding, and W. H. Boom. 2000. Mycobacterium tuberculosis inhibits MHC class II antigen processing in murine bone marrow macrophages. *Cellular immunology* 201: 63-74.
65. Noss, E. H., R. K. Pai, T. J. Sellati, J. D. Radolf, J. Belisle, D. T. Golenbock, W. H. Boom, and C. V. Harding. 2001. Toll-like receptor 2-dependent inhibition of macrophage class II MHC expression and antigen processing by 19-kDa lipoprotein of Mycobacterium tuberculosis. *J Immunol* 167: 910-918.
66. Ramachandra, L., E. Noss, W. H. Boom, and C. V. Harding. 2001. Processing of Mycobacterium tuberculosis antigen 85B involves intraphagosomal formation of peptide-major histocompatibility complex II complexes and is inhibited by live bacilli that decrease phagosome maturation. *The Journal of experimental medicine* 194: 1421-1432.
67. Elmore, S. 2007. Apoptosis: a review of programmed cell death. *Toxicologic pathology* 35: 495-516.
68. Creagh, E. M., H. Conroy, and S. J. Martin. 2003. Caspase-activation pathways in apoptosis and immunity. *Immunological reviews* 193: 10-21.
69. Riedl, S. J., and G. S. Salvesen. 2007. The apoptosome: signalling platform of cell death. *Nature reviews. Molecular cell biology* 8: 405-413.
70. Youle, R. J., and A. Strasser. 2008. The BCL-2 protein family: opposing activities that mediate cell death. *Nature reviews. Molecular cell biology* 9: 47-59.
71. Segal, M., S. Niazi, M. P. Simons, S. A. Galati, and J. G. Zangrilli. 2007. Bid activation during induction of extrinsic and intrinsic apoptosis in eosinophils. *Immunology and cell biology* 85: 518-524.
72. Lamkanfi, M., and V. M. Dixit. 2010. Manipulation of host cell death pathways during microbial infections. *Cell host & microbe* 8: 44-54.

73. Martin, C. J., M. G. Booty, T. R. Rosebrock, C. Nunes-Alves, D. M. Desjardins, I. Keren, S. M. Fortune, H. G. Remold, and S. M. Behar. 2012. Efferocytosis is an innate antibacterial mechanism. *Cell host & microbe* 12: 289-300.
74. Martin, C. J., K. N. Peters, and S. M. Behar. 2014. Macrophages clean up: efferocytosis and microbial control. *Current opinion in microbiology* 17: 17-23.
75. Golstein, P., and G. Kroemer. 2007. Cell death by necrosis: towards a molecular definition. *Trends in biochemical sciences* 32: 37-43.
76. Vanden Berghe, T., A. Linkermann, S. Jouan-Lanhouet, H. Walczak, and P. Vandenabeele. 2014. Regulated necrosis: the expanding network of non-apoptotic cell death pathways. *Nature reviews. Molecular cell biology* 15: 135-147.
77. Papayannopoulos, V., and A. Zychlinsky. 2009. NETs: a new strategy for using old weapons. *Trends in immunology* 30: 513-521.
78. Bauernfeind, F., and V. Hornung. 2013. Of inflammasomes and pathogens--sensing of microbes by the inflammasome. *EMBO molecular medicine* 5: 814-826.
79. Velmurugan, K., B. Chen, J. L. Miller, S. Azogue, S. Gurses, T. Hsu, M. Glickman, W. R. Jacobs, Jr., S. A. Porcelli, and V. Briken. 2007. Mycobacterium tuberculosis nuoG is a virulence gene that inhibits apoptosis of infected host cells. *PLoS pathogens* 3: e110.
80. Miller, J. L., K. Velmurugan, M. J. Cowan, and V. Briken. 2010. The type I NADH dehydrogenase of Mycobacterium tuberculosis counters phagosomal NOX2 activity to inhibit TNF-alpha-mediated host cell apoptosis. *PLoS pathogens* 6: e1000864.
81. Blomgran, R., L. Desvignes, V. Briken, and J. D. Ernst. 2012. Mycobacterium tuberculosis inhibits neutrophil apoptosis, leading to delayed activation of naive CD4 T cells. *Cell host & microbe* 11: 81-90.
82. Hinchey, J., S. Lee, B. Y. Jeon, R. J. Basaraba, M. M. Venkataswamy, B. Chen, J. Chan, M. Braunstein, I. M. Orme, S. C. Derrick, S. L. Morris, W. R. Jacobs, Jr., and S. A. Porcelli. 2007. Enhanced priming of adaptive immunity by a proapoptotic mutant of Mycobacterium tuberculosis. *The Journal of clinical investigation* 117: 2279-2288.
83. Edwards, K. M., M. H. Cynamon, R. K. Voladri, C. C. Hager, M. S. DeStefano, K. T. Tham, D. L. Lakey, M. R. Bochan, and D. S. Kernodle. 2001. Iron-cofactored superoxide dismutase inhibits host responses to Mycobacterium tuberculosis. *American journal of respiratory and critical care medicine* 164: 2213-2219.
84. Sun, J., V. Singh, A. Lau, R. W. Stokes, A. Obregon-Henao, I. M. Orme, D. Wong, Y. Av-Gay, and Z. Hmama. 2013. Mycobacterium tuberculosis nucleoside diphosphate kinase inactivates small GTPases leading to evasion of innate immunity. *PLoS pathogens* 9: e1003499.

85. Hsu, T., S. M. Hingley-Wilson, B. Chen, M. Chen, A. Z. Dai, P. M. Morin, C. B. Marks, J. Padiyar, C. Goulding, M. Gingery, D. Eisenberg, R. G. Russell, S. C. Derrick, F. M. Collins, S. L. Morris, C. H. King, and W. R. Jacobs, Jr. 2003. The primary mechanism of attenuation of bacillus Calmette-Guerin is a loss of secreted lytic function required for invasion of lung interstitial tissue. *Proceedings of the National Academy of Sciences of the United States of America* 100: 12420-12425.
86. Welin, A., D. Eklund, O. Stendahl, and M. Lerm. 2011. Human macrophages infected with a high burden of ESAT-6-expressing M. tuberculosis undergo caspase-1- and cathepsin B-independent necrosis. *PloS one* 6: e20302.
87. Simeone, R., A. Bobard, J. Lippmann, W. Bitter, L. Majlessi, R. Brosch, and J. Enninga. 2012. Phagosomal rupture by Mycobacterium tuberculosis results in toxicity and host cell death. *PLoS pathogens* 8: e1002507.
88. Kumar, D., and S. Narayanan. 2012. pknE, a serine/threonine kinase of Mycobacterium tuberculosis modulates multiple apoptotic paradigms. *Infection, genetics and evolution : journal of molecular epidemiology and evolutionary genetics in infectious diseases* 12: 737-747.
89. Wang, Q., S. Liu, Y. Tang, Q. Liu, and Y. Yao. 2014. MPT64 protein from Mycobacterium tuberculosis inhibits apoptosis of macrophages through NF-kB-miRNA21-Bcl-2 pathway. *PloS one* 9: e100949.
90. Gan, H., J. Lee, F. Ren, M. Chen, H. Kornfeld, and H. G. Remold. 2008. Mycobacterium tuberculosis blocks crosslinking of annexin-1 and apoptotic envelope formation on infected macrophages to maintain virulence. *Nature immunology* 9: 1189-1197.
91. Chen, M., H. Gan, and H. G. Remold. 2006. A mechanism of virulence: virulent Mycobacterium tuberculosis strain H37Rv, but not attenuated H37Ra, causes significant mitochondrial inner membrane disruption in macrophages leading to necrosis. *J Immunol* 176: 3707-3716.
92. Keane, J., H. G. Remold, and H. Kornfeld. 2000. Virulent Mycobacterium tuberculosis strains evade apoptosis of infected alveolar macrophages. *J Immunol* 164: 2016-2020.
93. Park, J. S., M. H. Tamayo, M. Gonzalez-Juarrero, I. M. Orme, and D. J. Ordway. 2006. Virulent clinical isolates of Mycobacterium tuberculosis grow rapidly and induce cellular necrosis but minimal apoptosis in murine macrophages. *Journal of leukocyte biology* 79: 80-86.
94. Divangahi, M., M. Chen, H. Gan, D. Desjardins, T. T. Hickman, D. M. Lee, S. Fortune, S. M. Behar, and H. G. Remold. 2009. Mycobacterium tuberculosis evades macrophage defenses by inhibiting plasma membrane repair. *Nature immunology* 10: 899-906.
95. Oddo, M., T. Renno, A. Attinger, T. Bakker, H. R. MacDonald, and P. R. Meylan. 1998. Fas ligand-induced apoptosis of infected human macrophages reduces the viability of intracellular Mycobacterium tuberculosis. *J Immunol* 160: 5448-5454.

96. Spira, A., J. D. Carroll, G. Liu, Z. Aziz, V. Shah, H. Kornfeld, and J. Keane. 2003. Apoptosis genes in human alveolar macrophages infected with virulent or attenuated Mycobacterium tuberculosis: a pivotal role for tumor necrosis factor. *American journal of respiratory cell and molecular biology* 29: 545-551.
97. Balcewicz-Sablinska, M. K., J. Keane, H. Kornfeld, and H. G. Remold. 1998. Pathogenic Mycobacterium tuberculosis evades apoptosis of host macrophages by release of TNF-R2, resulting in inactivation of TNF-alpha. *J Immunol* 161: 2636-2641.
98. Chen, M., M. Divangahi, H. Gan, D. S. Shin, S. Hong, D. M. Lee, C. N. Serhan, S. M. Behar, and H. G. Remold. 2008. Lipid mediators in innate immunity against tuberculosis: opposing roles of PGE2 and LXA4 in the induction of macrophage death. *The Journal of experimental medicine* 205: 2791-2801.
99. Behar, S. M., M. Divangahi, and H. G. Remold. 2010. Evasion of innate immunity by Mycobacterium tuberculosis: is death an exit strategy? *Nature reviews. Microbiology* 8: 668-674.
100. Bafica, A., C. A. Scanga, C. Serhan, F. Machado, S. White, A. Sher, and J. Aliberti. 2005. Host control of Mycobacterium tuberculosis is regulated by 5-lipoxygenase-dependent lipoxin production. *The Journal of clinical investigation* 115: 1601-1606.
101. Tobin, D. M., J. C. Vary, Jr., J. P. Ray, G. S. Walsh, S. J. Dunstan, N. D. Bang, D. A. Hagge, S. Khadge, M. C. King, T. R. Hawn, C. B. Moens, and L. Ramakrishnan. 2010. The lta4h locus modulates susceptibility to mycobacterial infection in zebrafish and humans. *Cell* 140: 717-730.
102. Mayer-Barber, K. D., B. B. Andrade, S. D. Oland, E. P. Amaral, D. L. Barber, J. Gonzales, S. C. Derrick, R. Shi, N. P. Kumar, W. Wei, X. Yuan, G. Zhang, Y. Cai, S. Babu, M. Catalfamo, A. M. Salazar, L. E. Via, C. E. Barry, 3rd, and A. Sher. 2014. Host-directed therapy of tuberculosis based on interleukin-1 and type I interferon crosstalk. *Nature* 511: 99-103.
103. Lee, J., H. G. Remold, M. H. Ieong, and H. Kornfeld. 2006. Macrophage apoptosis in response to high intracellular burden of Mycobacterium tuberculosis is mediated by a novel caspase-independent pathway. *J Immunol* 176: 4267-4274.
104. Lee, J., T. Repasy, K. Papavinasasundaram, C. Sassetti, and H. Kornfeld. 2011. Mycobacterium tuberculosis induces an atypical cell death mode to escape from infected macrophages. *PloS one* 6: e18367.
105. Lee, J., M. Hartman, and H. Kornfeld. 2009. Macrophage apoptosis in tuberculosis. *Yonsei medical journal* 50: 1-11.
106. Martens, G. W., M. C. Arikan, J. Lee, F. Ren, D. Greiner, and H. Kornfeld. 2007. Tuberculosis susceptibility of diabetic mice. *American journal of respiratory cell and molecular biology* 37: 518-524.
107. Wilson, A. A., G. J. Murphy, H. Hamakawa, L. W. Kwok, S. Srinivasan, A. H. Hovav, R. C. Mulligan, S. Amar, B. Suki, and D. N. Kotton. 2010.

Amelioration of emphysema in mice through lentiviral transduction of long-lived pulmonary alveolar macrophages. *The Journal of clinical investigation* 120: 379-389.

108. Murphy, G. J., G. Mostoslavsky, D. N. Kotton, and R. C. Mulligan. 2006. Exogenous control of mammalian gene expression via modulation of translational termination. *Nature medicine* 12: 1093-1099.
109. Ray, J. C., J. L. Flynn, and D. E. Kirschner. 2009. Synergy between individual TNF-dependent functions determines granuloma performance for controlling Mycobacterium tuberculosis infection. *J Immunol* 182: 3706-3717.
110. Fallahi-Sichani, M., M. El-Kebir, S. Marino, D. E. Kirschner, and J. J. Linderman. 2011. Multiscale computational modeling reveals a critical role for TNF-alpha receptor 1 dynamics in tuberculosis granuloma formation. *J Immunol* 186: 3472-3483.
111. Marino, S., M. El-Kebir, and D. Kirschner. 2011. A hybrid multi-compartment model of granuloma formation and T cell priming in tuberculosis. *Journal of theoretical biology* 280: 50-62.
112. Marino, S., I. B. Hogue, C. J. Ray, and D. E. Kirschner. 2008. A methodology for performing global uncertainty and sensitivity analysis in systems biology. *Journal of theoretical biology* 254: 178-196.
113. Kirschner, D. E., and J. J. Linderman. 2009. Mathematical and computational approaches can complement experimental studies of host-pathogen interactions. *Cellular microbiology* 11: 531-539.
114. McLean, R. A., W. L. Sanders, and W. W. Stroup. 1991. A unified approach to mixed linear models. *The American Statistician* 45: 54-64.
115. Corbeil, R. R., and S. R. Searle. 1976. Restricted maximum likelihood (REML) estimation of variance components in the mixed model. *Technometrics* 18: 31-38.
116. Daniel, W. W. 1990. *Applied Nonparametric Statistics*. Duxbury, Pacific Grove, CA.
117. Ordway, D., M. Henao-Tamayo, I. M. Orme, and M. Gonzalez-Juarrero. 2005. Foamy macrophages within lung granulomas of mice infected with Mycobacterium tuberculosis express molecules characteristic of dendritic cells and antiapoptotic markers of the TNF receptor-associated factor family. *J Immunol* 175: 3873-3881.
118. Wolf, A. J., B. Linas, G. J. Trevejo-Nunez, E. Kincaid, T. Tamura, K. Takatsu, and J. D. Ernst. 2007. Mycobacterium tuberculosis infects dendritic cells with high frequency and impairs their function in vivo. *J Immunol* 179: 2509-2519.
119. Gonzalez-Juarrero, M., T. S. Shim, A. Kipnis, A. P. Junqueira-Kipnis, and I. M. Orme. 2003. Dynamics of macrophage cell populations during murine pulmonary tuberculosis. *J Immunol* 171: 3128-3135.
120. Higgins, D. M., J. Sanchez-Campillo, A. G. Rosas-Taraco, J. R. Higgins, E. J. Lee, I. M. Orme, and M. Gonzalez-Juarrero. 2008. Relative levels of

M-CSF and GM-CSF influence the specific generation of macrophage populations during infection with Mycobacterium tuberculosis. *J Immunol* 180: 4892-4900.

121. Mayer-Barber, K. D., B. B. Andrade, D. L. Barber, S. Hieny, C. G. Feng, P. Caspar, S. Oland, S. Gordon, and A. Sher. 2011. Innate and adaptive interferons suppress IL-1alpha and IL-1beta production by distinct pulmonary myeloid subsets during Mycobacterium tuberculosis infection. *Immunity* 35: 1023-1034.
122. Gonzalez-Juarrero, M., and I. M. Orme. 2001. Characterization of murine lung dendritic cells infected with Mycobacterium tuberculosis. *Infection and immunity* 69: 1127-1133.
123. Khader, S. A., S. Partida-Sanchez, G. Bell, D. M. Jelley-Gibbs, S. Swain, J. E. Pearl, N. Ghilardi, F. J. Desauvage, F. E. Lund, and A. M. Cooper. 2006. Interleukin 12p40 is required for dendritic cell migration and T cell priming after Mycobacterium tuberculosis infection. *The Journal of experimental medicine* 203: 1805-1815.
124. Wolf, A. J., L. Desvignes, B. Linas, N. Banaiee, T. Tamura, K. Takatsu, and J. D. Ernst. 2008. Initiation of the adaptive immune response to Mycobacterium tuberculosis depends on antigen production in the local lymph node, not the lungs. *The Journal of experimental medicine* 205: 105-115.
125. Tian, T., J. Woodworth, M. Skold, and S. M. Behar. 2005. In vivo depletion of CD11c+ cells delays the CD4+ T cell response to Mycobacterium tuberculosis and exacerbates the outcome of infection. *J Immunol* 175: 3268-3272.
126. Murphy, J., R. Summer, A. A. Wilson, D. N. Kotton, and A. Fine. 2008. The prolonged life-span of alveolar macrophages. *American journal of respiratory cell and molecular biology* 38: 380-385.
127. Hagge, D. A., N. A. Ray, J. L. Krahenbuhl, and L. B. Adams. 2004. An in vitro model for the lepromatous leprosy granuloma: fate of Mycobacterium leprae from target macrophages after interaction with normal and activated effector macrophages. *J Immunol* 172: 7771-7779.
128. Lahiri, R., B. Randhawa, and J. L. Krahenbuhl. 2010. Infection of mouse macrophages with viable Mycobacterium leprae does not induce apoptosis. *The Journal of infectious diseases* 201: 1736-1742.
129. Gold, M. C., H. D. Ehlinger, M. S. Cook, S. K. Smyk-Pearson, P. T. Wille, R. M. Ungerleider, D. A. Lewinsohn, and D. M. Lewinsohn. 2008. Human innate Mycobacterium tuberculosis-reactive alphabetaTCR+ thymocytes. *PLoS pathogens* 4: e39.
130. Brinkmann, V., and A. Zychlinsky. 2007. Beneficial suicide: why neutrophils die to make NETs. *Nature reviews. Microbiology* 5: 577-582.
131. Brinkmann, V., U. Reichard, C. Goosmann, B. Fauler, Y. Uhlemann, D. S. Weiss, Y. Weinrauch, and A. Zychlinsky. 2004. Neutrophil extracellular traps kill bacteria. *Science* 303: 1532-1535.

132. Urban, C. F., D. Ermert, M. Schmid, U. Abu-Abed, C. Goosmann, W. Nacken, V. Brinkmann, P. R. Jungblut, and A. Zychlinsky. 2009. Neutrophil extracellular traps contain calprotectin, a cytosolic protein complex involved in host defense against Candida albicans. *PLoS pathogens* 5: e1000639.
133. Martens, G. W., T. Vallerskog, and H. Kornfeld. 2012. Hypercholesterolemic LDL receptor-deficient mice mount a neutrophilic response to tuberculosis despite the timely expression of protective immunity. *Journal of leukocyte biology* 91: 849-857.
134. Ramos-Kichik, V., R. Mondragon-Flores, M. Mondragon-Castelan, S. Gonzalez-Pozos, S. Muniz-Hernandez, O. Rojas-Espinosa, R. Chacon-Salinas, S. Estrada-Parra, and I. Estrada-Garcia. 2009. Neutrophil extracellular traps are induced by Mycobacterium tuberculosis. *Tuberculosis (Edinb)* 89: 29-37.
135. Gill, W. P., N. S. Harik, M. R. Whiddon, R. P. Liao, J. E. Mittler, and D. R. Sherman. 2009. A replication clock for Mycobacterium tuberculosis. *Nature medicine* 15: 211-214.
136. Ryan, R. C., M. P. O'Sullivan, and J. Keane. 2011. Mycobacterium tuberculosis infection induces non-apoptotic cell death of human dendritic cells. *BMC microbiology* 11: 237.
137. Bodnar, K. A., N. V. Serbina, and J. L. Flynn. 2001. Fate of Mycobacterium tuberculosis within murine dendritic cells. *Infection and immunity* 69: 800-809.
138. Martens, G. W., M. C. Arikan, J. Lee, F. Ren, T. Vallerskog, and H. Kornfeld. 2008. Hypercholesterolemia impairs immunity to tuberculosis. *Infection and immunity* 76: 3464-3472.
139. Lee, J., and H. Kornfeld. 2010. Interferon-gamma Regulates the Death of M. tuberculosis-Infected Macrophages. *Journal of cell death* 3: 1-11.
140. Kang, D. D., Y. Lin, J. R. Moreno, T. D. Randall, and S. A. Khader. 2011. Profiling early lung immune responses in the mouse model of tuberculosis. *PloS one* 6: e16161.
141. Keller, C., R. Hoffmann, R. Lang, S. Brandau, C. Hermann, and S. Ehlers. 2006. Genetically determined susceptibility to tuberculosis in mice causally involves accelerated and enhanced recruitment of granulocytes. *Infection and immunity* 74: 4295-4309.
142. Narasaraju, T., E. Yang, R. P. Samy, H. H. Ng, W. P. Poh, A. A. Liew, M. C. Phoon, N. van Rooijen, and V. T. Chow. 2011. Excessive neutrophils and neutrophil extracellular traps contribute to acute lung injury of influenza pneumonitis. *The American journal of pathology* 179: 199-210.
143. Repasy, T., J. Lee, S. Marino, N. Martinez, D. E. Kirschner, G. Hendricks, S. Baker, A. A. Wilson, D. N. Kotton, and H. Kornfeld. 2013. Intracellular bacillary burden reflects a burst size for Mycobacterium tuberculosis in vivo. *PLoS pathogens* 9: e1003190.

144. North, R. J., and A. A. Izzo. 1993. Mycobacterial virulence. Virulent strains of Mycobacteria tuberculosis have faster in vivo doubling times and are better equipped to resist growth-inhibiting functions of macrophages in the presence and absence of specific immunity. *The Journal of experimental medicine* 177: 1723-1733.
145. Chackerian, A. A., J. M. Alt, T. V. Perera, C. C. Dascher, and S. M. Behar. 2002. Dissemination of Mycobacterium tuberculosis Is Influenced by Host Factors and Precedes the Initiation of T-Cell Immunity. *Infection and immunity* 70: 4501-4509.
146. Keane, J., M. K. Balcewicz-Sablinska, H. G. Remold, G. L. Chupp, B. B. Meek, M. J. Fenton, and H. Kornfeld. 1997. Infection by Mycobacterium tuberculosis promotes human alveolar macrophage apoptosis. *Infection and immunity* 65: 298-304.
147. Altmann, C., A. Andres-Hernando, R. H. McMahan, N. Ahuja, Z. He, C. J. Rivard, C. L. Edelstein, L. Barthel, W. J. Janssen, and S. Faubel. 2012. Macrophages mediate lung inflammation in a mouse model of ischemic acute kidney injury. *American journal of physiology. Renal physiology* 302: F421-432.
148. Akbarshahi, H., M. Menzel, M. Posaric Bauden, A. Rosendahl, and R. Andersson. 2012. Enrichment of murine CD68+ CCR2+ and CD68+ CD206+ lung macrophages in acute pancreatitis-associated acute lung injury. *PloS one* 7: e42654.
149. Goyette, J., and C. L. Geczy. 2011. Inflammation-associated S100 proteins: new mechanisms that regulate function. *Amino acids* 41: 821-842.
150. Ehrchen, J. M., C. Sunderkotter, D. Foell, T. Vogl, and J. Roth. 2009. The endogenous Toll-like receptor 4 agonist S100A8/S100A9 (calprotectin) as innate amplifier of infection, autoimmunity, and cancer. *Journal of leukocyte biology* 86: 557-566.
151. Gopal, R., L. Monin, D. Torres, S. Slight, S. Mehra, K. C. McKenna, B. A. Fallert Junecko, T. A. Reinhart, J. Kolls, R. Baez-Saldana, A. Cruz-Lagunas, T. S. Rodriguez-Reyna, N. P. Kumar, P. Tessier, J. Roth, M. Selman, E. Becerril-Villanueva, J. Baquera-Heredia, B. Cumming, V. O. Kasprowicz, A. J. Steyn, S. Babu, D. Kaushal, J. Zuniga, T. Vogl, J. Rangel-Moreno, and S. A. Khader. 2013. S100A8/A9 proteins mediate neutrophilic inflammation and lung pathology during tuberculosis. *American journal of respiratory and critical care medicine* 188: 1137-1146.
152. Cox, J. S., B. Chen, M. McNeil, and W. R. Jacobs, Jr. 1999. Complex lipid determines tissue-specific replication of Mycobacterium tuberculosis in mice. *Nature* 402: 79-83.
153. Camacho, L. R., D. Ensergueix, E. Perez, B. Gicquel, and C. Guilhot. 1999. Identification of a virulence gene cluster of Mycobacterium

tuberculosis by signature-tagged transposon mutagenesis. *Molecular microbiology* 34: 257-267.

154. Parandhaman, D. K., and S. Narayanan. 2014. Cell death paradigms in the pathogenesis of Mycobacterium tuberculosis infection. *Frontiers in cellular and infection microbiology* 4: 31.
155. Davis, J. M., and L. Ramakrishnan. 2009. The role of the granuloma in expansion and dissemination of early tuberculous infection. *Cell* 136: 37-49.
156. Pan, H., B. S. Yan, M. Rojas, Y. V. Shebzukhov, H. Zhou, L. Kobzik, D. E. Higgins, M. J. Daly, B. R. Bloom, and I. Kramnik. 2005. Ipr1 gene mediates innate immunity to tuberculosis. *Nature* 434: 767-772.
157. Marzo, E., C. Vilaplana, G. Tapia, J. Diaz, V. Garcia, and P. J. Cardona. 2014. Damaging role of neutrophilic infiltration in a mouse model of progressive tuberculosis. *Tuberculosis (Edinb)* 94: 55-64.
158. Lammermann, T., P. V. Afonso, B. R. Angermann, J. M. Wang, W. Kastenmuller, C. A. Parent, and R. N. Germain. 2013. Neutrophil swarms require LTB4 and integrins at sites of cell death in vivo. *Nature* 498: 371-375.
159. Bournazou, I., J. D. Pound, R. Duffin, S. Bournazos, L. A. Melville, S. B. Brown, A. G. Rossi, and C. D. Gregory. 2009. Apoptotic human cells inhibit migration of granulocytes via release of lactoferrin. *The Journal of clinical investigation* 119: 20-32.
160. Amaral, E. P., S. C. Ribeiro, V. R. Lanes, F. M. Almeida, M. R. de Andrade, C. C. Bomfim, E. M. Salles, K. R. Bortoluci, R. Coutinho-Silva, M. H. Hirata, J. M. Alvarez, E. B. Lasunskaia, and M. R. D'Imperio-Lima. 2014. Pulmonary infection with hypervirulent Mycobacteria reveals a crucial role for the P2X7 receptor in aggressive forms of tuberculosis. *PLoS pathogens* 10: e1004188.
161. Nouailles, G., A. Dorhoi, M. Koch, J. Zerrahn, J. Weiner, 3rd, K. C. Fae, F. Arrey, S. Kuhlmann, S. Bandermann, D. Loewe, H. J. Mollenkopf, A. Vogelzang, C. Meyer-Schwesinger, H. W. Mittrucker, G. McEwen, and S. H. Kaufmann. 2014. CXCL5-secreting pulmonary epithelial cells drive destructive neutrophilic inflammation in tuberculosis. *The Journal of clinical investigation* 124: 1268-1282.
162. Berthelot, F., L. Fattoum, S. Casulli, J. Gozlan, V. Marechal, and C. Elbim. 2012. The effect of HMGB1, a damage-associated molecular pattern molecule, on polymorphonuclear neutrophil migration depends on its concentration. *Journal of innate immunity* 4: 41-58.
163. Lin, P. L., T. Coleman, J. P. Carney, B. J. Lopresti, J. Tomko, D. Fillmore, V. Dartois, C. Scanga, L. J. Frye, C. Janssen, E. Klein, C. E. Barry, 3rd, and J. L. Flynn. 2013. Radiologic responses in cynomolgous macaques for assessing tuberculosis chemotherapy regimens. *Antimicrobial agents and chemotherapy*.

164. el-Ahmady, O., M. Mansour, H. Zoeir, and O. Mansour. 1997. Elevated concentrations of interleukins and leukotriene in response to Mycobacterium tuberculosis infection. *Annals of clinical biochemistry* 34 (Pt 2): 160-164.
165. Pixley, F. J. 2012. Macrophage Migration and Its Regulation by CSF-1. *International journal of cell biology* 2012: 501962.
166. Colucci-Guyon, E., J. Y. Tinevez, S. A. Renshaw, and P. Herbomel. 2011. Strategies of professional phagocytes in vivo: unlike macrophages, neutrophils engulf only surface-associated microbes. *Journal of cell science* 124: 3053-3059.
167. Wong, K. W., and W. R. Jacobs, Jr. 2011. Critical role for NLRP3 in necrotic death triggered by Mycobacterium tuberculosis. *Cellular microbiology* 13: 1371-1384.
168. Francis, R. J., R. E. Butler, and G. R. Stewart. 2014. Mycobacterium tuberculosis ESAT-6 is a leukocidin causing Ca(2+) influx, necrosis and neutrophil extracellular trap formation. *Cell death & disease* 5: e1474.